FIELD-INSENSITIVE BOSE-EINSTEIN CONDENSATES AND AN ALL-OPTICAL ATOM LASER

Dissertation

zur Erlangung des Grades eines Doktors
der Naturwissenschaften

der Fakultät für Mathematik und Physik
der Eberhard-Karls-Universität zu Tübingen

vorgelegt von
Giovanni Cennini
aus Neapel

2004

Tag der mündliche Prüfung:	30. September 2004
Dekan:	Prof. Dr. H. Müther
1. Berichtstatter:	Prof. Dr. M. Weitz
2. Berichtstatter:	Prof. Dr. T. W. Hänsch
3. Berichtstatter:	Prof. Dr. T. Pfau

Abstract

Bose-Einstein condensates can be considered as sources of coherent matter. When atoms are extracted from a trapped Bose-Einstein condensate, a coherent, monoenergetic atomic beam is generated. Such a source is commonly referred to as an atom laser. Previous atom lasers were based on Bose-Einstein condensates of atoms in field-sensitive Zeeman states. Such atom lasers thus suffered form fluctuations of the chemical potential caused by stray magnetic fields.

In this work, a novel type of atom laser is demonstrated. A coherent atomic beam is generated by outcoupling of atoms from a magnetic field-insensitive Bose-Einstein condensate. The here developed experimental procedure does not require magnetic shielding of the apparatus in order to create quasi-continuous beams.

The presented experiments are based on quasistatic dipole traps for the confinement of cold ^{87}Rb atoms, which is realized with mid-infrared radiation emitted from a CO_2-laser operating near $\lambda = 10.6\,\mu m$. Because of the extreme laser detuning, a state-independent confinement is realized. Atoms in different spin-projections can be confined. Moreover, decoherence from photon scattering is negligible.

Evaporative cooling to quantum degeneracy ("all-optical BEC") is achieved in two optical dipole trapping geometries. In preliminary experiments, a crossed beams configuration was studied. This trap is formed by two CO_2-laser beams intersecting each other at a 90° angle, each of them having a 35 µm beam waist. The measured initial atom collision rate was about 7 kHz. A high initial atomic phase space density allowed to reach the quantum degenerate regime via evaporative cooling of the trapped atoms, which was accomplished through a continuous lowering of the optical confining potential. In this way, Bose-Einstein condensates with 1.0×10^4 were generated after 3 s of evaporative cooling.

In a second stage of this work, a single beam dipole trap was used for the confinement and the direct production of Bose-Einstein condensation of rubidium atoms. The trap was realized by tightly focussing a CO_2-laser beam to beam waist of 27 µm. In this trapping geometry, evaporative cooling successfully led to BEC after a forced evaporation period of 7 s. The number of atoms in the degenerate regime was measured to be 1.2×10^4.

In both trapping geometries, the state independent confinement allowed for the production of spinor condensates. In particular, $F = 1$ spinor condensates were generated: Bose condensed atoms populated the three spin-projections of the hyperfine ground state $|5S_{1/2}, F = 1\rangle$. The analysis of such spinor condensates was performed through a Stern-Gerlach experiment.

Particularly interesting is the possibility to achieve all-optical BEC in the single beam dipole trap. This represents the easiest realizable confining geometry for an optical dipole trap. Thus, experimental efforts towards all-optical Bose-Einstein condensation are considerably simplified.

In the single dipole trapping geometry, the confinement along the axis of the trapping beam is relatively weak. This feature allows one to remove atoms in field-sensitive states from the trap, when a moderate magnetic field gradient is applied throughout the forced evaporation phase. In the here presented experiments, an applied field gradient of 10 G/cm induces a force which is stronger than the confining optical dipole force. Atoms in $m_F = \pm 1$ states are removed from the trap, and only those in the field-insensitive state ($m_F = 0$ state) remain trapped and therefore reach quantum degeneracy.

This realizes a magnetic-field insensitive Bose-Einstein condensate. The stability of the chemical potential of this $m_F = 0$ Bose condensate is orders of magnitude higher than that of Bose-Einstein condensate based on atoms in field-sensitive states. The residual sensitivity to magnetic fields is as low as 14 fK/(mG)^2 and determined by the quadratic Zeeman effect only. The here demonstrated technique for the direct achieving of Bose-Einstein condensation of atoms in such $m_F = 0$ states may pave the way for the application of Bose condensates precision atom interferometry.

The work culminates in the demonstration of an all-optical atom laser. An output coupling of our optically trapped Bose-Einstein condensates is not possible with radiofrequency fields, as done in conventional atom lasers based on magnetic traps, since the optical dipole force acts on all Zeeman states. Instead, an output coupling of the field-insensitive Bose-Einstein condensate is achieved by smoothly lowering the CO_2-laser power in few hundreds milliseconds.

When the the optical dipole force does not sustain atoms against gravity anymore, a well collimated, monoenergetic atomic beam is observed. Unlike earlier devices, this atom laser is insensitive to stray magnetic fields. The generated atomic beam has an estimated brightness of typically 7×10^{27} atoms s^2 m^{-5}. The length and the flux of atoms in the beam can be adjusted by varying the lowering rate of the output coupling ramp. The transverse mode of the extracted coherent atomic beam does not suffer from lensing effects present in atom lasers based on RF-output coupling. This eliminates unwanted interference structure in the transverse mode of the atomic beam.

In future, atom lasers may allow for improved atom interferometers and atomic clocks. Furthermore, it is anticipated that field-insensitive states can also advance the field of precision atom optics for guided structures, which may allows, e.g., for improved atomic gyroscopes.

a Roberto e Rosaria

Table of Contents

Introduction

Einstein predicted in 1925 that an ideal gas of bosons of a given density, below a certain critical temperature would undergo a phase transition in which a macroscopic population of the lowest energy quantum state is measurable. This phenomenon is known as Bose-Einstein condensation (BEC) [1].

The quest for Bose-Einstein condensation in dilute atomic gases started in 1978 with studies based on spin-polarized hydrogen. It took almost two decades until the experimental demonstration of this new quantum phase transition: BEC was successfully observed in rubidium, sodium and lithium gases in 1995 [2, 3, 4], and in hydrogen gases in 1998 [5]. Undoubtedly, the success of those works on alkali atoms has to be ascribed to the ability of controlling and manipulating internal and external atomic degrees of freedom through laser cooling and atom trapping techniques, developed in the '80s and in the early '90s [6, 7, 8]. It has also built much on the understanding of the physics of atomic gases at very low temperatures that had been obtained using these techniques. The achievement of BEC and the impressive investigations of its properties were awarded by the Nobel prize in physics of 2001 [9, 10].

Efforts to reach BEC in dilute bosonic gases had been undertaken both in optical and magnetic traps. So far, many laboratories have succeeded in the production of the quantum degenerate regime in magnetic traps. The "conventional route" towards the quantum degenerate regime comprises an initial laser cooling and trapping of alkali atoms and a subsequent forced evaporation of magnetically trapped spin-polarized atoms [11]. In magnetic traps, evaporative cooling is accomplished by applying a radiofrequency radiation field, which removes the hottest atoms from the trap by spin-flip transitions. The remaining atoms rethermalize to a Maxwell-Boltzmann distribution of lower temperature, and eventually reach the critical temperature for the onset of the quantum degeneracy. Moreover, since the first demonstration of magnetic trapping of atoms [12], its technology has advanced a lot: today, e.g., magnetic traps offer new capabilities through miniaturization [13, 14].

On the other hand, the use of magnetic traps prevents the study of multiple spin-states species, diamagnetic atoms and molecules, since such traps only confine weak-field seeking spin states. Since the true ground state is always strong-field seeking, weak-field seeking states can inelastically scatter into the lowest energetic spin state. This so called dipolar

relaxation causes heating and losses of the trapped sample.

In addition, Bose-Einstein condensates in magnetic traps suffer from fluctuations of the chemical potential from stray magnetic fields. This imposes stringent limitations on precision experiments. Notably, the field of e.g. atomic clocks and atom interferometers benefits from the use of atoms in magnetic-field insensitive states ($m_F = 0$ states) [15].

While magnetic traps cannot confine atoms in such states, optical dipole traps certainly do. Indeed, for a suitable choice of the laser detuning with respect to the atomic frequency, such traps realize a state-independent confinement. Atoms in different spin-projections, diamagnetic atoms, and even molecules can be confined in far detuned optical traps [16].

Moreover, the use of laser light allows one to realize various confining geometries, ranging from spatially isotropic traps to optical lattices. Optical lattices are "microarrays" of well spatially ordered optical dipole traps, created by the interference of two or more laser beams. There is a huge amount of experimental work carried out with ultracold atoms confined in optical dipole traps and optical lattices [17]. Very recently, the application of dipole traps and optical lattices has opened a door to the physics of lower dimensions [18] and has permitted the observation of the Mott-insulator transition with an atomic gas [19]. In these experiments, involving Bose condensates, optical dipole traps served as secondary confining mechanism, as the quantum degenerate regime was first achieved in magnetic traps. It is clear that the formation of BEC directly in an optical dipole trap would definitely simplify these complex experiments.

By virtue of these and other considerations, the achievement of quantum degeneracy in optical dipole traps has been a longstanding goal in the atom physics community.

In 2001 Chapman's group demonstrated Bose-Einstein condensation by direct evaporative cooling of rubidium atoms in a CO_2-laser crossed dipole trap [20]. Because of the state-independent confinement realized by far detuned optical dipole traps, evaporative cooling cannot be achieved by radiofrequency transitions into untrapped states, as usually performed in magnetic traps. Instead, evaporative cooling most simply proceeds through a continuous lowering of the optical trapping potential. Since then, three other experimental groups achieved Bose-Einstein condensation with only optical methods. The group of Grimm and collaborators achieved Bose-Einstein condensation of cesium atoms in 2002 in a levitating optical dipole trap [21]. Also fermionic degeneracy has been demonstrated by all-optical methods in a CO_2-laser optical dipole trap by Thomas and collaborators in 2002 [22]. In March 2003, our group at Tübingen University observed BEC in these initial experiments using a CO_2-laser crossed dipole trap [23]. In the same year, Bose-Einstein condensation of ytterbium atoms was reported by Takasu *et al*. [24].

Although the experimental procedure for an "all-optical formation" of BEC is conceptually simple and offers both technical and theoretical advantages over the conventional root pursued in magnetic traps, the demanding initial conditions on the atomic phase space density and on the atom collision rate represent a major obstacle. Previously, Friebel *et al*. had shown that, in quasistatic dipole traps, simple polarization gradient optical cooling techniques alone can accumulate atoms to phase space densities three orders of magnitude below the onset of BEC [25]. However, the absence of a "runaway regime" in the evaporation course, as observed in pioneering works by Chu in Yag-laser dipole traps [26],

was seen as an insurmountable obstacle for the success of this cooling technique.

In this work, I report on the all-optical formation of Bose-Einstein condensation in quasistatic dipole traps and on the realization of a novel type of atom laser. One of the distinctive features of this work is the possibility to directly Bose condense alkali atoms in a running wave dipole trap realized by tightly focussing a CO_2-laser beam [23]. This is the easiest realizable geometry for an optical dipole trap. Note that previous experiments on BEC in optical dipole traps required more alignment sensitive geometries [20] or Feshbach resonances to enhance the atom collision rate [22, 21].

Bose-Einstein condensation is considered as a starting point of complex experiments which explore the research areas of, e.g., strongly correlated systems and quantum computing in optical lattices. All-optical BEC, according to the scheme here developed, might become a workhorse for future experiments, since it simplifies the experimental efforts towards the quantum degeneracy.

Bose-Einstein condensates which are described by three or more order parameters (so called "spinor condensates") display a rich, although complex dynamics [27]. Magnetic traps prevent the formation of spinor condensates. Usually, the study of such systems is carried out in a far-detuned optical dipole trap after the transfer from a magnetic trap [28]. In our experiments, spinor condensates are directly created by evaporative cooling atoms in CO_2-laser dipole traps. This dramatically reduces the complexity of experiments on spin dynamics.

Another focal point of this work is the direct creation of magnetic-field insensitive Bose-Einstein condensates [23]. When a sufficiently strong magnetic field gradient is applied, the resulting magnetic force can be larger than the confining optical dipole force along the weakly confining axes of the CO_2-laser beam. As results, atoms in field-sensitive states are removed in the final stage of the forced evaporation. Only atoms in field-insensitive states ($m_F = 0$ states) remain trapped and therefore are allowed to reach the quantum degeneracy. The chemical potential of a $m_F = 0$ Bose-Einstein condensate displays an exceptional robustness against any stray magnetic field. Let us point out that the chemical potential of a Bose-Einstein condensate of spin-polarized atoms is subjected to fluctuations on the order of $\Delta B \times 67\,\mathrm{nK/mG}$, where ΔB is the fluctuation in the magnetic field. On the contrary, the residual magnetic-field sensitivity of a $m_F = 0$ Bose condensate is determined only by the quadratic Zeeman effect. The stability of the chemical potential is in this way increased to a value of $\simeq 10\,\mathrm{fK/(mG)^2}$.

Let us observe that an alternative way to produce magnetic-field insensitive Bose condensates is to use spin-singlet ground state atoms as, e.g., recently demonstrated by Takasu *et al*. with Yb atoms. Nevertheless, our technique is reliable, easy to implement and might open Bose-Einstein condensation a door to atom interferometry and metrology fields, for which atoms in $m_F = 0$ states are widely used.

One of the most striking physical properties of a Bose-Einstein condensate is the existence coherence. Interference between two spatially overlapped Bose condensates has been observed [29]. Moreover, the spatial coherence of such a degenerate system of bosons has been measured [30]. On the other hand, the formation of a Bose-Einstein condensate

is based on bosonic stimulation [31, 32]. Because of these two embedded properties, Bose-Einstein condensates are considered as sources of "coherent matter". Indeed, it is possible to extract atoms from a trapped Bose-Einstein condensate and therefore produce coherent, diffraction limited, monoenergetic beams, which in literature are usually referred to as "atom lasers" [33, 34, 35, 36, 37].

For the first time, in this work an all-optical atom laser is demonstrated. This atom laser is based on atoms extracted from a $m_F = 0$ Bose condensate, and therefore displays an exceptional robustness to stray magnetic fields [37]. Hitherto, atom lasers were produced out of magnetic-field sensitive Bose condensates, where the output coupling is realized by transfer from field-sensitive into field-insensitive spin-projections, as first demonstrated by Ketterle and coworkers [33]. Such atom lasers experienced first-order sensitivity to magnetic field fluctuations. Inevitably, glitches in the magnetic field caused a reduction of the temporal coherence of an atom lasers, and only a pulsed operation could be realized. Hänsch and collaborators showed that an appropriate magnetic shielding of the experimental apparatus can reduce such detrimental effects [36]. Although successful, this technique cannot be easily scaled: reductions of fluctuations of the chemical potential on the order of fK seem unattainable with the present technology employed in magnetically trapped spin-polarized Bose-Einstein condensates. The scenario dramatically changes if one considers Bose-Einstein condensates of atoms in field-insensitive states, as achieved in this work.

Because the optical confining potential is not Zeeman selective, the here developed experimental procedure does not require radiofrequency fields or magnetic shielding of the experimental apparatus to create a quasi-continuous output coupler. Once a $m_F = 0$ Bose condensate is formed in a single CO_2-laser dipole trap, the confining potential is smoothly ramped down over a period of few hundreds milliseconds. When the optical confining potential does not sustain the condensed cloud against gravity any more, the atoms near the chemical potential surface spill out and a well collimated atomic beam is observed. A high brightness of the atomic beam is achieved. Moreover, changing the lowering rate of the optical power, it is possible to vary the flux of the extracted atoms and the length of the realized atomic beams. In this way, a well collimated atomic beam of up to 1 mm length can be observed.

Very recently, experiments characterizing some of the physical properties of atom lasers have been performed. For example, the temporal coherence of a quasi-continuous laser beam has been measured by Köhl *et al*. [38]. Moreover, the angular divergence of an atom laser has been determined by Aspect and collaborators [39]. An interesting result of that experiment was that the angular divergence here is primarily caused by interactions between the atoms in the laser beam and the remaining atoms inside the Bose condensate. On the other hand, this interaction can be described as an interactive lensing effect which leads to a interference structure in the transverse mode of the atomic beam [40]. For the sake of clarity it is important to note that these experiments have been carried out with atom lasers based on magnetically trapped Bose condensates, for which the extraction mechanism was based on spin-flip transitions of the trapped atoms inside the condensate.

In this work, instead, the output coupling mechanism does not require radiofrequency

transitions, and the output coupled atoms are those which are near the (downward directed) side of the condensate. In this way, the extracted beam does not transit the residing atomic cloud, eliminating an unwanted interference pattern in the atom laser mode.

Thesis structure

In the first chapter the theory of Bose-Einstein condensation in dilute gases is introduced. Most of the experimentally observed phenomena can be described in the framework of a mean field theory. The limit of negligible kinetic energy, namely the Thomas-Fermi regime, is reviewed. In this regime, it is possible to derive hydrodynamic equations for a trapped Bose condensate, which can be used to describe the output coupling of the all-optical atom laser demonstrated in this work.

In the second chapter an introduction to optical dipole traps for neutral atoms is presented. I will focus on the possibility to realize a state-independent confinement by employing quasistatic dipole traps. The relevant physical parameters as the potential depth and the trap frequencies are studied for two trapping geometries, realized by using CO_2-laser radiation.

In the third chapter the experimental apparatus for the study of ultracold atoms in quasistatic dipole traps is presented. The system has been built in the laboratories at Tübingen Universität and allows for a reliable production of Bose-Einstein condensates of atoms in magnetic-field insensitive states.

The fourth chapter is devoted to the experimental description of the "all-optical path" towards BEC. This relatively new experimental approach is accomplished both in a single and a crossed dipole trap geometry. Based on the single beam geometry, we demonstrate a novel technique for generating magnetic-field insensitive Bose-Einstein condensation (BEC in $m_F = 0$ states).

In the last chapter, I report on the realization of the all-optical atom laser. Gravity is used to achieve a quasi-continuous output coupling of the Bose condensed atoms. A simple model which describes the used extraction process is developed. Measurements on the brightness and on the beam profile will be presented and discussed.

Chapter 1

Bose-Einstein condensation in dilute atomic gases

The concept of Bose statistics was introduced in 1924 by Bose [41] to derive the Plank's law using a statistical argument. One year later, Einstein extended the Bose statistics to massive particles [1]. Below a critical temperature, trapped bosons undergo a phase transition, where a macroscopic occupation of the lowest energy state of the system is achieved. Bosons in this regime are described quantum mechanically by a unique macroscopic "condensate" wave function, which can be measured and manipulated in the laboratory.

One major problem encountered to test Einstein's predictions is that at densities and temperatures required for BEC, almost all materials equilibrate towards the solid state (He^4 is an exception because it is fluid even at $T = 0$). To date, this limitation has been sidestepped by studying very dilute systems, for which the relaxation to the solid state is dramatically reduced.

In this chapter, Bose-Einstein condensation in dilute, trapped gases is introduced. In the first part, the model of non-interacting trapped atoms is reviewed. This allows to extract useful physical quantities as the critical temperature (T_c) and the fraction of condensed atoms below T_c, namely N_c. Current experiments are carried out in dilute regime, where the interparticle interaction are essentially binary collisions. The physics in this regime of negligible thermal component (when $T \simeq 0$) is described by a Gross-Pitaevskii equation (GP equation). When the interparticle energy is greater than kinetic energy, the properties of the condensed system are well described in the so called Thomas-Fermi approximation. As conclusion of the chapter, the hydrodynamics of a trapped Bose condensate is introduced. This theory allows one to discuss the output coupler process in the formation of an "all-optical atom laser".

Henceforth, for a description of the Bose-Einstein condensation (BEC) in inhomogeneous systems, the approaches outlined in the review papers [42] and [43] are followed.

1.1 Bose-Einstein condensation of non interacting gases

The center of mass motion of N bosonic atoms, trapped in an external harmonic potential, can be approximated, under certain conditions, by a N harmonic oscillators, each having potential

$$V_{ext}(\mathbf{r}) = \frac{m}{2}(\omega_x^2 x^2 + \omega_y^2 y^2 + \omega_z^2 z^2), \tag{1.1}$$

where m is the mass of the bosons and $\omega_{x,y,z}$ are the trap frequencies of the harmonic confining potential. If the atom-atom interaction is neglected, the many-body Hamiltonian is the sum of single-particle Hamiltonian, each with an energy spectrum given by the well known formula:

$$\epsilon_{n_x n_y n_z} = \hbar\omega_x\left(n_x + \frac{1}{2}\right) + \hbar\omega_y\left(n_y + \frac{1}{2}\right) + \hbar\omega_y\left(n_y + \frac{1}{2}\right). \tag{1.2}$$

In the context of grand canonical ensemble, the mean number of atoms $\bar{n}$ in the single-energy eigenstate $|n_x, n_y, n_z\rangle$ with energy $\epsilon_{n_x n_y n_z}$ is given by

$$\bar{n}_i = \frac{1}{e^{(\epsilon_{n_x n_y n_z} - \mu)/k_B T} - 1}, \tag{1.3}$$

where μ is the chemical potential and is fixed by the total number of bosons

$$N = \sum_{\{n_x, n_y, n_z\}} \frac{1}{e^{(\epsilon_{n_x n_y n_z} - \mu)/k_B T} - 1}. \tag{1.4}$$

The chemical potential is large and negative for $T \to \infty$. As the temperature decrease, it increases monotonically. If at some temperature T_c (critical temperature) the condition (1.4) can be met with $\mu \to \mu_c = \epsilon_{0,0,0}$, then below T_c the occupation of the lowest single-particle state ($|0,0,0\rangle$) is of the order N, while the other $\bar{n}$ are still of the order unity or less[1]. This condition is the occurrence of BEC, namely a macroscopical occupation of the quantum ground state of the system. The critical temperature is calculated transforming the sum (1.4) into an integral. The validity of this "semiclassical" approximation implies that the relevant excitation energies are much larger than the level spacing fixed by the trap frequencies:

$$N = \int_0^\infty \frac{dn_x dn_y dn_z}{exp\left[(\epsilon_{n_x n_y n_z} - \mu)/k_B T\right] - 1} + N_c. \tag{1.5}$$

In this last equation the contribution of the lowest state (the ground state), indicated with N_c, is separated out [44, 45]. The integral (1.5) gives

$$N - N_c = \xi(3)\left(\frac{k_B T}{\hbar\omega_{ho}}\right)^3, \tag{1.6}$$

[1] The possibility of a fragmentated condensate is not discussed here

where $\xi(n)$ is the Riemann function and $\omega_{ho} = (\omega_x\omega_y\omega_z)^{1/3}$ is the geometric average of the oscillator frequencies. For a detailed account of trapped BEC conditions see [46]. The critical temperature is obtained by imposing $N_c \to 0$ at $T = T_c$:

$$k_B T_c = \hbar\omega_{ho}\left(\frac{N}{\xi(3)}\right)^{1/3} \simeq 0.94\hbar\omega_{ho}N^{1/3}. \tag{1.7}$$

For temperatures higher than T_c the chemical potential is smaller than μ_c and becomes a function on N. The thermodynamic limit is obtained by letting $N \to \infty$ and $\omega_{ho} \to 0$ while keeping $N\omega_{ho}^3$ constant. The fraction of condensed atoms for $T < T_c$ is given by the well known relation[2]

$$\frac{N_c}{N} = 1 - \left(\frac{T}{T_c}\right)^3. \tag{1.8}$$

As conclusion of this paragraph, it is worth pointing out that bosons can be considered as quantum mechanical object whose wavepackets have a spatial extent of the order of $\lambda_{\mathrm{dB}} = \sqrt{2\pi\hbar^2/(mk_BT)}$. This quantity can be regarded as the position uncertainty associated with the thermal momentum distribution. The lower the temperature, the larger is λ_{dB}. When the atomic temperature is close T_c, λ_{dB} becomes comparable to the interparticle distance, and the atomic wavepackets start to overlap. As results, the indistinguishability of particles becomes important, and the Bose statistic plays a role. At this temperature, the trapped bosons undergo a phase transition, with almost all bosons occupying the same quantum mechanical state. The occurrence of BEC may be regarded as an effect of the Bose statistics only. Actually, It is possible to demonstrate that this phase transition is reinforced in case of interactions among bosons [43]. This tendency of bosons to "cluster" is very generic [47].

1.2 Weakly interacting Bose gas

In the previous section, the bosonic system has been assumed to be composed of non interacting particles. A richer panorama is revealed when interparticle interactions are taken into account. In a Bose-Einstein condensate the ground state wave function is the product of the single-particle harmonic oscillator wave functions:

$$\Phi(\mathbf{r_1}, \ldots, \mathbf{r_N}) = \prod_{i=1}^{N} \phi_0(\mathbf{r_i}) \tag{1.9}$$

with $\phi_0(\mathbf{r}) = [m\omega_{ho}/(\pi\hbar)]^{3/4} exp\big[-(m/2\hbar)(\omega_x x^2 + \omega_y y^2 + \omega_z z^2)\big]$ being the ground state wave function of each particle. The density distribution is then $n(\mathbf{r}) = N|\phi_0(\mathbf{r})|^2$, in which N is the total number of atoms in the condensate. It is important to notice that, in this

[2] In a homogeneous gas the dependence on the temperature is $N_c/N = 1 - (T/T_c)^{3/2}$

approximation, the size of the Bose condensed cloud is independent on N and equals the harmonic oscillator length:

$$a_{ho} = \left(\frac{\hbar}{m\omega_{ho}}\right)^{1/2}. \tag{1.10}$$

However, experiments show that the size of the condensed cloud is somewhat larger than a_{ho}. This is the clear evidence of the presence of interparticle interactions.

The easiest way to take into account interparticle-interactions is to introduce a mean field approach. This approach describes a weakly interacting system of bosons, in the limit of negligible thermal compound and high condensate's fraction. The many-body Hamiltonian, describing N interacting bosons confined in an external potential V_{ext}, in the second quantization picture reads

$$\hat{H} = \int d\mathbf{r}\hat{\Psi}^{\dagger}(\mathbf{r})\big[-\frac{\hbar^2}{2m}\nabla^2 + V_{ext}\big]\hat{\Psi}(\mathbf{r}) + \frac{1}{2}\int d\mathbf{r}d\mathbf{r}'\hat{\Psi}^{\dagger}(\mathbf{r})\hat{\Psi}^{\dagger}(\mathbf{r}')V_{int}(\mathbf{r}-\mathbf{r}')\hat{\Psi}(\mathbf{r}')\hat{\Psi}(\mathbf{r}), \tag{1.11}$$

where $\hat{\Psi}^{\dagger}(\mathbf{r})$ and $\hat{\Psi}(\mathbf{r})$ are the boson field operators of creation and annihilation, respectively, and $V_{int}(\mathbf{r}-\mathbf{r}')$ is the interparticle potential. In dilute regime, the scattering length is much smaller than the interparticle distance:

$$n|a|^3 \ll 1, \tag{1.12}$$

where a is the scattering length [3]. Because of diluteness, the interaction potential is assumed to be punctual [48]:

$$V = g\delta(\mathbf{r}-\mathbf{r}'), \tag{1.13}$$

where g is the coupling constant [44, 48], and its value is given by

$$g = \frac{4\pi\hbar a}{m}. \tag{1.14}$$

The idea of mean field theory was introduced by Bogoliubov [49], and it consists in separating out the condensate contribution to the bosonic field operator. The field operators are considered as linear combinations of single particle operators of annihilation and creation, namely $\hat{\Psi}(\mathbf{r}) = \sum_{\alpha}\Psi_{\alpha}(\mathbf{r})a_{\alpha}$, where $\Psi_{\alpha}(\mathbf{r})$ are single-particle wave functions and a_{α} are the corresponding annihilation operators. In Fock space, the bosonic operators of creation and annihilations are defined through the relations

$$\begin{aligned} a_{\alpha}^{\dagger}|n_0, n_1, \ldots, n_{\alpha}, \ldots\rangle &= \sqrt{n_{\alpha}+1}|n_0, n_1, \ldots, n_{\alpha}+1, \ldots\rangle \\ a_{\alpha}|n_0, n_1, \ldots, n_{\alpha}, \ldots\rangle &= \sqrt{n_{\alpha}}|n_0, n_1, \ldots, n_{\alpha}-1, \ldots\rangle \end{aligned} \tag{1.15}$$

where n_{α} are the eigenvalues of the number operator $\hat{n}_{\alpha} = a_{\alpha}^{\dagger}a_{\alpha}$.

[3] Here the modulus appears since Nature has provided atomic species with negative scattering length as well.

Bose-Einstein condensation occurs when the number of atoms in the ground state $n_0 \equiv N_0 \gg 1$. In this limit, $N_0 + 1 \simeq N_0$ and the operators $a_0^\dagger = a_0 = \sqrt{N_0}$ become c-numbers. The field operator is then

$$\hat{\Psi}(\mathbf{r}, t) = \Phi(\mathbf{r}, t) + \hat{\Psi}'(\mathbf{r}, t). \tag{1.16}$$

The quantity $\Phi(\mathbf{r}, t)$ is called "order parameter" [50, 51], and it is the average value of the bosonic field operator: $\Phi(\vec{r}, t) \equiv \langle \hat{\Psi}(\vec{r}, t) \rangle$. Its modulus fixes the condensate density

$$n_0(\mathbf{r}, t) = |\Phi(\mathbf{r}, t)|^2. \tag{1.17}$$

On the other hand, the quantity $\hat{\Psi}(\mathbf{r}, t)'$ is the remaining quantum microscopic contribution of the bosonic field. It is worth noticing that this residual part describes the excitations caused by the thermal component. Neglecting this last term, the equation of motion for the order parameter becomes [42, 52]

$$i\hbar \frac{\partial \Phi(\mathbf{r}, t)}{\partial t} = \left(-\frac{\hbar^2 \nabla^2}{2m} + V_{ext} + g|\Phi(\mathbf{r}, t)|^2 \right) \Phi(\mathbf{r}, t) \tag{1.18}$$

This is known as the time dependent Gross-Pitaevskii equation. The term $g|\Phi(\mathbf{r}, t)|^2$ is the interaction potential. The time independent GP equation is derived when the following ansatz is done: $\Phi(\mathbf{r}, t) = \phi(\mathbf{r}) exp(-i\mu t/\hbar)$, where μ is the chemical potential and ϕ is a real function such that $\int d\vec{r} \phi^2 = N_0$. The GP equation in the stationary case reads

$$\left(-\frac{\hbar^2 \nabla^2}{2m} + V_{ext} + g|\phi|^2 \right) \phi(\mathbf{r}) = \mu \phi(\mathbf{r}) \tag{1.19}$$

This is a non linear Schrödinger equation, because of the term $n(\mathbf{r}) = |\phi(\mathbf{r})|^2$. In case of negligible interparticle interaction, the quadratic term in ϕ vanishes, and the condensate wave function is the harmonic ground state function, as it has been shown at the beginning of this section.

1.3 Thomas Fermi approximation

Generally, the GP equation can be solved numerically. However, it is possible to obtain an analytical solution in the limit of strong interparticle interactions. Comparing the interaction energy and the kinetic energy possessed by the bosons, one finds

$$\frac{E_{int}}{E_{kin}} \propto \frac{N|a|}{a_{ho}}. \tag{1.20}$$

In current experiments on BEC, this ratio is much greater than 1, and in the GP-equation the kinetic energy can be neglected. This is the Thomas Fermi (TF) regime, and is met even if $n|a|^3 \ll 1$. In the TF regime, the density of the trapped Bose-Einstein condensate is then described by the following equation

$$n(\mathbf{r}) = |\phi(\mathbf{r})|^2 = \frac{1}{g}\left[\mu - V_{ext}\right]. \tag{1.21}$$

In our work the ratio $E_{int}/E_{kin} \sim 100$ and the TF approximation is valid. Equation (1.21) is valid where $\mu \geq V_{ext}$, otherwise the condensate density is assumed $n = 0$. The peak density is

$$n_0 = \frac{\mu}{g}. \tag{1.22}$$

The relation between the chemical potential and the total number of particles in this regime is given through the relation

$$\mu = \frac{\hbar\omega_{ho}}{2}\left(\frac{15Na}{a_{ho}}\right)^{2/5}. \tag{1.23}$$

The density profile has the form of an inverted parabola, which vanishes at the turning point R defined by the condition $\mu = V_{ext}$. For a spherical harmonic potential:

$$R = a_{ho}\left(\frac{15Na}{a_{ho}}\right)^{1/5} \tag{1.24}$$

The Thomas-Fermi density is inadequate to describe the system only near the turning point R [53]. The shape of the outer part of the condensate is fixed by the balance of the zero-point kinetic energy and the external potential. In order to take into account the effect, one usually introduces the "healing length", defined as the minimum distance over which the order parameter "heal": the distance over which the density grows from 0 to n. This distance is given from the balance between the kinetic energy and the interaction energy [42, 43]:

$$\xi = (8\pi n_{max} a)^{-1/2} \tag{1.25}$$

In typical Bose-Einstein condensates, the healing length is large in comparison with the scattering length, but generally smaller than the typical trap dimensions.

1.4 Hydrodynamic equations

As conclusion of this chapter, we would like to extend the Thomas-Fermi approximation to the time dependent case. In this case, the system is described by a Newton's equation, and the Bose condensed cloud behaves as a classical particles under the effect of an external potential. Based on this approximation, it is possible to describe the output couple dynamics of the all-optical atom laser demonstrated in this work [37]. For completeness, let us note that the time dependent Thomas-Fermi approximation is commonly encountered in the experiments in which the external trapping potential has a temporal dependency, e. g. in ballistic expansion, or in the collective excitation of a Bose condensate to modulations of the trap frequency [11].

For this purpose, it is convenient to write the complex order parameter Φ according the well known hydrodynamic representation (a modulus plus a phase):

$$\Phi(\mathbf{r}, t) = \sqrt{n(\mathbf{r}, t)}e^{iS(\mathbf{r},t)} \tag{1.26}$$

the phase $S(\mathbf{r},t)$ fixes the velocity field as follows:

$$n(\mathbf{r},t)\mathbf{v}(\mathbf{r},t) = \frac{\hbar}{2im}(\Phi^*\nabla\Phi - \Phi\nabla\Phi^*), \tag{1.27}$$

so that

$$\mathbf{v}(\mathbf{r},t) = \frac{\hbar}{m}\nabla S(\mathbf{r},t). \tag{1.28}$$

The GP equation (1.18) can be rewritten in the form of two coupled equations for the density and the velocity field:

$$\frac{\partial}{\partial t}n + \nabla\cdot(\mathbf{v}n) = 0 \tag{1.29}$$

$$m\frac{\partial}{\partial t}\mathbf{v} + \nabla\big(V_{ext} + gn - \frac{\hbar^2}{2m\sqrt{n}}\nabla^2\sqrt{n} + \frac{mv^2}{2}\big) = 0 \tag{1.30}$$

The first one is the equation of continuity, while the second establishes the irrotational nature of the superfluid motion.

The classical hydrodynamic approximation consists in neglecting the quantum pressure term $\frac{\hbar^2}{2m\sqrt{n}}\nabla^2\sqrt{n}$ in the equation (1.30). If we denote with d the typical length scale of variation of the condensate density n, and with ξ the healing length (see equation (1.25)), then the condition for neglecting the quantum pressure is [54]

$$d \gg \xi. \tag{1.31}$$

Remembering that $\nabla(\frac{1}{2}mv^2) = m(\mathbf{v}\cdot\nabla)\mathbf{v}$, equation 1.30 can be cast into:

$$m(\frac{\partial}{\partial t} + \mathbf{v}\cdot\nabla)\mathbf{v} = -\nabla(V_{ext} + gn). \tag{1.32}$$

This is a Newton's equation in presence of an external force field written in Euler's point of view (the quantity in the brackets on the left side is the convective derivative).

In the case of the atom laser, the external potential is the sum of two terms: $V_{ext} = V_{ho} + V_{grav}$. However, since the gravitational term is stronger than the interparticle potential gn, it is possible to neglect this last term. The equation (1.32) becomes

$$m\frac{d^2}{dt^2}\mathbf{r}(t) = \mathbf{F}(\mathbf{r},t) = -\nabla(V_{ho} + V_{grav}). \tag{1.33}$$

The condensate behaves as a classical particle in a force field given by the sum of the optical and the gravitational potentials. Based on this equation it is possible to estimate the output emission time of the atom laser as will be explained in the chapter on the realization of the atom laser.

Chapter 2

Optical Dipole Traps

An optical dipole trap consists of a laser field configuration with one or more points of stable equilibrium for the atomic motion, such that any displacement of an atom from these points results in an average restoring force. The trapping force (the optical dipole force) arises from the coherent interaction between the electric field associated with a far detuned laser field and the induced atomic dipole moment [55, 56, 57]. Such traps are suitable for storing particles. Indeed, for a suitable choice of the laser detuning with respect to the atomic frequency such traps realize a state-independent confinement. Atoms in different spin-projection states can be trapped, as well as diamagnetic atoms and molecules. This is an advantage over magnetic traps, for which only spin polarized atoms can be confined. The photon scattering rate, which is responsible for the maximum lifetime of the trapped atoms, can be reduced by increasing the laser detuning. Moreover, laser light fields allow one to realize a great variety of different trap geometries, ranging from symmetric to anisotropic traps, from mesoscopic traps to spatially ordered optical lattices [17, 58, 59].

In this chapter, the optical dipole potential for an atom in a detuned laser light field is derived. First, a classical model based on the concept of the atomic polarizability is introduced. From this picture, it is possible to get an easy and rapid insight in the matter. Subsequently, an approach based on the ac-Stark shifts of the atomic levels in the presence of a detuned laser field is presented. With these theoretical tools, it is possible to gain a better understanding of the properties of optical dipole traps. Afterwards, the study of two CO_2-laser optical dipole trap geometries is exposed. The relevant physical parameters as the potential depth and the trap frequencies in both laser field configurations are extracted.

2.1 Optical potential and photon scattering rate

The force acting on an atom placed in a laser field can be viewed as the Lorentz force exerted by the electric field associated to the laser light on the induced atomic dipole moment. The force has three components resulting, respectively, from the absorption, spontaneous emission, and induced emission of photons by the atoms. The first two of these represent the scattering force, which is used for dissipating the atomic kinetic energy. For far-detuned laser radiation, the scattering force is negligible and the third contribution plays a role in the atom-laser interaction. This contribution is called optical dipole force; it has a dispersive nature, and is directed along the gradient of the laser field intensity. For the sake of completeness, off-resonant absorption and subsequent spontaneous emission play a fundamental role in the heating rate of the trapped atoms.

It is already possible to get an insight in the matter, if the laser field is treated classically and the atom as an harmonic oscillator (as long as the saturation effects can be neglected). If an atom is placed in a laser field, the electric field $\vec{E}$ associated to the laser light, oscillating at pulsation $\omega_L = 2\pi\nu_L$, induces an oscillating atomic dipole moment $\vec{d}$. If the electric field is given by $\vec{E}(\vec{r},t) = \hat{e}E(\vec{r})e^{-i\omega_L t} + h.c.$, then the induced atomic dipole moment reads $\vec{d}(\vec{r},t) = d\hat{e}(\vec{r})e^{-i\omega_L t} + h.c.$, where $\hat{e}$ is the unit polarization vector, and d is the amplitude of the induced dipole moment, which is related to the atomic polarizability $\alpha(\omega)$ through the relation

$$d = \alpha(\omega)E. \tag{2.1}$$

Note that α is a complex function, depending on the laser frequency. The interaction potential of the induced dipole moment $\vec{d}$ in the driving field $\vec{E}$ is given by

$$V_{dip} = -\langle \int_0^E \vec{d}(E') \cdot d\vec{E}' \rangle = -\frac{1}{2}\langle \vec{d} \cdot \vec{E} \rangle = -\frac{1}{2}\langle \alpha E^2 \rangle, \tag{2.2}$$

where the angular brackets denote the usual time average over the rapidly oscillating terms; the factor $1/2$ is present because the atomic dipole moment is not permanent but induced. It is easy to show that the optical potential is related to the laser field intensity by

$$V_{dip}(\mathbf{r}) = -\frac{1}{2\epsilon_0 c} Re(\alpha) I(\mathbf{r}), \tag{2.3}$$

where $I = 1/2\epsilon_0 c|\vec{E}|^2$ is the laser light intensity. Note that the dipole potential is proportional to the real part of the atomic polarizability. The optical dipole force is given by the gradient of the optical dipole potential:

$$F_{dip}(\mathbf{r}) = -\vec{\nabla} V_{dip} = -\frac{1}{2\epsilon_0 c} Re(\alpha) \vec{\nabla} I(\mathbf{r}). \tag{2.4}$$

It is evident that this force is directed along the gradient of the laser field intensity.

The residual photon scattering rate, which leads to a heating of the atoms, is calculated as follows. In a classical picture, between the times t and dt the atomic electron moves

from $\mathbf{r}$ to $d\mathbf{r}$ and the driving electric field carries out a work $dW = e\vec{E} \cdot d\mathbf{r}$ on it. The average power absorbed by the atom is $P_{abs} = \vec{E} \cdot \langle \dot{\vec{d}} \rangle$. The photon scattering rate is inferred as the averaged absorbed power per photon energy:

$$\Gamma_{sc} = \frac{P_{abs}}{\hbar\omega_L} = \frac{1}{\hbar\epsilon_0 c} Im(\alpha) I(\mathbf{r}). \tag{2.5}$$

Expressions (2.4) and (2.5) are valid for any polarizable particle in an oscillating electric field, *i.e.* for an atom in a far off-resonant laser field or a molecule in a microwave field as well. The frequency dependency of the atomic polarizability can be calculated by using the Lorentz's model of a classical damped oscillator in an external driving field. The oscillator has a characteristic frequency ω_A corresponding to the optical transition. The damping rate is given by the well known Larmor formula of a radiating accelerated charge [60]:

$$\alpha = 6\pi\epsilon_0 c^3 \frac{\Gamma/\omega_A^2}{\omega_A^2 - \omega_L^2 - i\frac{\omega_L^3}{\omega_A^2}\Gamma}, \tag{2.6}$$

where Γ is the on-resonant damping rate which can be calculated quantummechanically by introducing the simple model of a two-level atom:

$$\Gamma = \frac{\omega_A^3}{3\pi\epsilon_0\hbar c^3} |\langle e|\vec{d}|g\rangle|^2, \tag{2.7}$$

with $\vec{d}$ representing the dipole atomic operator. The above expressions allow to write down the strength of the optical potential and the photon scattering rate in the regime of negligible saturation:

$$V_{dip}(\mathbf{r}) = -\frac{3\pi c^2}{2\omega_A^3}\left(\frac{\Gamma}{\omega_A - \omega_L} + \frac{\Gamma}{\omega_A + \omega_L}\right) I(\mathbf{r}) \approx \frac{3\pi c^2}{2\omega_A^3}\frac{\Gamma}{\Delta} I(\mathbf{r}) \tag{2.8}$$

$$\Gamma_{sc} = \frac{3\pi c^2}{2\hbar\omega_A^3}\left(\frac{\omega_A}{\omega_L}\right)^3\left(\frac{\Gamma}{\omega_A - \omega_L} + \frac{\Gamma}{\omega_A + \omega_L}\right) I(\mathbf{r}) \approx \frac{3\pi c^2}{2\hbar\omega_A^3}\left(\frac{\Gamma}{\Delta}\right)^2 I(\mathbf{r}), \tag{2.9}$$

where $\Delta = \omega_L - \omega_A$ is the laser detuning relative to the atomic resonance.

Note that, on the right side of the equations (2.8) and (2.9) the rotating wave approximation is assumed[2], which is valid when the detuning $\Delta \gg \Gamma$, and $\Delta \ll \omega_A$. The optical dipole potential is proportional to the laser field intensity. Depending on the sign of the laser detuning, two typologies of optical dipole traps are possible, as it is shown in Fig. 2.1.

For *blue traps* ($\Delta > 0; \omega_L > \omega_A$) the optical potential has the same sign as the laser field intensity. This causes that the minima of the atomic motion coincide with the minima of the laser field. In this case, the dipole force attracts atoms towards the minima of the light field. On the other hand, for *red traps* ($\Delta < 0; \omega_L < \omega_A$) the minima of the atomic motion correspond to the maxima of the laser light field. In this latter case, the optical dipole force pushes atoms towards the maxima of the laser field.

[2]In the rotating wave approximation, the counter-rotating term, which oscillates at frequency $\omega_L + \omega_A$ is neglected.

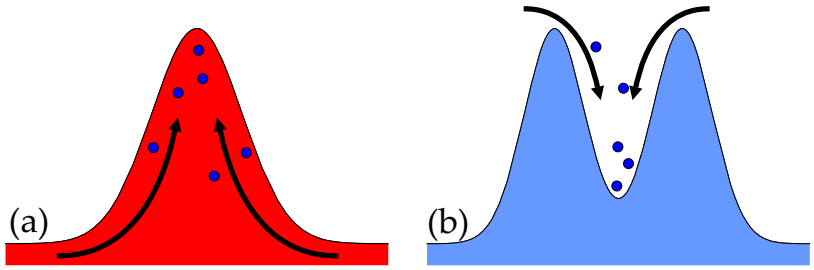

Figure 2.1: Optical Dipole Traps: (a) Scheme of a red detuned dipole optical trap ($\Delta < 0$); the intensity of the laser light has a gaussian form, and atoms are attracted towards the maxima of the laser light. (b) Blue detuned optical dipole trap ($\Delta > 0$); such traps can be realized with, e.g., "hollow beams" that is by using Laguerre-Gauss beams or Bessel-Gauss beams. In this case, atoms are dragged towards the minima of the laser light field.

It is clear that the choice of the laser detuning is important. In general, it depends on the trapping geometry, on the total amount of laser power available and the maximum photon scattering rate that atoms are allowed to experience. The photon scattering rate as a function of the optical potential reads

$$\Gamma_{sc} = \frac{\Gamma}{\Delta} V_{dip}. \tag{2.10}$$

The maximum kinetic energy that the confined atoms can posses in an optical dipole trap is referred to as the potential depth of the trap. This is a fundamental concept in the physics of atom trapping. Each time an atom absorbs a photon from the laser light field, its kinetic energy increases in average by one recoil energy $E_{rec} \simeq \hbar^2 k^2/m$, where k is the photon wave-vector and m the atomic mass. Therefore, the absorbed photons limit the lifetime of the trapped atoms, since they increase the atomic kinetic energy. It is necessary to operate at a large laser detuning Δ in order to guarantee long trapping times. On the other hand, larger laser detuning means shallower optical potential depth, see equation (2.8). However, because in near resonant dipole traps the optical potential scales as I/Δ whereas the scattering rate as I/Δ^2, there is room for adjusting the laser detuning in order to minimize the number of absorbed photons, and, at the same time, to guarantee sufficiently strong potential depths.

2.2 Multi-level atoms

The expressions of the dipole potential and the scattering rate have been derived for a two-level atom model. In reality, atoms have a rich multi-level structure. For multi-level atoms the expressions previously obtained get more complicated. However, this is not a merely

drawback, since a richer panorama of phenomena emerges, e. g. a laser polarization dependency of the atomic dipole potential [17].

The interaction between a laser light field and a multi-level atom is better described in the dressed-state approach [61]. The effect of off-resonant laser light on the atomic levels can be treated as a perturbation in second order of the electric field. We calculate this light shift in a dressed atom approach. For non degenerate states, the energy shift of the i-th state is given by the well known formula

$$\Delta E_i = \sum_{j \neq i} \frac{|\langle j|H_{int}|i\rangle|^2}{\epsilon_i - \epsilon_j}, \tag{2.11}$$

where the atom-laser interaction is included in the term $H_{int} = -\vec{d} \cdot \vec{E}$, and ϵ_i is the unperturbed energy of the i-th state, considering the atom plus the laser field as an unique system. In its ground state $|g\rangle$, the atom has zero energy, whereas the laser field has an energy equal to $n\hbar\omega_L$, with n the number of photons. The energy of the ground state of the "atom+field" system is $\epsilon_g = n\hbar\omega_L$. If one photon is absorbed from the laser field, the atom undergoes an electronic transition to the excited state $|e\rangle$, and the total energy of the system is $\epsilon_e = \hbar\omega_A + (n-1)\hbar\omega_L = -\hbar\Delta + n\hbar\omega_L$. These two states are coupled by the laser field. After some algebra, the formula (2.11), in the limit $\Delta \gg \Gamma$, reads

$$\Delta E_{g/e}(\mathbf{r}) = \pm \frac{|\langle e|\vec{d}|g\rangle|^2}{\Delta} |\vec{E}|^2 = \pm \frac{3\pi c^2}{2\omega_A^3} \frac{\Gamma}{\Delta} I(\mathbf{r}), \tag{2.12}$$

where the signs $\pm$ correspond to the ground and excited state, respectively.

It is worth pointing out that this formula has been derived for a laser field with detuning Δ much below the optical frequency ω_A, and for a two-level atom. Optical dipole traps which relay on this approximation are called "near-resonant" dipole traps. For such a system, the sign of the light shifts depends on the laser detuning, realizing a state dependency on the detuning Δ, as represented in Fig 2.2.

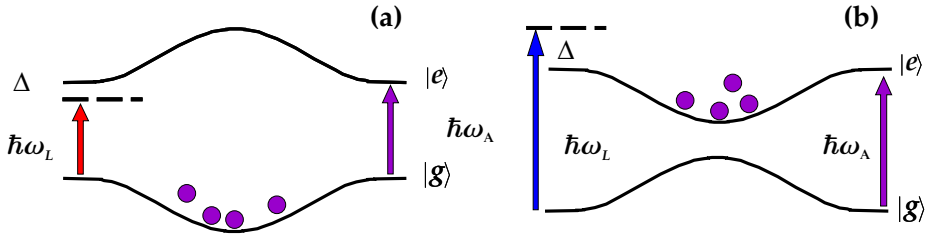

Figure 2.2: Scheme of ac-Stark shifts. (a) The atom-laser interaction shifts the atomic energy levels downwards or upwards. For $\Delta < 0$, with a laser beam which presents a maximum in space, the ground state is trapping in the maxima of the light, while the excited level is anti-trapping. (b) When $\Delta > 0$, the excited state becomes trapping.

The scenario dramatically changes as soon as atoms are regarded as objects with an electronic substructure. In this case, one has to sum over all possible excited states $|e_j\rangle$ starting from a specific ground state $|g_i\rangle$ (of which one wants to calculate the light shift). The dipole matrix element for these transitions is given by the well known formula $\mu_{ij} = c_{ij} \parallel \mu \parallel$, where $\parallel \mu \parallel$ is the reduced matrix element and c_{ij} is the relative line strength of the involved transition. The energy shift of an electronic ground state $|g_i\rangle$ is

$$\Delta E_i = \frac{3\pi c^2 \Gamma}{2\omega_A^3} I \sum_j \frac{c_{ij}^2}{\Delta_{ij}}, \tag{2.13}$$

where Γ is the spontaneous decay rate, I the laser intensity, and Δ_{ij} the laser detuning relative to the involved transitions.

Many experiments on laser cooling and atom trapping employ alkali atoms, which of course have a complex electronic structure. In particular, in this thesis isotope ^{87}Rb of rubidium atom has been investigated. The spin-orbit coupling, being responsible for the fine structure, leads to the D-line doublet $5S_{1/2} \rightarrow 5P_{1/2}, 5P_{3/2}$, with an energy splitting $\hbar\Delta'_{FS} \approx 7200\,\text{GHz}$. The two D-lines are at wavelength of 794.8 nm (D1-line) and 780.2 nm (D2-line), respectively. Moreover, the coupling with the nuclear spin $I = 3/2$ is responsible for the hyperfine splitting of both ground and excited states, with energies $\hbar\Delta_{HFS} \approx 6.8\,\text{GHz}$ and $\hbar\Delta'_{HFS} \approx 500\,\text{MHz}$. It is evident that the three splitting energies represent three relevant atomic energy scales: $\Delta'_{FS} \gg \Delta_{HFS} \gg \Delta'_{HFS}$. For example, when the laser detuning $\Delta \gg \Delta'_{HFS}$ the optical potential becomes [17, 62]

$$V_{dip} = \frac{3\pi c^2 \Gamma}{2\omega_A^3} \left(\frac{2 + P g_F m_F}{\Delta_{2,F}} + \frac{1 - P g_F m_F}{\Delta_{1,F}} \right) I(\mathbf{r}), \tag{2.14}$$

in which g_F is the Landé factor and P is the laser polarization ($P = 0$ for linearly polarized laser light and $P = \pm 1$ for circularly $\sigma^{\pm}$ light, respectively). The two detunings $\Delta_{2,F}$ and $\Delta_{1,F}$ refer to the energy difference between the particular ground state $5S_{1/2}F$ and the center of the hyperfine splitting $5P_{1/2}$ and $5P_{3/2}$, respectively.

As a further example, let us consider the case of a laser detuning which greatly exceeds the fine-structure splitting Δ'_{FS}. If Δ denotes the laser detuning with respect to the center of the D-line doublet, then $\Delta_{2,F} = \Delta_{1,F} = \Delta \gg \Delta'_{FS}$. The hyperfine splitting is therefore negligible, and expression (2.14) can be approximated by

$$\frac{3\pi c^2}{2\omega_A^3} \frac{\Gamma}{\Delta} \left(1 + \frac{1}{3} P g_F m_F \frac{\Delta'_{FS}}{\Delta} \right) I(\mathbf{r}). \tag{2.15}$$

Deeper discussions about the role of the laser detuning in optical dipole traps go beyond the aim of this work. It is nevertheless interesting to point out that, in this last case, if a laser with linearly light is employed ($P = 0$) all magnetic sub-levels are shifted of an equal quantity, contrarily to that of a $\sigma^{\pm}$ laser light, which induces light shifts that depend on the m_F spin-projection.

2.3 Quasistatic dipole traps

So far, we have assumed that the laser detuning Δ is much smaller than the absolute laser frequency. In this approximation, the counter-rotating term in the expression of the atom-field interaction in equations (2.8) and (2.9) can be neglected.

In the case of CO_2-laser dipole traps, the laser wavelength is one order of magnitude bigger than the wavelength associated to $D1$ and $D2$ lines, and both the hyperfine and fine atomic structures are not resolved. As a result, the rotating and the counter-rotating terms contribute to the optical potential with roughly the same weight [63].

The trapping potential is given by the lowest order perturbation theory expression for the Stark-shift of a ground state$|g\rangle$, due to the excited states $|e\rangle$ [61, 64]:

$$\Delta E_g = -\frac{1}{4\hbar}\sum_e |\vec{d_{eg}}\cdot\vec{E}|^2\left[\frac{1}{\omega_{eg}-\omega_L}+\frac{1}{\omega_{eg}+\omega_L}\right], \tag{2.16}$$

where $\omega_{eg} = (E_e - E_g)/\hbar$. This expression can be simplified using the atomic polarizability. In general, when the laser frequency ω_L is much smaller than any of the resonant atomic frequencies ω_{eg}, the scalar polarizability can be approximated by the expression [65]

$$\alpha(\omega_L) = \frac{e^2}{m}\sum_{e\neq g}\frac{f_{ge}}{\omega_{eg}^2-\omega_L^2}, \tag{2.17}$$

where f_{ge} is the absorption oscillator strength of the $g \rightarrow e$ transition:

$$f_{ge} = \frac{2m\omega_{eg}}{3\hbar(2J_g+1)e^2}\mid\langle gJ_g||\hat{p}||eJ_e\rangle\mid^2, \tag{2.18}$$

Fig. 2.3 shows the behavior of the rubidium dynamic polarizability versus the exciting laser frequency (in cm^{-1}), both for the ground and excited states of rubidium atoms. By means of equations (2.17) and (2.18), the light shift formula (2.16) becomes

$$V_{dip} = -\frac{1}{2}\frac{\alpha_S}{[1-(\omega_L/\omega_1)^2]}|\vec{E}|^2, \tag{2.19}$$

where ω_1 is the frequency of the first dipole transition ($D1$-line), and α_S denotes the static atomic polarizability (in the limit $\omega_L \rightarrow 0$).

At the CO_2-laser wavelength ($\lambda \simeq 10.6\,\mu m$) this latter equation approaches the static value (in the limit $\omega_L \rightarrow 0$):

$$V_{dip} = -\frac{1}{2}\alpha_S|\vec{E}|^2. \tag{2.20}$$

The value of the static polarizability of the rubidium ground state $5S_{1/2}$ used in this experimental work is $5.26\times10^{-39}Cm^2/V$ [66, 67, 68]. For the sake of completeness, let us note that in addition to the electric dipole force, there is a light shift contribution from the magnetic dipole interaction with the ground state hyperfine levels. This shift is a factor

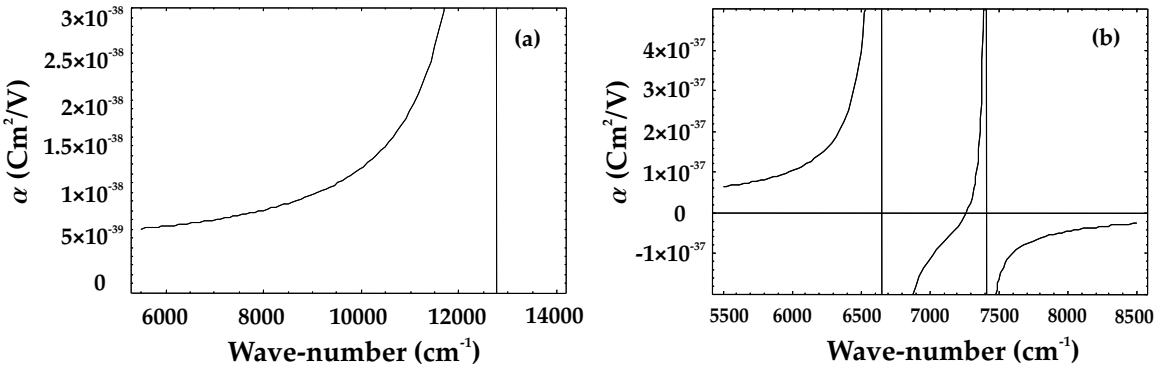

Figure 2.3: Rubidium dynamic polarizability. (a) Ground state dynamic polarizability. At CO_2-laser frequency, the dynamic polarizability approximately equals the static values. (b) Dynamic polarizability of the first electronic excited state $5P$.

$2\mu_{Bohr}^2/(\hbar\alpha_S\omega_L)$ smaller than the Stark-shift [69]. In the case of ^{87}Rb atoms this factor is of the order of 10^{-8}.

One advantage of such quasistatic dipole traps, is the possibility to realize a state-independent confinement. For example as it is shown in Fig. 2.3, the static atomic polarizability of rubidium atoms is positive both for the ground- and the excited states $5S$ and $5P$, respectively, in contrast to near-resonant dipole traps, for which the excited states are antitrapping (when $\Delta < 0$). This applies also to other alkali atoms. Moreover, because the laser wavelength is 10.6 µm, fine and hyperfine structures are not resolved. As result, all hyperfine components of the ground state $5S_{1/2}$ and excited states $5P_{1/2}$ and $5P_{3/2}$ are trapped.

The photon scattering rate is estimate in this way. For a multi-level atom, the total scattering rate is composed by two terms: $\Gamma_{sc} = \Gamma_{Rayleigh} + \Gamma_{Raman}$. The first one is the contribution of the Rayleigh scattering describing an elastic process, the latter term is the Raman scattering, which leaves the atom in a different hyperfine or Zeeman sublevels *i.e*. initial and final states are different [70]. The Rayleigh scattering is given by the usual formula

$$\Gamma_{Rayleigh} = \frac{8\pi r_0^2 I\omega_L^3}{3\hbar}\left[\sum_e \frac{f_{eg}}{\omega_{eg}^2}\right]^2, \tag{2.21}$$

where r_0 is the classical electron radius. At the CO_2-laser radiation ($\omega_L \simeq \omega_1/10$) this formula is almost exact. At laser frequency $\omega_L \simeq \omega_1/2$ the Rayleigh scattering is within 70% exact. In particular, for alkali atoms, the ratio between the Raman and Rayleigh scattering, e. g., at frequency $\omega_L \simeq \omega_1/2$ is approximately given by

$$\frac{\Gamma_{Raman}}{\Gamma_{Rayleigh}} \approx \frac{8}{9}\left[\frac{\Delta'_{FS}\omega_L}{\omega_1^2}\right]^2. \tag{2.22}$$

In the case of CO_2-laser radiation this ratio is negligible.

If a gaussian laser beam is used for trapping atoms (laser intensity $I = 2P/(\pi w_0^2)$ with P the laser power), then the Rayleigh photon scattering rate reads

$$\Gamma_{Rayleigh} = \frac{16 r_0^2 P}{3\hbar w_0^2} \left(\frac{m_e \alpha_S}{e^2}\right)^2 \omega_L^3, \tag{2.23}$$

where w_0 is the beam waist of the gaussian beam. Typical values of this photon scattering rate in our experiments with ^{87}Rb are 1 photon scattered every 10 minutes. This results in a realization of a conservative trap, where decoherence caused by absorption of laser photons is highly suppressed.

2.4 Dipole trapping geometries

In the experiments carried out in this work, Bose-Einstein condensation is reached by "all-optical methods" in CO_2-laser optical dipole traps. Two laser beam geometries have been realized for this purpose: a single running wave tightly focussed optical dipole trap, and a crossed beams configuration. In Fig. 2.4 is presented a scheme of the two CO_2-laser beam geometries. The laser wavelength of the trapping radiation in our experiment is

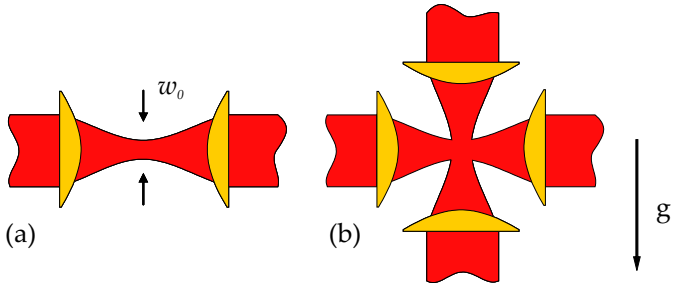

Figure 2.4: Scheme of two CO_2-laser optical dipole traps. (a) Single running wave configuration. Inside a UHV chamber a couple of ZnSe lenses tightly focuses a laser beam down to a beam waist w_0. Atoms are trapped in the focus of the laser beam. (b) Crossed beams geometry. Two tightly focussed CO_2-laser beams intersect each other in the beam waist plane. The overlapping zone defines the trap.

near 10.6 µm, and the ratio between the laser frequency and the frequency of the doublet $D1 - D2$ (of ^{87}Rb) is $\lesssim 1/10$. The approximation of quasi-electrostatic trap applies here, see equation (2.20). Moreover, because the laser detuning is negative, the dipole force attracts the cold rubidium atoms towards the maxima of the laser light field.

In the experiments with a single running wave geometry, the optical dipole trap has been realized by focussing a gaussian laser beam. The CO_2-laser beam travels inside an

ultra high vacuum chamber along the z axis, which is perpendicular to the gravity axis (x axis). According to the equation (2.20), the optical potential realized by a single tightly focussed gaussian beam is

$$V_{dip} = -V_{depth} \frac{1}{\left[1 + \left(z/z_0\right)^2\right]} exp\left(-2\frac{r^2}{w_0^2} \frac{1}{1 + (z/z_0)^2} \right), \tag{2.24}$$

where $z_0 = \pi w_0^2/\lambda$ is the Rayleigh length, w_0 is the beam waist of the gaussian beam, and $r^2 = x^2 + y^2$ [71]. The quantity $V_{depth} = \alpha_s P/(\pi\epsilon_0 c w_0^2)$ is the potential depth at the focus (in $r = 0$ and $z = 0$). In Fig. 4.9 a numerical simulation of a single optical dipole trap is shown. The inferred potential depth for an optical power of 28 W and a beam waist of 27 µm is about 1.4 mK. The available laser power sets the maximum temperature of the trapped cold atomic ensemble, for a fixed laser beam waist.

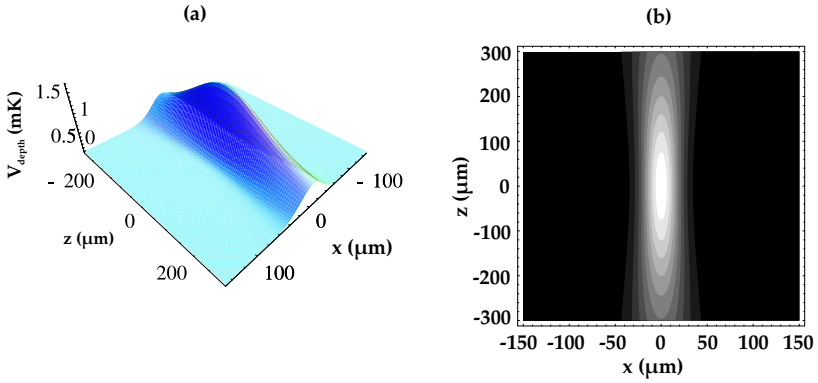

Figure 2.5: Single optical dipole trap. The optical power is 28 W and the beam waist is 27 µm. (a) 3D view (xz-plane view) of a focussed gaussian beam realizing a single running wave optical dipole trap. The vertical scale gives the potential depth in mK. (b) Contour plot of the laser beam intensity(xz-plane view). The brighter areas correspond to higher intensity values.

The analytical expression for the optical potential of a crossed dipole trap is somewhat more complicated in the case of two generic laser beams, with different polarizations ϵ_1 and ϵ_2, different k-vectors k_1 and k_2, and with frequencies ω_{L_1} and ω_{L_2} intersecting at an arbitrary angle ϕ. However, in the realized experimental setup two linearly polarized CO_2-laser beams, separated 40 MHz in frequency, crossing each other at 90 degree, are employed. The frequency separation allows one to neglect any contribution to the optical potential arising from interference of the two laser beams. In this case, the total dipole potential is given by the sum of the two independent dipole potentials.

Let $\{O, x, y, z\}$ be a cartesian reference system, oriented in such a way that one beam propagates along z and the other one along x and with the origin in the intersection point

(at this point the two beams are focussed to beam waists w_{01} and w_{02}, respectively). The total dipole potential reads:

$$V_{cross} = -V^1_{depth}\frac{1}{\left[1+\left(z/z_0\right)^2\right]}exp\left(-2\frac{x^2+y^2}{w^2_{01}}\frac{1}{1+(z/z_0)^2}\right)$$
$$-V^2_{depth}\frac{1}{\left[1+\left(x/x_0\right)^2\right]}exp\left(-2\frac{y^2+z^2}{w^2_{02}}\frac{1}{1+(x/x_0)^2}\right). \quad (2.25)$$

The potential depth of the crossed trap is the sum of the two individual ones:

$$V_{depth} = -\frac{\alpha_S P_1}{\pi c \epsilon_0 w^2_{01}} - \frac{\alpha_S P_2}{\pi c \epsilon_0 w^2_{02}} \quad (2.26)$$

where $P_1$and P_2 are the laser powers.

In the experiment presented in this work, the optical power in each beam has been chosen to be nearly the same. In general, one has to add also the gravitational potential energy mgx which the trapped atoms posses. However, in many experiments the optical confinement is stronger than the gravity, and it is possible to neglect this additional force. This issue will be discussed later in the context of the realization of a novel type of atom laser. In Fig. 2.6 a numerical simulation of a CO_2-laser optical dipole trap in the crossed geometry is represented. The optical power is 12 W, and each beam waist is 35 µm. It is clear that with respect to a single beam geometry, a crossed beams configuration offers a stronger spatial confinement, although the potential depth is the same in both cases.

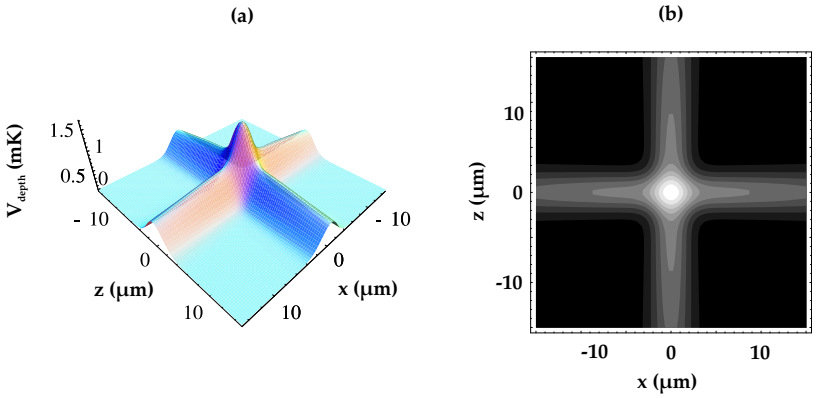

Figure 2.6: Crossed optical dipole trap. Both beams have the same optical power (12 W) and the same beam waist (35 µm), which reproduce the experimental features of the real trap. (a) 3D view (xz-plane view). The vertical scale gives the potential depth in mK. (b) Contour plot of the laser beam intensity(xz-plane view). The brighter areas correspond to higher intensity values.

The motion of ultracold atoms in the optical dipole traps, can be well approximated by an harmonic oscillator. Since the optical potential has a minimum in the laser beam focus region, it is possible to expand the confining optical potential to the second order in the coordinates. The hamiltonian of the center of mass of a trapped atom is given by:

$$H = \frac{1}{2m}\sum_{i}^{3} p_i^2 + \frac{1}{2}\sum_{i}^{3} k_i x_i^2 \tag{2.27}$$

where p_i is the momentum conjugated to x_i, and k_i are the spring constants derived by a diagonalisation of the $\partial^2 V_{dip}/\partial x_i \partial x_j\big|_0$ matrix of the second derivatives of the optical potential V_{dip}.
For a single CO_2-laser beam dipole trap, the vibrational frequencies are:

$$\begin{aligned} \nu_r &= \frac{1}{2\pi}\sqrt{\frac{4\alpha_S P}{\pi c \epsilon_0 m w_0^4}} \\ \nu_z &= \frac{1}{2\pi}\sqrt{\frac{2\alpha_S P \lambda_L^2}{\pi^3 c \epsilon_0 m w_0^6}} \end{aligned} \tag{2.28}$$

where ν_r is the vibrational frequency in the transversal x,y plane and ν_z in the longitudinal direction, i.e. along the laser beam propagation axis. Typical experimental values in our experiment are $\nu_r = 4.8\,\text{kHz}$ and $\nu_z = 350\,\text{Hz}$, for a laser power of 28 W and a beam waist of $w_0 = 27\,\mu\text{m}$. The trap has a cigar shape geometry. The tightly confining plane is the xy-plane.

Instead, for a crossed dipole trap with beams crossing at a 90 degree angle, one can expect that all vibrational frequencies are of the same order of magnitude:

$$\begin{aligned} \nu_x &= \frac{1}{2\pi}\left(\frac{4\alpha_S}{\pi c \epsilon_0 m}\right)^{1/2}\left(\frac{P_1}{w_{01}^4} + \frac{P_2 \lambda_L^2}{2\pi^2 w_{02}^6}\right)^{1/2} \\ \nu_y &= \frac{1}{2\pi}\left(\frac{4\alpha_S}{\pi c \epsilon_0 m}\right)^{1/2}\left(\frac{P_1}{w_{01}^4} + \frac{P_2}{w_{02}^4}\right)^{1/2} \\ \nu_z &= \frac{1}{2\pi}\left(\frac{4\alpha_S}{\pi c \epsilon_0 m}\right)^{1/2}\left(\frac{P_1 \lambda_L^2}{2\pi^2 w_{01}^6} + \frac{P_2}{w_{02}^4}\right)^{1/2} \end{aligned} \tag{2.29}$$

With a typical CO_2-laser power of 12 W in each beam and typical beam waists $w_{01} = w_{02} = 35\mu\text{m}$, the trap frequencies are near 1.7 kHz in all three directions.

In the next chapter, we will describe the experimental setup constructed within this work for the realization and the characterization of such optical dipole traps for ultracold rubidium atoms.

Chapter 3

Experimental apparatus

For this experimental work, a complete new experimental setup has been built. The used experimental setup allows for a direct condensation of ^{87}Rb atoms in purely optical dipole traps. In order to reach the quantum degenerate regime in dilute alkali gases, laser cooling and atom trapping techniques have been implemented. Such techniques required reliable laser sources, with tunable radiation and frequency stabilization against frequency fluctuations. For the formation of a Bose-Einstein condensate is mandatory to reduce three body collisions. This condition is met in dilute atomic gases. Diluteness is reached when bosonic gases are trapped in conservative traps (optical traps and magneto-optical traps) in conditions of ultra-high vacuum (UHV).

A vacuum system which guarantees a pressure of the background gases of 1×10^{-10}mbar has been assembled. One of the characteristics of this system is the possibility to have good optical access for realizing and optically resolving 1D and 2D mesoscopic optical lattices.

After the description of the vacuum system, the diode laser sources for the preparation of the cold atomic ensemble are presented. Bose-Einstein condensation is reached by evaporatively cool ultracold ^{87}Rb atoms in a CO_2-laser optical dipole trap. This cooling technique is accomplished by lowering the purely optical confining potential over time: a suitable control of the optical confining power is required. The employed optics for the pure optical dipole trapping of atoms are presented. This optical system has been optimized for the realization of both a single single beam dipole trap and a crossed beams dipole trap, employing radiation derived from a commercial CO_2-laser. Finally, the absorption imaging system, which permits to analyze the trapped quantum degenerate atomic cloud at the end of an experimental run, is presented.

3.1 Vacuum system

The vacuum system permits to reach a pressure of the background gas of roughly 1×10^{-10}mbar. Such a low value is mandatory to achieve sufficiently long trap lifetimes, which permit to employ more effective evaporative cooling techniques on longer time scales. The vacuum system is made out of steel. It is composed by two parts: a main vacuum chamber, in which experiments on ultracold atoms are performed, and a vacuum pump body, where the vacuum pumps are installed. The main vacuum can has a spherical form with an average diameter of 162 mm, as Fig. 3.1 shows. The pump system body has

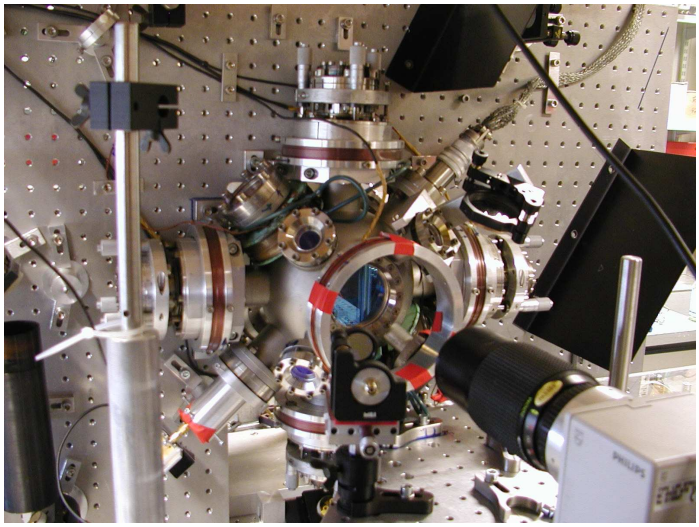

Figure 3.1: Front view of the vacuum chamber.

a cylindric form (with a diameter of 11 cm and a height of 18 cm), and presents a big optical window. This window is used for coupling a near-resonant laser beam employed for absorption imaging technique. This vacuum pump body is attached to the main vacuum can through a CF63 flange. In Fig. 3.2 the rear part of the vacuum system is shown. An ion pump (VTS, 25l/s) is attached to the vacuum pump can, through a UHV-valve, and allows to reach background pressure of 5×10^{-9}mbar. This ion pump is always on and it is placed ~ 50 cm away from the center of the main vacuum chamber. Moreover, in the vacuum pump body, a titan-sublimation pump and a pressure gauge (Ionivac) are installed. The Ti:sublimation pump is activated regularly once in two-three weeks, to maintain the desired background pressure of 1×10^{-10} mbar.

This main chamber has several windows for the optical access of resonant light and mid-infrared light. The designed vacuum system allows for a realization of different optical dipole trap geometries, and in particular it permits to realize and optically resolve mesoscopic 1D and 2D optical lattices [72]. For all these purposes, a total of 16 flanges are

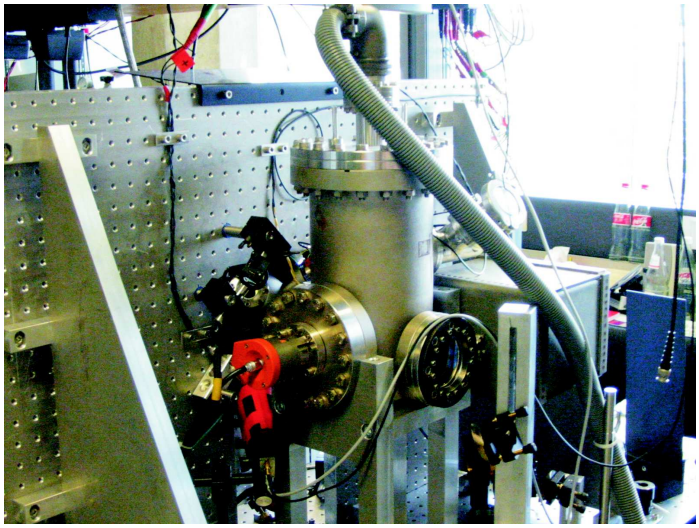

Figure 3.2: Pump system body

present on the main vacuum chamber. There are eight standard flanges (CF38). In particular, four of them mount ZnSe windows for coupling in and out the vacuum chamber CO_2-laser light. Other three standard flanges mount quartz plates. Two of these are used for the optical access of the MOT beams propagating along the axis of the MOT magnetic coils, and the third one for the detection of fluorescence light from the trapped atoms, using a calibrated photodiode. The last standard flange is used for the rubidium getters. The remaining eight flanges require non standard mountings and are used as optical ports. Their inner diameter is of 20 mm. These flanges present quartz windows for coupling near resonant laser light. These windows are attached to the flanges by using Helicoflex elements (type HNV 200 Al, from Cefilac).

Moreover, the main vacuum can has one big optical windows, mounted on standard CF63 flanges, as displayed in Figs. 3.1. The imaging system (lenses plus CCD camera) is placed in front of this big window. This window is 66 mm away from the center of the main vacuum chamber, and allows for a solid angle of approximately 57.4 degree. This angle is suitable for high resolution imaging of 1D and 2D mesoscopic optical lattices.

The alkali atom source consists of three metal filaments (model RbNS 34/12FT, by SAES Getters S.p.A.), enriched with RbCr, which release rubidium atoms when current flows through them. These rubidium dispensers are mounted in the main vacuum chamber at a distance of 3 cm away from the center of the chamber. Typical values of the heating current are $2.7 - 3$ A.

3.2 MOT system

To date, magneto-optical traps (MOT) represent a workhorse for the production of ultracold atoms in quantum optics experiments. Atoms in a MOT experience a dissipative force, which depends on the atomic velocity, and an optical restoring force because of the presence of an external inhomogeneous magnetic field. The dissipative force allows to reach atomic velocities corresponding to an atomic temperature on the order of 10 µK. The position dependent force is realized, when a radial quadrupole magnetic field is employed in conjunction with three pairs of counterpropagating laser beams with oppositely circular polarizations $\sigma^{\pm}$ travelling along the three axes of a cartesian reference frame [73]. The laser beams are detuned few MHz to the red side of a strong atomic resonance. They intersect each other in the zero of the quadrupole magnetic field.

In Fig. 3.3 the scheme of the realized MOT. The MOT coils are oriented at an 45° angle with respect to the propagation axes of the CO_2-laser beams.

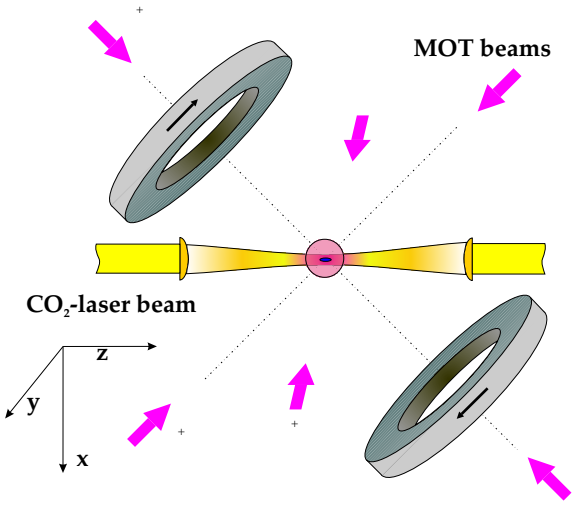

Figure 3.3: Scheme of the realized MOT and optical dipole trap. Three $\sigma^{\pm}$ pairs of counterpropagating laser beam intersect in the center of the vacuum chamber, at the zero of a magnetic quadrupole field. The magnetic coils are placed outside the vacuum chamber. The CO_2-laser optical dipole trap is overlapped with the MOT.

For a MOT with ^{87}Rb atoms, two laser sources are needed: a "cooling" laser, whose frequency is red detuned with respect to the hyperfine transition $|5S_{1/2}, F = 2\rangle \rightarrow |5P_{3/2}, F' = 3\rangle$, and a"repumping" laser whose frequency radiation is resonant with the hyperfine transition $|5S_{1/2}, F = 1\rangle \rightarrow |5P_{3/2}, F' = 2\rangle$. The repumping laser is necessary to "close"the cooling transition. The existence of off-resonant excitations drive populations into $|F' = 2\rangle$, from which atoms decay into the $|F = 1\rangle$ state. Atoms in this level need to be repumped into the cooling cycle.

3.2.1 Cooling laser

The laser light, tuned near the cooling transition, is provided by a grating stabilized diode laser system (master laser), whose radiation is amplified by a second, high power diode laser (slave laser). The corresponding optical scheme is shown in the lower half of Fig. 3.4. The lasers is controllable in frequency and stabilized against frequency fluctuations. The external cavity reduces the spectral width of the emitted radiation, and the grating permits a selection of the radiation wavelength. The mechanical setup of these laser diodes is temperature stabilized. These laser sources are frequency stabilized by employing electronic servo loops, which stabilize their feed current.

The master laser has an extended cavity in Littrow configuration [74] (diode laser Hitachi 7851G, with nominal power of 50 mW). This light passes an optical isolator (Gsänger 60 dB), with a transmission efficiency of 85 %. After this isolator, almost 1 mW of the master's light is used for the injection technique. Nearly 2 mW of this light is sent to a saturation spectroscopy line, which gives a reference signal for a rough alignment of the resonance. The rest of the master laser light is used for the frequency stabilization. For splitting this laser light combinations of $\lambda/2$ wave-plates ($\lambda/2$ plates) and cube polarizer beam splitters (PCB) are used.

The slave laser (diode CW-C1-780.015S-PD, SLI, with nominal power of 150 mW) is a free-running wave diode laser, and it is injected by the master light derived by the first pair $\lambda/2$ plate PCB. The light from the slave laser, passes an optical isolator (Gsänger 60 dB), with a transmission efficiency of 90%, and then afterwards also an acousto-optic modulator (IntraAction, with operative frequency of 40 MHz). The first diffraction order from this AOM is used for the MOT. In order to increase the efficiency of the first order diffracted light (up to values of 80 %), the diameter of the laser beam is reduced to less than 1 mm. After the AOM, the light form the first order of diffraction is divided in two. A beam with few hundreds of microwatts is coupled into a single mode optical fiber, and sent to the vacuum chamber for imaging diagnostic. The other beam is spatially filtered by a 50 µm pin-hole, and then expanded by a telescope to a beam diameter of 2 cm (the lenses of this telescope have focal lengths $f_1 = 50$ mm and $f_2 = 700$ mm). The optical power after the pin-hole is 45 mW, see Fig. 3.4. Additional optical elements are used for dividing the beams in three and to give the correct polarizations $\sigma^{\pm}$, to realize a 3-beams MOT.

3.2.2 Repumping laser

The repumping light is delivered by another laser source, see the upper half of Fig. 3.4. This is a grating stabilized diode laser (Sanyo DL7140-201, with nominal power of 70 mW). An optical isolator (Gsänger 60 dB) prevents retro-reflection of light into the laser cavity. The transmission from this isolator is 85 %. The optical power after this optical isolator is 20 mW. About 2 mW of this light is sent to a spectroscopy line for a frequency stabilization. The remaining light is split again. Nearly 3 mW of this repumping light is sent to a frequency offset locking system. The remaining light travels through an acousto-optic modulator (IntraAction, with operative frequency of 80 MHz). The light in the first

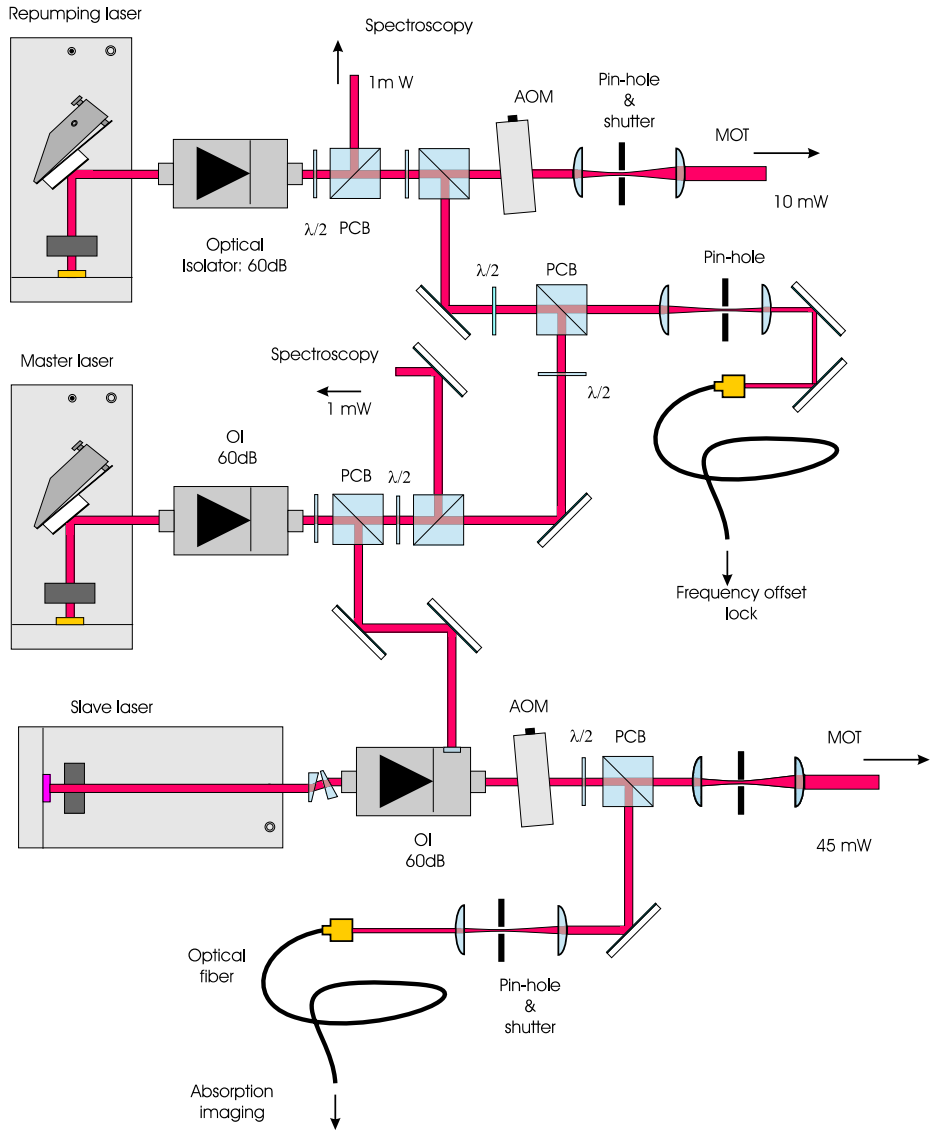

Figure 3.4: Scheme of the MOT laser system. OI: optical isolator; PCB: polarizer cube beam-splitter

diffraction order is almost 90 %. This light is spatially filtered by a 50 µm pin-hole and then expanded by a telescope to a beam diameter of nearly 2 cm. The optical power after the pin-hole is 10 mW. The beam is spatially overlapped with the cooling laser radiation, and then sent to the vacuum chamber for realizing the MOT.

3.2.3 Frequency Offset Lock

For the frequency stabilization of the cooling laser source, a novel lock scheme has been developed [75]. Light from the cooling laser is superimposed to that of the repumping laser (which acts as a reference oscillator) on a fast photodiode. The beat signal between the two laser frequency (about 6.8 GHz), is mixed with a microwave reference signal, derived from a frequency synthesizer. Let us remember that the difference in frequency between the two lasers nearly equals the hyperfine splitting of the ground state $5S_{1/2}$. After the mixing, the signal is split in two. One part is sent to a spectrum analyzer (for monitoring the mixed down signal) and the other part to an error-signal-circuit (ESC). The output of this ESC is an error signal which is sent to an electronic servo loop. The main advantages of this new lock technique is to have a steep slope of the signal error and to change in few hundreds of microsecond the lock point frequency, by varying the frequency of the microwave local oscillator. The capture range is of several hundreds MHz. This allows for a fast frequency detuning of the cooling laser source in the different phases of the experiment (MOT-phase, dark-MOT phase and detection).

3.2.4 MOT magnetic field coils

To generate a quadrupole magnetic field, a pair of coils, in anti-Helmholtz configuration, (each of them has 300 copper wire windings) is used. These coils are centered on two CF38 flanges and their axis is at 45 degree with respect to the horizontal and vertical CO_2-laser beam directions. Moreover, they have the middle point 91.5 mm far away from the center of the vacuum chamber. Their mean diameter is 33 mm. The value of the gradient field used in the experiment for MOT and dark-MOT phase is nearly 10 Gauss/cm, relatively to a current $I = 4.5$ A. In order to produce a magnetic field offset, three pairs of Helmholtz coils (about 30 copper wire windings each) are used. These compensation coils have a mean diameter of 15 cm. Two pairs have as axes the horizontal and vertical axes of the vacuum chamber(namely the CO_2-laser beam axes). The axes of the third pair is perpendicular to the plane individuated by the two CO_2laser beams.

3.3 Dipole trapping laser optics

After collecting a cold atomic cloud of ^{87}RB atoms in the MOT, these atoms are transferred to a quasistatic dipole trap. The dipole trapping radiation is derived from a commercial, RF-excited CO_2-laser (GEM-50S Coherent-Laser). The maximum optical power is 54 W for $\lambda = 10.6$ µm. A tunable grating is mounted inside the laser cavity for adjusting the laser wavelength within the range $(9.3 - 10.6)$ µm. The free spectral range, defined as

$\nu_{FRS} = c/(2L)$, is 111 MHz, where L is the laser cavity length (135 cm). The used laser model has a piezoelectric actuator which allows to change the length of the laser cavity in a range $15 - 25\,\mu$m. In the setting up of the laser system, the single frequency operation of the CO_2-laser has been checked. This task has been accomplished by using a Fabry-Perot interferometer, with a free spectral range of ~ 300 MHz.

The scheme of the CO_2-laser optics is shown in Fig. 3.5. The mid-infrared light emitted by the laser passes an acousto-optical modulator (Weiss & Schulz, with RF drive frequency of 40.68 MHz, and RF power of 60 W), which is used to control the optical power during the experiment and to allow for an optical isolation of the laser. Almost 60% of the incoming light is transferred into the first diffraction order, which is used for trapping the rubidium atoms. After this AOM (master AOM) the mid-infrared light passes a 2.5 : 1 telescope, formed by ZnSe lenses (L1 and L2, with focal length $f_1 \simeq 10$ cm and $f_2 = 3.8$ cm, from Coherent). After the telescope, the mid-infrared laser light passes a second AOM. This AOM has a function of a beam divider, and it is used only in the experiments carried out with CO_2-laser crossed dipole traps. Note that the zero's and first order diffracted beams differ in frequency, which eliminates unwanted standing-wave effects. By controlling the RF drive radiation, it is possible to balance the optical power in each diffracted beam. In general, a ratio of 50% is chosen. For experiments with a single running wave CO_2laser optical dipole trap, this AOM beam divider is omitted and the mid-infrared laser beam is directed to the vacuum chamber directly after the telescope.

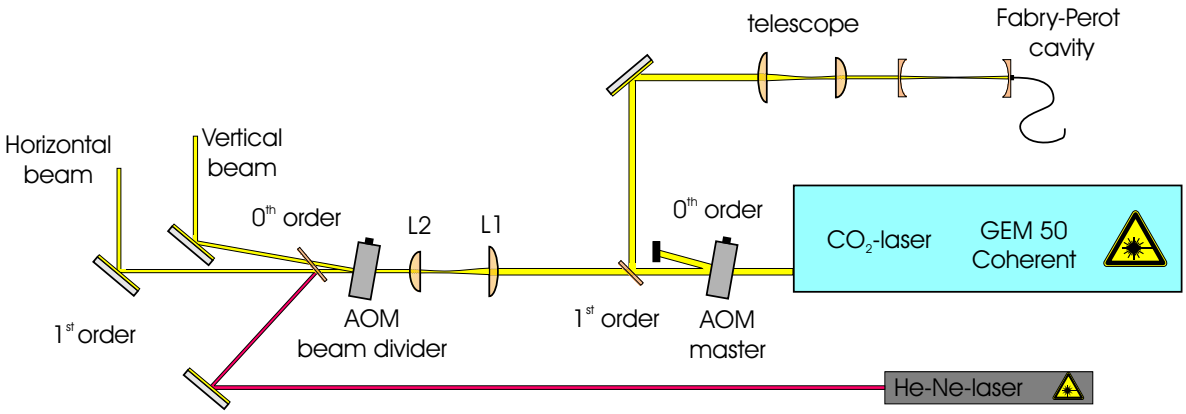

Figure 3.5: Scheme of CO_2-laser optics. Mid-infrared laser light is derived from a commercial RF-excited CO_2-laser. The optical power is controlled by using the first AOM (master AOM). The beam waist is adjusted by acting on a telescope L1-L2. For crossed trap geometries, a second RF-driven AOM is used. A visible He-Ne laser is employed to get a rough alignment of the invisible CO_2-laser beams.

For a rough alignment of the CO_2-laser beams, a visible guiding laser beam is used. This guiding light is derived from a He-Ne laser (wavelength $\lambda = 632$ nm) and is spatially

overlapped with the mid-infrared light using a beam-combiner (P/N 033-084-01, Coherent) placed after the beam divider AOM, as shown in Fig.3.5. After the beam divider, the CO_2-laser beams are stirred using gold mirrors, and they enter the vacuum chamber through ZnSe windows. The CO_2-laser radiation propagates through the vacuum chamber along two perpendicular axes: the horizontal axis z and the vertical axis x of the vacuum chamber (x is gravity axis). In particular, for the horizontal beam the first diffraction order is employed. Inside the vacuum chamber, correspondingly to the CO_2-laser axes, are placed spherical corrected ZnSe lenses in order to focus the mid-infrared radiation beams down to a minimum beam waist of 20 µm. These diffraction limited lenses (Coherent, $f = 38$ mm) are installed in 20 cm long steel holders. Micrometers screws allow one to move and to translate these holders [76].

The size of the CO_2-laser beam waist is adjusted by acting on the external telescope. For the crossed trap geometry, a beam waist of 35 µm is chosen, whereas for a single running wave geometry a beam size of 27 µm in the trapping region is used.

In optical dipole traps, evaporative cooling proceeds by reducing the optical potential depth with time. In the experiments presented here, this task is performed by decreasing the RF drive power supplied to the first AOM (master AOM) with time. The AOM RF-drivers have a both a digital and analog input. The digital input is used for switching on and off the RF, while the latter one is used for controlling the RF drive power level. The switching time of the RF drive power is less than 1 µs. By regulating the analog voltage, the RF drive power is controlled. The digital level for operation is 1.5 V. The analog input has been varied from a maximum of 10 V to a minimum of -3 V. The values for the beam divider AOM are 1.5 V for the digital input, and 3.3 V for the analog input.

3.4 Absorption imaging technique

The knowledge of the properties of Bose-Einstein condensates and in general of ultracold atoms (such as the number of trapped atoms, the atomic temperature and the atomic density as well) is inferred from the analysis of time of flight images (TOF). In particular, in this thesis absorption imaging technique is employed. This is a suitable technique for optically dense atomic cloud, as for example an atomic Bose-Einstein condensate. The method is destructive, since it is based on the absorption of resonant photons and subsequent incoherent emission of them. A collimated spatially filtered laser beam irradiates the ultracold atoms during their ballistic fall, after having switched off the CO_2-laser optical dipole traps. Shadows of atomic clouds are imaged onto a CCD camera, as shown in Fig. 3.6.

When laser light propagates through a medium, atoms in general absorb and phase shift this light [70]. In the performed experiments, since resonant light is employed, only absorption occurs [1].

Let y be the direction of propagation of a collimated, linearly polarized laser light beam. If I_0 is the laser intensity before the interaction with the atomic cloud, then the transmitted

[1] Other imaging techniques rely on phase shift effects such as phase contrast imaging, where off-resonant laser light is used.

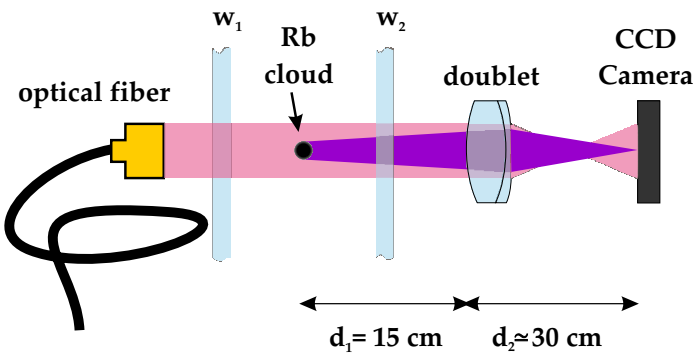

Figure 3.6: Scheme of the setup for optical absorption imaging. A resonant beam excite atoms, which absorbs photons from this beam. A shadow of the atomic cloud is imaged onto a CCD camera, by employing a doublet lens. w_1 and w_2 are the two big windows in the experimental setup.

laser intensity I after the interaction is

$$I = I_0 e^{\sigma_\pi \int n(x,y,z)dy} \tag{3.1}$$

where $n(x,y,z)$ is the atomic density and σ_π the photon cross section for linearly polarized light, given by the following equation

$$\sigma_\pi = \frac{7}{15}\frac{3\lambda^2}{2\pi}\frac{1}{1+\left(\frac{2\Delta}{\Gamma}\right)^2} \tag{3.2}$$

Let us note that these two equations are valid in regime of negligible saturation. Integrating the equation (3.1) along the interaction direction y, it is possible to extract information about the atomic density distribution in the imaging plane (x,z):

$$\frac{1}{\sigma_\pi}D(x,z) = \int n(x,y,z)dy = -\frac{1}{\sigma_\pi}\ln\frac{I(x,z)}{I_0(x,z)} \tag{3.3}$$

From this last relation, it is clear that the knowledge of $I(x,z)$ and $I_0(x,z)$ allows one to extract information on the atomic density.

The light for the absorption imaging of cold atoms is derived from the cooling laser source, as it is shown in Fig. 3.4. During the detection phase, the laser frequency is tuned exactly into resonance with respect to the $|5S_{1/2}, F = 2\rangle \rightarrow |5P_{3/2}, F' = 3\rangle$ optical transition. After the cooling laser AOM, part of the first order diffracted light is split by using a pair $\lambda/2$ plate cube polarizer beam splitter. By controlling the RF-power of the laser cooling AOM, it is possible to reduce in 1 µs the amount or resonant light to values of 20 nW. In order to completely extinguish this resonant light, a mechanical shutter is used (closing time $\sim$ 400 µs). This shutter is open only during the detection time, namely for less then

100 ms. The probing beam dimensions are reduced by using a 2:1 telescope (see Fig. 3.4). This collimated beam is injected into a single mode optical fiber (Schäfter+Kirchhoff, PMC-850-5,5-NA011-3-APC-300P, and 60SMS-1-4-A8-02 for the coupling optics), and then sent to the vacuum chamber. This probing beam enters the vacuum chamber from the back side (from the big window present in the pump body), and travels inside the vacuum chamber along the y direction. A small angle with this axis minimizes interference patterns due to multiple reflections on the windows.

The laser beam diameter after the optical fiber is 8 mm. The light intensity at this point is about $150\,\mu W/cm^2$. This value is well below the D2-line saturation intensity $I_s = 1.16\,mW/cm^2$, and relations (3.1) and (3.2) hold. The probing light pulses are 80 µs long. This allows to detect atomic density distribution with a reduced blurring effect. Indeed, it is possible to show, see [11], that if in a time Δt an atom scatters N_p photons, it acquires a random velocity $v_{rms} = \sqrt{N_p} v_{rec}$, which leads to a random position $r_{rms} = (\sqrt{N_p/3}) v_{rec} \Delta t$, where v_{rec} is the recoil velocity. Here, the number of scattered photons is about 60, and this leads to a random position of 2 µm.

The images of the shadow of the atomic cloud is created onto a slow-scan CCD camera (Sony XC-55 progressive, 659×494 pixels with a cell size of 7.4 µm), placed outside the vacuum chamber. A spherically corrected doublet lens (Melles Griot, $f = 145$ mm) is used to provide a magnification of nearly 2.6.

All physical information necessary to study the ultracold atomic clouds is embedded in the atomic density distribution given in equation (3.3). Our aim is to extract $D(x,z)$ from the recorded shadow images. For this purpose, three images are taken. An image is taken with atomic cloud present is recorded. The image onto the CCD camera is denoted by $I_{exp}(x,z)$. Soon after, a second image is taken without atoms, in order to have only the laser intensity distribution $I_{0,exp}(x,z)$. Afterwards, a third image is taken without probing beam and without atomic cloud, to have a background offset $I_{bg}(x,z)$. All these images are taken with the same exposure time.

If we account for the camera background, we can determine the ratio $I(x,z)/I_0(x,z)$ in equation (3.3) from our experimental data using the formula:

$$\frac{I_{exp}(x,z) - I_{bg}(x,z)}{I_{0,exp}(x,z) - I_{bg}(x,z)}. \tag{3.4}$$

The systematics errors, due to laser time intensity drift are minimized by repeating this procedure at the end of each experimental cycle. The discussion of the image analysis of the thermal and Bose condensed clouds is exposed in Appendix A.

3.5 Experiment control

For a successful operation of the experiment, various laser beams must be switched on and off during the experimental cycle following an exact temporal sequence. Moreover, the laser frequency of the cooling laser must be tuned during the several experimental phases,

with precision of tenths of microseconds. All these tasks are accomplished by using a "real time" system control device.

The used device is an AD-Win System from Keithley, and it has a CPU unit (SHARC-DSP ADSP21062 with a clock of 40 MHz, and local memory of 256 kByte, and a RAM memory of 16 MByte). The system is modular, with analog and digital cards. The digital input-output (I/O) module has 32 channels. In the experiments this module is programmed to have TTL-logic pulses for controlling the opening and closing times of mechanical shutters employed for each laser light beam, as well as to initialize digital oscilloscopes to trigger the CCD camera, and to switch on and off all the magnetic fields. Moreover, electronic switches for controlling the starting time of external function generators is activated by TTL pulses from the I/O module as well. Besides, an analog module with eight channels is used. Each analog channel supplies a signal in the voltage range between ± 10 V, with a maximum output current of 5 mA, through an 16Bit D/A converter. Analog output signals are employed to control the analog inputs of each AOM RF-driver in the experiment (for the cooling laser, the repumping laser and the CO_2-laser), in order to have the desired laser light power during each experimental phase, as described in detail in [76].

Chapter 4

Bose-Einstein condensation in optical dipole traps

In the past years, several laser cooling techniques have been developed in order to reach the critical temperature for the onset of the quantum degeneracy in optical dipole traps [77, 78, 79, 80, 81, 82, 83]. However, absorption effects, heating and trap losses due to excited-state collisions are the main roadblocks to Bose-Einstein condensation by using laser cooling techniques alone. To date, these limitations have been circumvented by forced evaporation of the trapped atoms.

In this chapter, experiments on direct Bose-Einstein condensation (all-optical BEC) of rubidium atoms in CO_2-laser optical dipole traps are presented. The quantum degenerate regime has been reached via a forced evaporative cooling of atoms both in a single running wave beam dipole trap and in a crossed beams dipole trap. Particularly interesting is the possibility to achieve all-optical BEC in the single beam dipole trap. This undoubtedly represents an experimental simplification towards the achievement of the quantum degenerate regime.

The preparation of the cold thermal cloud of rubidium atoms in the magneto-optical trap (MOT) is the same for both geometries and it will be presented at the beginning of this chapter. Afterwards, the initial experiments on all-optical BEC in CO_2-laser crossed dipole traps will be shown. From these first experiments we gained insight in the evaporative cooling process to resort to a single beam CO_2-laser dipole trap in a later stage of the experimental work. Optimization of the initial trapping conditions (as the atomic temperature and atomic density) is discussed for both geometries. Subsequently, all-optical BEC in a tightly focussed CO_2-laser dipole trap is presented.

As conclusion of this chapter, a novel technique for generating magnetic-field insensitive Bose-Einstein condensates ($m_F = 0$ Bose condensates) is described. This procedure suppresses fluctuations of the chemical potential from stray magnetic fields. Such a magnetic field insensitive Bose condensate is of interest in the context of atom interferometry, atom lasers and precision atomic clocks. This $m_F = 0$ Bose condensate constituted the source of coherent matter for the generation of an all-optical atom laser.

4.1 Precooling and collection of alkali atoms

The starting point of the described experiments on ultracold rubidium atoms (^{87}Rb isotope) is the realization of a MOT. In the previous chapter, the main requirements for the realization of such a trap have been outlined.

In our experiments, rubidium atoms are collected into the MOT from the thermal background gas emitted by rubidium alkali dispensers. The duration of the MOT phase has been chosen in order to maximize the number of the trapped atoms into the CO_2-laser optical dipole traps. Since two types of dipole trapping geometries are implemented, the duration of the MOT phase is different for the two geometries. In particular, a 5 s long MOT phase is used in experiments with a crossed beams geometry, whereas a 30 s long phase in experiments with a single running wave dipole trap. In both cases, the number of atoms in the MOT saturates after ~ 30 s. When a 5 s long phase is chosen, the number of collected atoms in the MOT is about 1×10^7.

The MOT fluorescence signal is recorded with a calibrated photodiode, such that the number of the trapped atoms can be inferred. Neglecting two and three body losses, the number of atoms captured in the MOT grows according the following equation [84]:

$$N(t) = N_0(1 - e^{t/\tau}) \tag{4.1}$$

By fitting this function to the experimental data, the MOT loading time is derived, which was typically around $\tau \simeq 12$ s in our experiments. The value of the loading time gives information about the lifetime of the MOT due to background collisions, which in the present experimental setup are caused by thermal atoms emitted by the rubidium dispensers. During the MOT phase, the total cooling optical power is 45 mW, whereas that of the repumping laser is 10 mW. These values of the optical power correspond to laser intensities well below the saturation intensity. The cooling laser detuning is chosen to maximize the number of the trapped rubidium atoms, and it is approximately 18 MHz to the red of the cycling transition $|5S_{1/2}, F = 2\rangle \rightarrow |5P_{3/2}, F' = 3\rangle$. The frequency of the repumping laser is locked on the resonance $|5S_{1/2}, F = 1\rangle \rightarrow |5P_{3/2}, F' = 2\rangle$. Fig. 4.1 shows a temporal scheme which reproduces the main events of a typical experimental run. The MOT magnetic field gradient has been set to 10 G/cm in the zero region. At this stage, the atomic temperature is measured using time of flight imaging. The magnetic quadrupole is suddenly switched off and the probe beam irradiates the falling atoms at different times. Typical observed atomic temperatures are of order 40 µK, which is clearly below the Doppler temperature ($\simeq 140$ µK) [76, 85].

Although it is possible to adjust the experimental parameters, to achieve lower atomic temperatures in the MOT stage, we have noted that during this precooling phase is more valuable to obtain a number of trapped atoms as high as possible. The estimated atomic density is 2.32×10^{10} atoms/cm^3. This leads to an atomic phase space density of 4.2×10^{-7}.

It is important to note that in a MOT the maximum atomic density achievable is limited by collisions between ground- and excited state atoms during which part of the excitation energy can be transformed into kinetic energy, and by repulsive forces between atoms

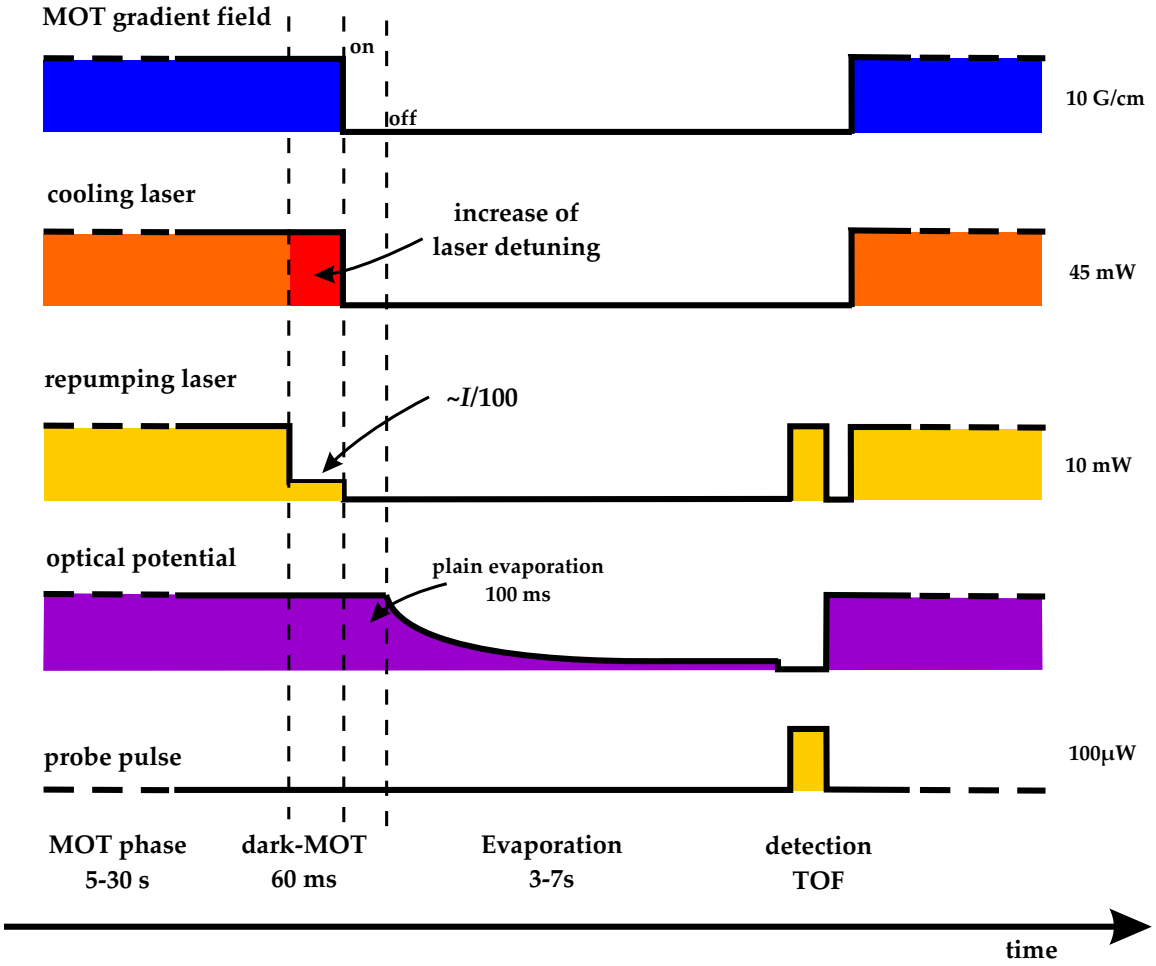

Figure 4.1: Time sequence of a typical experimental cycle. The duration of the MOT phase depends on the adopted CO_2-laser beam geometry. After the dark-MOT phase, both cooling and repumping lasers are extinguished. Before ramping down the confining CO_2-laser optical power, a 100 ms long time is waited allowing for a natural evaporation of atoms. After condensation, and subsequent manipulation of the trapped atoms, a TOF imaging is applied as diagnostic tool.

caused by reabsorption of scattered photons from the interior of the trap, as reported in [86, 87, 88]. These limitations can be circumvented by applying a temporal dark-MOT phase.

Indeed, at the end of the MOT stage, the cooling laser is further detuned to the red of the cooling transition. At the same time, the repumping laser intensity is decreased by nearly a factor 100, as it is shown in Fig. 4.1. This dark-MOT phase lasts 60 ms (for both CO_2-laser dipole trapping geometries), during which the atomic cloud is compressed. To this aim, the cooling laser detuning is changed in time. In an initial stage of the experiment, the cooling laser detuning was directly ramped up to a value of 160 MHz in few hundreds microseconds. In a later stage of this work, improved results were obtained by first changing the cooling laser detuning to an intermediate value of $\Delta_1 \simeq 40$ MHz for a 20 ms period. Subsequently, this frequency is ramped linearly up to 160 MHz in 20 ms and kept constant to the this final value for an additional 20 ms long period. The use of such a temporally tailored ramp yielded an improved transfer efficiency into the optical dipole trap of nearly 40 % compared to a dark-MOT with a temporally constant value of some final frequency detuning. Sometimes, we refer to this improved dark-MOT phase as a "soft" dark-MOT. Fig. 4.2 shows the cooling laser detuning during the improved dark-MOT stage over time.

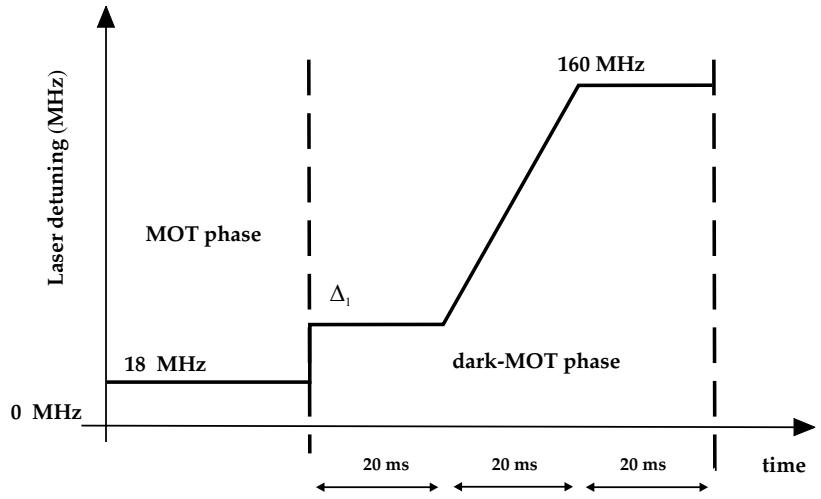

Figure 4.2: Temporal dark-MOT phase. During the dark-MOT phase the cooling laser is further "red" detuned with respect to the cooling transition. The choice of the starting detuning Δ_1 is done by maximizing the total number of transferred atoms to the CO_2-laser dipole traps. A typical value for Δ_1 is 40 MHz.

We observe that, in general, a reduction of repumping light intensity results in an increased accumulation of rubidium atoms in the lowest hyperfine ground state $|5S_{1/2}, F = 1\rangle$. At the end of the dark-MOT phase, the MOT magnetic field is turned off in few hundreds milliseconds, and both cooling and repumping light are reduced to nW level by suddenly switching off two independent acousto-optic modulators (AOMs). The switch-

ing time of these AOMs is shorter than 1 µs. Additional mechanical shutters are used in order to completely extinguish this residual near resonant light. The closing time of these shutters was measured to be $\simeq 200 - 400$ µs. To prevent losses due to hyperfine changing collisions, almost all rubidium atoms are pumped in the lowest hyperfine ground state: $|5S_{1/2}, F = 1\rangle$. This atom pumping is accomplished by setting a delay between the closing time of the mechanical shutters for the two MOT lasers. In particular, the repumping light is closed 2 ms before the cooling light. Note that this is a variation of the spatial dark-MOT first realized by Ketterle *et al*. [89].

This compression and optical pumping stage is mandatory in our experiments, since without it the number of trapped atoms in CO_2-laser dipole traps would be smaller than 10^4, and this would prevent the success of evaporative cooling towards BEC. During the MOT and dark-MOT phases, the CO_2-laser power is kept at the maximum value. The focus of this laser beam is overlapped to the MOT center. At the end of the dark-MOT phase, the atoms are confined by the purely optical potential alone. The atomic cloud is prepared for subsequent evaporative cooling, which takes place in the optical dipole traps alone.

In the next paragraph, a simple model of forced evaporative cooling is reviewed. The study of this model allows a quite sufficient understanding of the evaporative process in optical dipole traps, i.e. of the physical quantities which play a major role in the success of this cooling technique.

4.2 Evaporative cooling in optical dipole traps

Evaporative cooling of atoms was originally proposed by Hess, for the case of atomic hydrogen [90]. It consists of the selective removal of atoms in the high-energy tail of the thermal distribution and the subsequent equilibration of the remaining atoms to an energy distribution of lower temperature. In optical dipole traps, evaporative cooling is usually accomplished by lowering the confining optical potential during time, as first demonstrated by the group of Chu [26]. However, in that experiment the cooling process stopped already three order of magnitude away form the onset of the degenerate regime.

The key parameter in evaporative cooling is the ratio between the potential depth and the atomic temperature of the trapped ensemble: $\eta = U/k_B T$ [91, 92]. When the atomic temperature drops, the evaporation rate decreases and at a certain point stagnates. In fact, the number of colliding pairs atoms with enough energy for leaving is proportional to $e^{-\eta}$. In the experiments presented in this thesis, after the plain evaporation (as it will be explained later) η is about $9 - 10$, and this implies a suppression of evaporation by a factor $e^{-9} - e^{-10}$. To achieve further cooling, a continuous lowering of the optical potential U is needed, as it is schematically represented in Fig. 4.3.

It is possible to show that if the confining optical potential is harmonic, and if the atoms have a temperature $k_B T \ll U$ (the atoms then vibrate near the bottom of the optical potential), the total energy change due to evaporation of atoms $\dot{N}$ and change of potential

$\dot{U}$ is

$$\dot{E} = \dot{N}(U + \alpha k_B T) + \frac{\dot{U}}{U}\frac{E}{2}, \tag{4.2}$$

where $E/2$ is the average potential energy and $\alpha = (\eta - 5)/(\eta - 4)$. On the other hand, the variation of the total energy is $\dot{E} = 3Nk_B\dot{T} + 3\dot{N}k_B T$. Therefore, the change in temperature is $\dot{T} \propto \dot{N}(U + \alpha k_B T - 3k_B T)$, proportional to the difference between the average energy carried away per particle and the thermal energy $3k_B T$.

If equation (4.2) is solved for a fixed value of $U/k_B T = \eta$, the number of trapped atoms is found to vary with the trap depth as

$$\frac{N}{N_i} = \left(\frac{U}{U_i}\right)^{3/[2(\eta'-3)]}, \tag{4.3}$$

where i denotes the initial conditions at $t = 0$, and $\eta' = \eta + \alpha$ [93].

The phase-space density in the classical regime is $\rho = N(h\nu)^3/(k_B T)$, where $\nu = \nu(t) \propto \sqrt{U(t)}$ is the geometric mean of the trap oscillation frequencies. Using equation (4.3), we get

$$\frac{\rho}{\rho_i} = \left(\frac{U_i}{U}\right)^{3(\eta'-4)/[2(\eta'-3)]} = \left(\frac{N_i}{N}\right)^{\eta'-4}. \tag{4.4}$$

In typical experiments the potential depth is lowered from initial 28 W to a final value of 200 mW. For $\eta \approx 10$ (as indeed measured in a preliminary stage of this work), it is possible to have an increase in the phase space density of a factor 600. It is interesting to estimate the drop in the collision rate caused by the evaporation. For an energy-independent scattering cross section, the elastic collision rate for a Bose gas in an harmonic trap is $\gamma = 4\pi N m\sigma\nu^3/(k_B T)$ scales as:

$$\frac{\gamma}{\gamma_i} = \left(\frac{U}{U_i}\right)^{\eta'/[2(\eta'-3)]}, \tag{4.5}$$

where $\sigma = 8\pi a^2$ is the collision cross section for bosons. When $\eta \approx 10$ the collision rate is reduced by a factor 25 if the confining potential depth is decreased by a factor 100. It is possible to show that η remains constant when the optical potential follows the time law

$$U(t) = \frac{U_i}{(1 + t/\tau)^{\beta}}, \tag{4.6}$$

where $\beta = 2(\eta' - 3)/\eta'$, and τ a time constant given by

$$\frac{1}{\tau} = \frac{2}{3}\eta'(\eta' - 4)exp(-\eta)\gamma_i. \tag{4.7}$$

If one wants to include background losses Γ_{bg}, then the previous equations hold as long as the τ is replaced with $\left[1 - exp(-\Gamma_{bg}\tau)/\Gamma_{bg}\right]$.

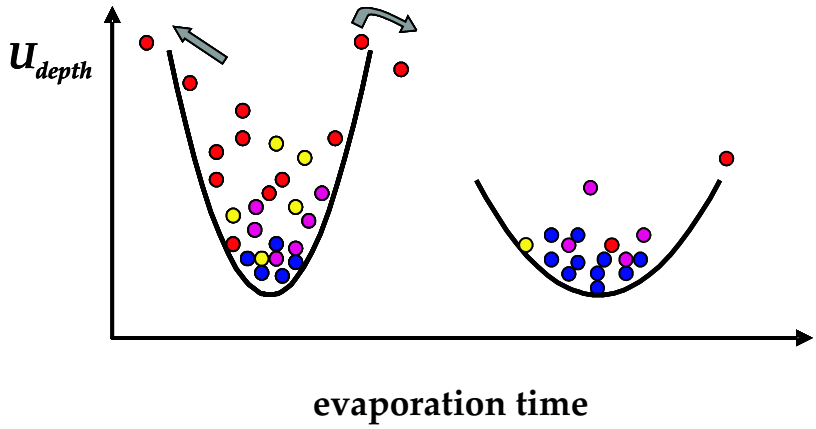

Figure 4.3: Scheme of evaporative cooling in an optical dipole trap. In far-detuned optical dipole traps, forced evaporation is usually accomplished by lowering the optical confining potential with time. However, this leads to a weakening of the confinement of the atoms and therefore to a reduction of the atom collision rate. For low potential depths longer rethermalization times are thus expected.

4.3 Quasistatic dipole traps and phase space density

So far, only few experimental groups have achieved quantum degeneracy by means of "all-optical methods". The reason is that, in contrary to magnetic traps, where the application of rf transitions into untrapped states allows one to work with temporally constant confinement, in optical dipole traps the so called "runaway regime" in the course of evaporative cooling is never met. In fact, when the optical potential is lowered with time, the trap compression decreases and rethermalization towards lower atomic temperatures requires longer relaxation times. On the other hand, because of gravity, it is not possible to ramp down the potential depth to extremely low values.

In the light of these considerations, a good strategy for the success of evaporative cooling towards BEC in optical dipole traps is to start with a high atom collision rate and a high atomic phase space density. Indeed, in quasistatic dipole traps, significantly high initial atomic phase space densities have been achieved by laser cooling alone.

Although theoretical and experimental works have been produced to model the loading mechanism of atoms into extremely far-detuned optical dipole traps [93, 94], yet it is not properly understood the reasons why in such traps high atomic phase space densities can be observed.

A possible explanation, we propose here, relates to the behavior of the atomic polarizability of alkali atoms in extremely far detuned laser light fields. In contrast to more closely resonant dipole traps, in CO_2-laser optical traps the atomic polarizability is positive for both the electronic ground- and excited states of alkali atoms. In the case of rubidium

atoms, the excited state $5P_{3/2}$ has a polarizability $\alpha_{5P_{3/2}} = 16.8 \times 10^{-39}$ Cm^2/V. This makes the excited state a factor ~ 2.7 more trapping than the electronic ground state $5S_{1/2}$, which has a static polarizability $\alpha_{5P_{3/2}} = 5.26 \times 10^{-39}$ Cm^2/V.

With the here used typical experimental parameters of the CO_2-laser dipole trap, the ground state $5S_{1/2}$ is lowered by 40 MHz with respect to the unperturbed value, whereas the excited state $5P_{3/2}$ experiences a 100 MHz red shift from the unperturbed value.

During the dark-MOT phase, the cooling laser is red shifted by an amount of 160 MHz away from the cooling transition, while the repumping laser is locked on the repumping transition. By doing so, the energy levels for an atom in the center of the trap are shifted by 60 MHz to the red side of the D2-line transition frequency, with respect to a free atom. This leads to an enhancement of the friction force experienced by an atom passing the CO_2-laser beam focus during the dark MOT phase. Therefore, the probability for an atom to remain captured in the CO_2-laser focus is higher than in the case of near resonant optical dipole traps. This is assumed to be at least partially responsible for the observed accumulation of atoms to very high atomic densities.

This argumentation might account for the surprising feature of the occurrence of high initial atomic phase space densities of the laser cooled ensembles. Certainly, a more realistic model of the atom loading must take into account the complex dynamics of the trapped atoms in laser light field and their thermalization with a bath of cold atoms represented by the dark-MOT cloud.

4.4 CO_2-laser crossed dipole trap

In this section, experiments producing Bose-Einstein condensation in a CO_2-laser crossed dipole trap are presented. This trap is formed by two CO_2-laser beams with nearly the same beam waist. The laser beams intersect each other at a 90° angle, as it has been explained in chapters 2 and 3.

In initial experiments, the quasistatic dipole traps have been characterized and optimized. It has been taken a great care of the maximization of the atom transfer efficiency from the MOT to the purely optical dipole traps. Moreover, the initial atomic temperature of the ensemble trapped in the CO_2-laser radiation has been optimized as well. The CO_2-laser beams overlap the MOT region, and the trap loading time extends throughout the precooling phases. The used precooling phase lasts 5 s + 60 ms (MOT + dark-MOT), as explained in section 4.2. Fig. 4.4 shows an image of a typical trapped rubidium ensemble in a crossed CO_2-laser optical dipole trap.

The trap frequencies are measured by parametrically exciting the trapped rubidium atoms. The intensity of the mid-infrared radiation is modulated by periodically varying the power of the RF driving signal of the acousto-optic modulator, which controls the CO_2-laser beams intensity. A loss in the number of trapped atoms is observed when the frequency modulation is twice a trap frequency. With 12 W in each CO_2-laser trapping beam, the observed parametric resonance corresponds to a mean trap frequency of $\nu = 1.7$ kHz (this is the geometric average of the three trap frequencies). From this measurement the

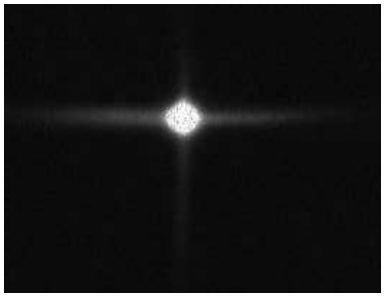

Figure 4.4: CO_2-laser crossed dipole trap. Absorption image of the trapped atoms. The image is taken few microseconds after the end of the dipole trapping phase. More than one million of atoms are trapped with a temperature about 100 µK.

value of the laser beam waist is extracted: $w_0 = 35\,\mu m$. For a crossed beam geometry, the vibrational frequencies along the three axes are similar, and the trap has a spherical shape. In the current setup, it is possible to adjust the laser beam waist by varying the distance of the two lenses (L1 and L2) forming a telescope for the CO_2-laser radiation, see Fig. 3.5. The estimated potential depth for this crossed beams configuration is about 1.2 mK.

Subsequently to the characterization of the trap, the trap lifetime and the atomic temperature have been measured as follows. After having loaded the CO_2-laser dipole trap, the mid-infrared trapping radiation was kept on at a fixed constant value for a variable time (delay time), and then switched off, allowing for a free falling expansion of the atomic cloud. The number of atoms and the atomic temperature were recorded by using absorption imaging technique at different delay times. The shortest used delay time is 70 ms. For earlier delay times, the atoms which have not been transferred into the CO_2-laser dipole traps have not fallen out of the detection region. This procedure was repeated for different values of the confining potential depth (different values of the CO_2-laser optical power). In all measurements, the CO_2-laser loading time remains the same. Figs. 4.5 and 4.6 show the measured number of atoms and relative atomic temperatures for two different values of the total CO_2-laser trapping power. In particular, the data displayed in Fig. 4.5 refers to a total CO_2-laser optical power of 30 W (15 W in each beam), whereas in Fig. 4.6 a total trapping power of 10 W was used (5 W in each beam).

If this two sets of measurements are compared, one can observe that, despite the almost equal number of the trapped atoms, the atomic temperature is lower for smaller laser trapping powers, see Figs. 4.5b and 4.6b. This dependency of the atomic temperature on the trapping power is ascribed to the failure of the sub-Doppler cooling mechanism for high CO_2-laser power.

Moreover, for the different values of the confining optical power, the behavior of the number of the trapped atoms is the same: one can observe an initial fast decay and then a slow one, as shown in Figs. 4.5a and 4.6a. If one compares the behavior of the number of atoms and the atomic temperature with time, it is evident that a plain evaporation

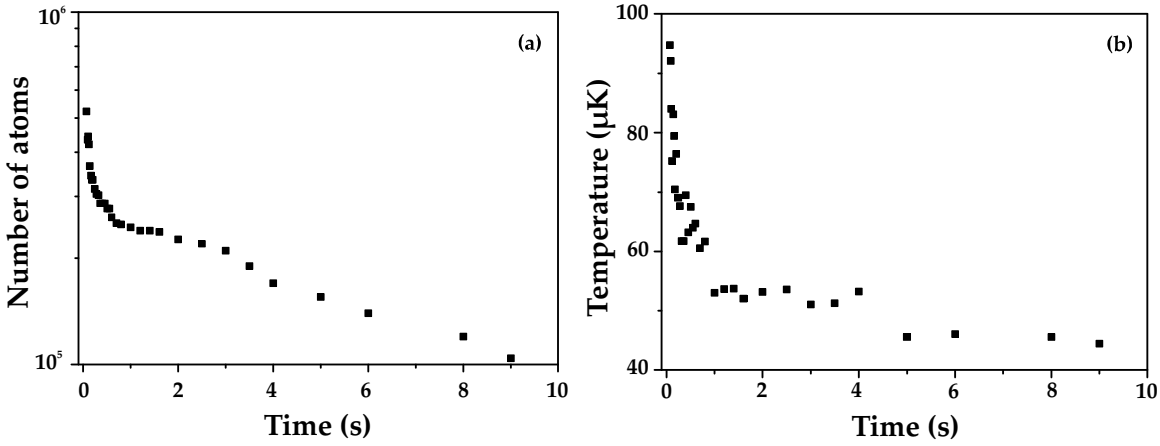

Figure 4.5: Typical trap parameters for a crossed dipole trap with total CO_2-laser power of 30 W and beam waist of $w_0 = 35\,\mu m$). (a) Number of atoms versus trapping time (log scale). The fast decay can be described by a double exponential decay with a fast and a slow time constant. (b) Atomic temperature decreases fast within the first second of the dipole trapping phase, and then continues to decrease slowly.

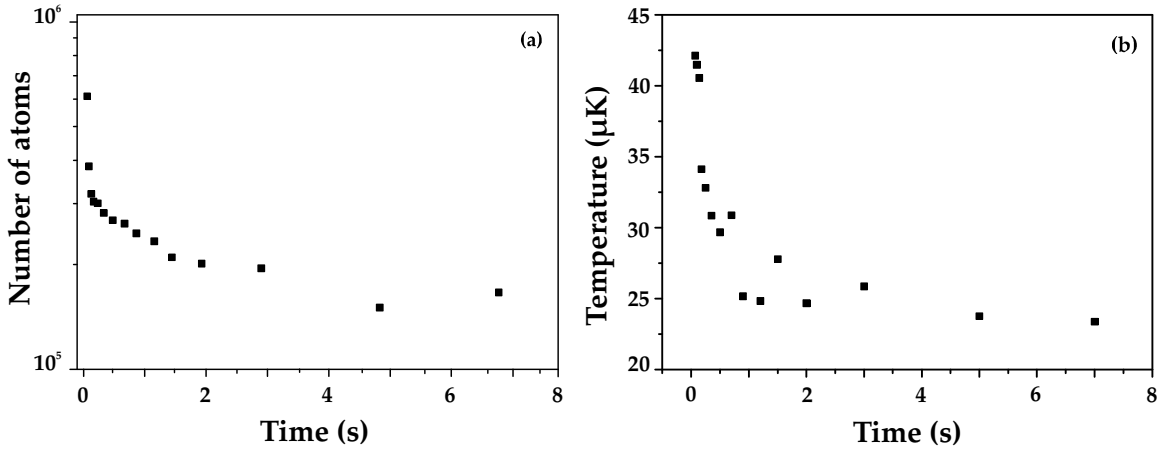

Figure 4.6: Typical trap parameters for a crossed dipole trap with total CO_2-laser power of 10 W and beam waist of $w_0 = 35\,\mu m$). (a) Number of atoms versus trapping time (log scale). The fast decay can be described by a double exponential decay with a fast and a slow time constant. (b) Atomic temperature decreases fast within the first second of the dipole trapping phase, and then continues to decrease slowly.

happens after the dark-MOT phase. Let us point out that the number of trapped atoms in Figs. 4.5, 4.6 is not well optimized yet. For these measurements, the dark-MOT phase was still realized by suddenly increasing the detuning of the cooling laser from a value of 18 MHz to 160 MHz, with a step function in time.

However, when a "soft" dark-MOT phase is realized, as it was described before in section 4.2 (see Fig. 4.2), the number of the transferred atoms into the CO_2-laser dipole trap becomes higher than 10^6. It is important to note that even in case of not well optimized atom transfer, it is possible to observe a fast loss of atoms attributed to a rethermalization process. Fig. 4.7 shows a set of data corresponding to the optimized dark-MOT phase. These data correspond to a CO_2-laser optical power in each beam of 12 W and to a beam waist of 35 µm.

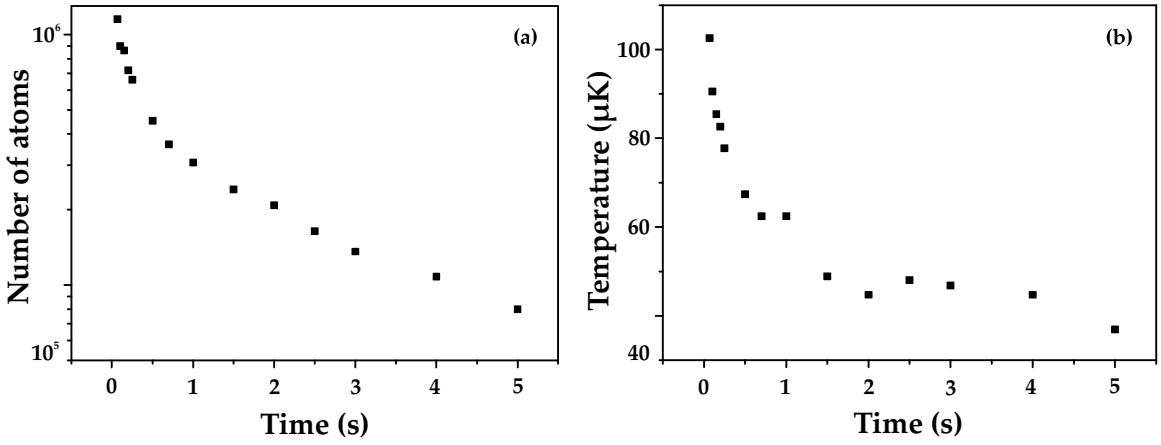

Figure 4.7: Characterization of a crossed dipole trap with a "soft" dark-MOT phase. The total CO_2-laser power is 24 W and the beam waist is 35 µm. (a) Number of atoms versus trapping time. The initial number of atoms is here above 1×10^6. (b) Atomic temperature during the dipole trapping phase versus time.

If the data are fitted with a double exponential function, one can approximate the behavior of the trapped atoms with time considering two characteristic decay phases: a fast and a slow decay with time constants near 100 ms and 12 s, respectively. The slow decay is attributed to losses due to collisions with background gas, which ultimately limit the available trapping time. On the other hand, the fast decay of atoms and the reduction of the atomic temperature with time are attributed to a "plain evaporation" of the highest energetic atoms. This process is effective only for small trapping times when the loss rate is large.

The measured atomic density after a delay time of 500 ms is 1×10^{13} atoms/cm^3. The measured atomic temperature is about 60 µK and the inferred phase space product $n\lambda_{dB}^3 \simeq 1/500$, which corresponding to a 1/1500 phase space density if we assume equal distri-

bution of spin-projections. The inferred collisional rate is 7 kHz [23]. These results are comparable to previous results observed in CO_2-laser optical lattice and crossed dipole geometries [25].

With these parameters, the initial conditions for a successful further forced evaporation towards Bose-Einstein condensation are met.

4.4.1 BEC in a crossed dipole trap

Once the ultracold bosonic ensemble is prepared, as explained in the previous sections, the experimental sequence towards BEC proceeds as follows.

After the dark-MOT phase, the CO_2-laser optical potential is not immediately ramped down. A 100 ms long period is waited. After this period, the mid-infrared power is reduced in a 3.5 s long ramp time from initially 12 W to a final value of 75 mW in each of the trapping beams according the formula (4.6). In these crossed dipole experiments, optimum cooling was achieved using $\tau = 0.3\,\mathrm{s}$ and $\beta = 1.5$ as parameters in the temporal function (4.6). When the confining potential is ramped down, an increasing of the optical density is observed . For a characterization of the cooling, shadow images of the expanded atomic cloud at the end of the evaporation process are analyzed. In Fig. 4.8, absorption images of the formation of a Bose condensate are shown. The images are taken for a time of flight (TOF) of 15 ms.

Fig. 4.8a shows data for a final total trapping power 300 mW, corresponding to an average trap vibrational frequency of 350 Hz. The expanded cloud here has a spherical symmetry, since the trapped ensemble is still purely thermal. The measured atomic temperature here is 240 nK. The optical density is well fitted by a gaussian distribution (dashed line). The phase space density increases when the confining CO_2-laser power is ramped down further. Fig. 4.8b refers to data recorded when the final power is 200 mW, where a typical bimodal distribution corresponding to an atomic cloud near the transition point is observed. The central feature corresponds to atoms in the Bose-condensate, while the wings represent thermal atoms, with a temperature of 200 nK. The critical temperature is estimated to be $T_c = 190\,\mathrm{nK}$. For a final power of 150 mW, an almost pure condensate is obtained, as shown in Fig. 4.8c. No thermal component is discernible here.

The pure condensate contains about 1.0×10^4 atoms distributed among the three m_F states of the electronic hyperfine ground state $F = 1$. This is referred to as a spinor condensate. A Bose-Einstein condensate which is described by an order parameter with three or more components is called spinor condensate [27]. In other measurements, we have applied a magnetic quadrupole field during the course of the evaporation by leaving on the MOT coils. This leads to a condensate with about 70 percent population in the $m_F = 1$ and 30 percent in the $m_F = 0$ spin projection. For these trap parameters, the magnetic field gradient leads to a predominant population of one field-sensitive Zeeman state.

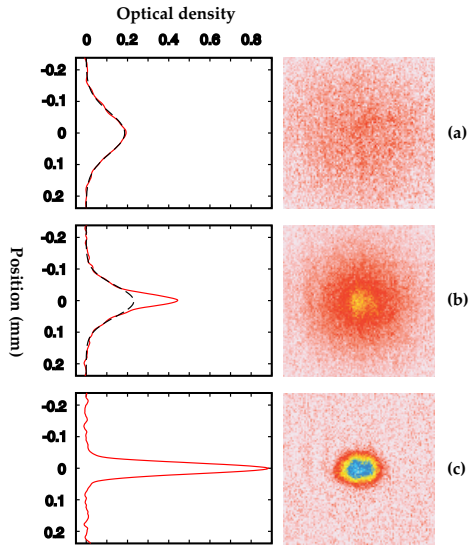

Figure 4.8: Shadow images of Bose-Einstein condensation in the crossed beams optical dipole trap. (a) Final trapping power of 300 mW for the cooling ramp. In this measurement, the ensemble is still thermal. The optical column density is fitted by a Boltzmann distribution. (b) For a final potential depth of 200 mW a bimodal distribution is observable. The measured atomic temperature is 200 µK. (c) At 150 mW final trap power, a pure condensate is discernible. The number of the condensed atoms is 1.0×10^4, which are distributed among the three spin-projection states $m_F = \pm 1, 0$.

4.5 CO_2-laser single dipole trap

From the preliminary experiments on all-optical BEC in a CO_2-laser crossed dipole trap, we gained insight in the evaporation process: a fundamental role in the all-optical BEC was played by the initial conditions of the forced evaporation as the atomic collisional rate, which had to be maintained high throughout the cooling process. Based on this understanding, we resorted to the single dipole trap geometry. This is the easiest realizable geometry for a red detuned optical dipole trap. However, despite the experimental simplicity of this configuration, successful evaporative cooling is more difficult to achieve here. Indeed, evaporative cooling process might stop before the onset of the quantum degenerate regime, since the atom collision rate in a single beam geometry is lower than that in a crossed beams configuration of same beam focus. As successful strategy, we decided to tightly focuss the CO_2-laser beam to a smaller beam waist. Our experimental setup allowed us for the generation of extremely focussed traps with beam waists down to 20 µm. We found that a good compromise between number of trapped atoms and trap frequencies was met, when the beam waist of the CO_2-laser beam was chosen in the range $25 - 30$ µm.

In previous experiments on direct BEC in optical dipole traps, this problem had been

circumvented by enhancing the atom collision rate either using a more alignment-sensitive crossed dipole trap geometry [20] or Feshbach resonances [22, 21]. However, it is here demonstrated that by choosing a relatively small laser beam waist the initial atom collision rate is high enough such that forced evaporation to quantum degeneracy can be successfully accomplished in this trapping geometry.

4.5.1 Crossed versus single dipole traps

Compared to the crossed dipole trap geometry, a single running wave dipole trap gives a weaker confinement along the beam propagation axis. The cloud has a cigar shape with the longest symmetry axis z, perpendicular to the gravity axis x. Fig. 4.9 shows an absorption image of the rubidium cloud confined in a single running wave CO_2-laser dipole trap realized in this work.

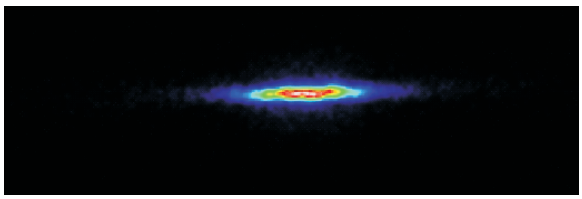

Figure 4.9: Absorption image of a single beam dipole trap. The rubidium cloud is confined in a cigar shaped CO_2-laser dipole trap, whose longest axis corresponds to the propagation direction of the mid-infrared laser beam. The image has been taken few microseconds after the switching off of the trapping radiation.

The ratio between the longitudinal and the radial frequencies in a single running wave dipole trap is

$$\frac{\nu_z}{\nu_r} = \frac{\lambda_L}{w_0 \pi \sqrt{2}}. \tag{4.8}$$

Whereas for a crossed beams CO_2-laser dipole trap this ratio is $\simeq 1$, in a single beam CO_2-laser dipole trap with a beam waist of 35 µm, the ratio is $\simeq 1/15$. For a fixed beam waist and for a given value of the optical power, the mean trap frequency in a single dipole trap is smaller than that in a crossed beams dipole trap. It is easy to show that, if γ_1 and γ_2 denote the atom collision rates for two different values of the geometric mean of the trap vibrational frequencies ν_1, and ν_2, respectively, the following relation holds

$$\frac{\gamma_1}{\gamma_2} = \left(\frac{\nu_1}{\nu_2}\right)^3 \tag{4.9}$$

It is clear that the achievable atomic collisional rate in a single dipole trap is a factor 15 smaller than the case of a crossed dipole trap, for which $\nu_z \simeq \nu_r$, under the assumption

of equal beam waist and confining power (and same number of atoms and atomic temperature). However, if one reduce the beam waist of the single CO_2-laser dipole trap, it is possible to again increase the atom collision rate. Indeed, if the dependency of the trap frequencies on the beam waist is inserted in equation (4.9), we obtain:

$$\frac{\gamma_1}{\gamma_2} = \left(\frac{w_2}{w_1}\right)^7 \tag{4.10}$$

Based on this relation, we have reduced the beam waist of the laser beam down to a value of $w_2 = 27\,\mu m$. With this values, the ratio (4.10) is about a factor 35 higher than the case of a trap with a 35 µm beam waist. The atom collision rate is still expected to be smaller that for a perfectly aligned 35 µm crossed dipole trap. However, the single running wave geometry is far less alignment sensitive.

4.5.2 Dipole trap characterization

Before the study of evaporative cooling, the single beam CO_2-laser dipole trap was characterized as follows. ^{87}Rb atoms are precooled and collected in the MOT. The MOT loading phase is chosen to be 30 s, during which 6×10^7 atoms are captured. The laser cooling is 18 MHz red detuned to the cooling transition. Afterwards, a 60 ms long "soft" dark-MOT phase is realized as explained before in section 4.1. At the end of this precooling stage, all near-resonant optical beams are extinguished, switching off the AOMs and closing the mechanical shutters. Hyperfine changing collisions are reduced by extinguishing the repumping light 1 ms before the cooling light. At the end of this dark-MOT stage, the magnetic quadrupole field is turned off as well. Throughout the precooling stage the CO_2-laser is kept at maximum power. The CO_2-laser beam, which overlaps with the MOT region, travels inside the vacuum chamber along the z horizontal axis, orthogonal to the x gravity axis, as it has been described in chapters 2 and 3.

In typical experiments, 4×10^6 atoms are captured in the single beam running wave dipole trap. At full CO_2-laser power (28 W), the measured trap frequencies are $\nu_r = 4.8\,kHz$ and $\nu_z = 350\,Hz$, corresponding to vibrations orthogonal and collinear respectively to the beam axes. In this single beam geometry, there is no spherical symmetry and the longitudinal trap frequency is about 11 times smaller than the radial one. The geometry of the trapped atomic cloud is cigar shaped, as shown Fig. 4.9.

As the case of the crossed beam geometry, the shortest used delay time is 70 ms after the end of the dark-MOT phase. At 70 ms the number of atoms in the CO_2-laser dipole trap is 4×10^6, and the corresponding atomic temperature is measured to be 140 µK. Here, the atomic temperature approaches the Doppler temperature. A trap loss with a decay time faster than vacuum limited rate is observed. At a total dipole trapping time of 100 ms (100 ms after the dark-MOT phase), the number of trapped atoms has decreased to one third (*i.e.* in only 30 ms the number of trapped atoms drops by a factor 3) and the temperature has reduced to 90 µK. Fig. 4.10 shows both the number of the trapped atoms and the atomic temperature in the single dipole trap as function of time.

Similarly to the crossed dipole trap geometry, the number of the trapped atoms and the atomic temperature display a fast and a slow decay time constant. The first one is attributed to a fast "natural" evaporation of the trapped atoms, and the latter to collisions with the background gas.

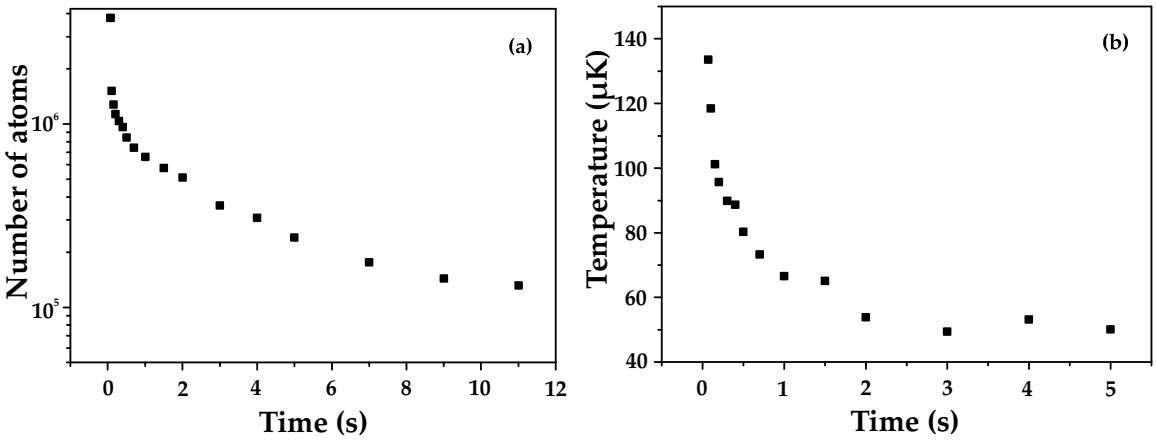

Figure 4.10: Characterization of the single running wave CO_2-laser optical dipole trap (optical power 28 W, beam waist 27 μm). (a) Number of the trapped atoms versus delay time. A fast decay with a characteristic time of 100 ms is observed. (b) Atomic temperature during versus delay time. The temperature decreases at the beginning of the dipole trapping phase.

After the initial fast decay, the trap loss slows down and the trap gradually reaches its vacuum limited lifetime of 12 seconds. The inferred atomic density at 70 ms dipole trapping time is $n \simeq 1.2 \times 10^{13}\,\mathrm{cm}^{-3}$, and the collisional rate is 6.2 kHz. The atomic phase-space product at this stage is $n\lambda_{dB}^3 \simeq 1.2 \times 10^{-4}$. Since the CO_2-laser dipole trap confines all spin-projection states of the hyperfine ground state $|5S_{1/2}, F = 1\rangle$, the phase space density of each of those sub-levels is 4×10^{-5}, as long as equal population of Zeeman components is assumed. However, already some 30 ms later, the product $n\lambda_{dB}^3$ has already increased to 0.0016. This high value represents an favorable starting point for a successful forced evaporative cooling towards BEC.

4.5.3 BEC in a single optical dipole trap

The experimental cycle for directly achieving Bose-Einstein condensation in a single CO_2-laser dipole trap has already been shown in Fig. 4.1. After a delay time of 100 ms, the power of the mid-infrared beam is ramped down to induce a time-dependent trap potential according equation (4.6). Optimum cooling is observed when choosing parameter values of the ramp near $\tau = 0.45$ s and $\beta = 1.4$. The optical trapping power is reduced in 7 s from an initial value of 28 W to a final power of 200 mW.

Fig. 4.11 shows the formation of the condensate at a free falling expansion time of 10 ms. For the data shown in Fig. 4.11a, the evaporation ramp ended at a final CO_2-laser power of 500 mW. In this case, a thermal distribution is observed. The measured atomic temperature is 350 nK. This means that the confining potential should be lowered further in order to get BEC. When the final CO_2-laser power is around 240 mW, it is possible to recognize the onset of condensation. In Fig. 4.11b a typical bimodal distribution is recorded. The thermal component has a temperature of 180 nK. Here, the mean vibrational trap frequency is 250 Hz. It is possible to obtain almost pure condensates when the power is reduced below 200 mW, as shown in Fig. 4.11c. The final optical power of the evaporation ramp here is 200 mW and the corresponding mean trap frequency is 190 Hz. The critical temperature for the onset of the quantum degenerate regime is estimated to be 180 µK. The number of atoms in the almost pure Bose-Einstein condensate is measured to be 1.2×10^4. The measured peak density of the pure Bose-Einstein condensate is $1.3 \times 10^{14}\,\mathrm{cm}^{-3}$.

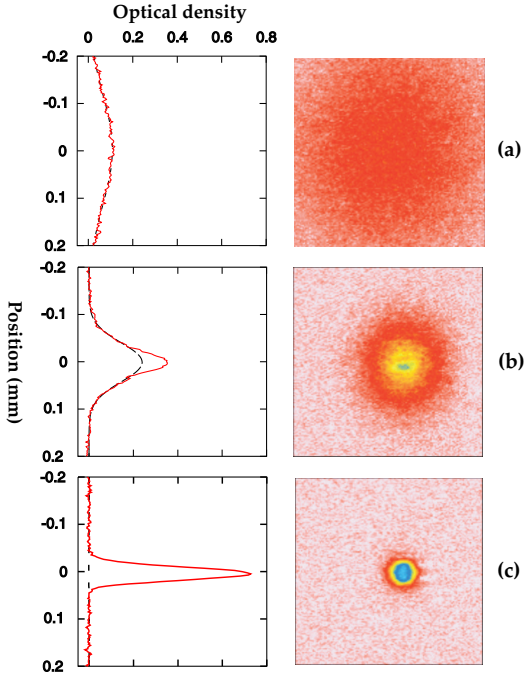

Figure 4.11: BEC formation in a single running wave dipole trap. Absorption images at TOF=10 ms. (a) When the evaporation ramp ends at a laser power of 500 mW there is only thermal cloud. (b) At 240 mW it is possible to observe bimodal distribution. (c) An almost pure condensate with 1.2×10^4 atoms is observed when the trapping laser power is ramped down to 200 mW.

It is interesting to note that in Fig. 4.11c the shape of the condensate appears near spherical in the x, z imaging plane, although the confining trap has a cigar shape, see Fig 4.9. This

behavior is easily understood when one considers that in this asymmetric trap geometry, soon after the release from the trap, the cloud expands faster along the tightest radial direction than along the axial one, because of the anisotropic release of mean field energy; see Appendix C for an explanation. This results in a fast expansion of the condensate along the tightest confining axes (x, y).

In Fig. 4.12 a time-of-flight (TOF) sequence is shown. This sequence illustrates how the shape of a released Bose condensate changes in a ballistic expansion. The first image

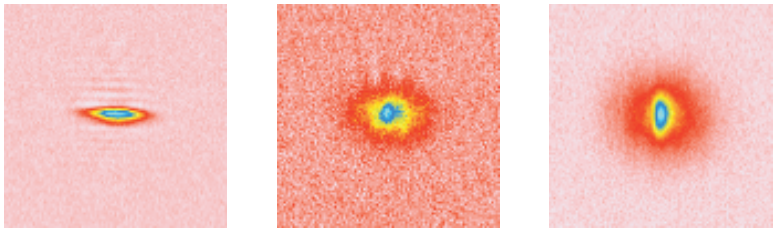

(a) **(b)** **(c)**

Figure 4.12: Free expansion of a Bose-Einstein condensate. The images are take at different times after extinguishing the trapping potential. (a) Condensed cloud soon after the release from the optical trap. The cloud has a cigar shape along the z axis. (b) TOF image at 8 ms. Because of the anisotropic release of the mean field energy, the condensate expands mostly in the tightest confined directions (x, y). (c) TOF picture after 15 ms. The field of view is (for each image) 240 µm $\times$ 240 µm.

shows a condensate soon after switching off the confining CO_2-laser potential (almost no expansion). At this stage the cloud has a cigar shape and is elongated along the weakly confining axis. Subsequently, the interaction energy is released and converted into kinetic energy, causing an expansion in the x, y plane faster than that along the z axis. Figs. 4.12b and 4.12c give TOF images recorded after a 8 ms, and 15 ms respectively. In particular, in Fig. 4.12b, the cloud is almost symmetric, while in the final image the symmetry axis is inverted.

The so formed Bose-Einstein condensate has a spinor nature. Condensed atoms are distributed among the three Zeeman levels ($|m_F = \pm 1, 0\rangle$) of the hyperfine ground state $|5S_{1/2}, F = 1\rangle$. To analyze the distribution of the three Zeeman components, a Stern-Gerlach experiment is performed. After the Bose condensate production, the CO_2-laser optical dipole trap is turned off, and a weak magnetic field gradient is applied during the free expansion. The induced magnetic force spatially separates the different Zeeman components. Fig. 4.13 shows a typical measurement, where a separation into three clouds with different spin projections is clearly visible. The produced condensates here have typically 12000 atoms distributed among the $|F = 1, m_F = \pm 1, 0\rangle$ Zeeman components.

In the next section a technique for producing Bose condensates into magnetic field

insensitive states will be discussed.

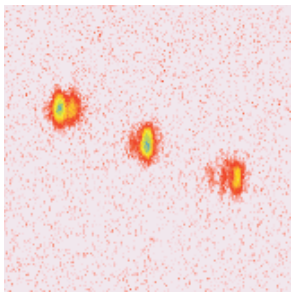

Figure 4.13: Stern-Gerlach experiment. A weak magnetic gradient field induces a spatial separation of the three condensed clouds during the free expansion of the Bose condensate. TOF of 15 ms. The field of view is 380 µm $\times$ 380 µm.

4.6 Magnetic-field insensitive BEC

Far detuned optical dipole traps can confine atoms independently on their spin orientation, offering the possibility of studying multiple spin components ensembles as well as the properties of spinor condensates. Recently, evolution of spin domains in spinor condensates have been experimentally observed [95, 96, 97, 98].

In this work, spinor condensates are directly created in CO_2-laser optical dipole traps, both for a single beam and a crossed beams geometry. However, we can also create Bose-Einstein condensates of atoms in magnetic field-insensitive states ($m_F = 0$ states). An alternative way to produce Bose-Einstein condensates in field-insensitive states is to use spin-singlet ground state atoms as, e.g., alkali-earth atoms. Indeed, very recently Takasu *et al*. demonstrated BEC with Yb atoms in a Yag-laser crossed dipole trap.

When an inhomogeneous magnetic field is applied throughout the forced evaporation phase, only atoms in the field-insensitive state $|F = 1, m_F = 0\rangle$ are allowed to condense. In fact, in the final stages of the evaporative cooling, the optical dipole trap cannot then anymore confine atoms in $m_F = \pm 1$ states, because of the presence of a magnetic force. Only the atoms in the $m_F = 0$ state remain trapped and condense, as shown in Fig. 4.14.

This is already the case when a relatively weak magnetic field gradient of 10 G/cm is added to the optical dipole potential for a laser power depth of 200 mW [2]. Fig. 4.14a displays a Stern-Gerlach experiment with no magnetic gradient applied during the evaporation time. In this case, a spinor condensate is formed with almost 12000 atoms distributed among the three m_F spin-projections. In Fig. 4.14b only a scalar condensate (in particular

[2]Note that in our setup the minimum of the magnetic field does not coincide with the center of the CO_2-laser dipole trap.

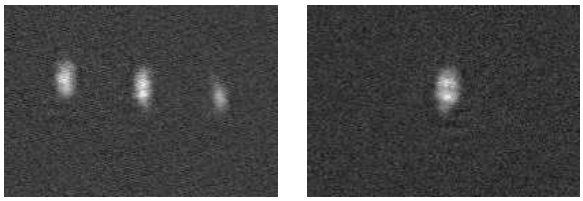

(a) (b)

Figure 4.14: Results of Stern-Gerlach experiments of Bose-Einstein condensates for a 15 ms free expansion time. (a) A spinor condensate is analyzed, by applying a weak gradient field during the detection time. Here, in the dipole trap a mixture of $|m_F = 0, \pm 1\rangle$ condensates was present, which spatially separate into three clouds during the expansion. (b) Stern-Gerlach image of an $|m_F = 0\rangle$ Bose condensate.

an $m_F = 0$ condensate) is formed, when a magnetic field gradient is applied throughout the evaporation phase. Both images refer to a free expansion time of 15 ms.

It is interesting to note that the number of atoms in the $m_F = 0$ Bose condensate is 7000. This value is larger than one third of the number of atoms of the corresponding spinor condensate. We ascribe this phenomenon to a sympathetic cooling which favors population of the $m_F = 0$ spin-projection.

Note that the fluctuations of the chemical potential $\Delta\mu$ of such a $m_F = 0$ Bose condensate caused by any stray magnetic field are dramatically reduced. Let us remember that the expression of the chemical potential, in case of zero fluctuation of the magnetic field, has been already derived in chapter 1, see equation (1.23). For atoms in magnetic field sensitive states, the fluctuations of the chemical potential are of the order $\mu_B \Delta B / k_B$ ($\cong \Delta B \times 67\,\mathrm{nK/mG}$), where μ_B is the Bohr magneton and B the value of the magnetic field. In our experiments, the residual fluctuations of the chemical potential of a $m_F = 0$ Bose condensate can estimated using the Breit-Rabi formula [99]:

$$\mu \sim \frac{(g_F - g_I)^2}{4} \frac{(\mu_B B)^2}{E_{HFS} k_B}, \tag{4.11}$$

where E_{HFS} is the hyperfine energy, and g_F and g_I are the electron and the nuclear g-factors, respectively. In our experiments, the residual fluctuations of the chemical potential are as low as $14\,\mathrm{fK/(mG)^2}$.

Based on this result, we have realized a novel type of atom laser, as will be presented in the next chapter.

4.6.1 Condensate lifetime

To measure the condensate lifetime, once BEC is achieved, the confining potential depth is kept constant and Stern-Gerlach analysis is performed after different delay times. The

measured lifetime of the Bose condensates is 5 s. This value is shorter than that imposed by the pressure of the background gas, which is 12 s. The inferred peak density for the generated $m_F = 0$ Bose-Einstein condensate is $n \simeq 1.1 \times 10^{14}\,\mathrm{cm}^{-3}$. On the other hand, the value of the three body recombination rate for Bose condensed atoms is $K_3 = 5.8 \times 10^{-30}\,\mathrm{cm}^6\mathrm{s}^{-1}$, as measured by Burt *et al*. [100]. The product $K_3 n^2$ leads to a time decay constant of 14 s. This value is well above the vacuum limited lifetime that we measured. We assume that the discrepancy between this three body decay time and the condensate lifetime derives from the experimental uncertainty on the peak density. This hypothesis must be corroborated by further measurements in future experiments.

It is interesting to note that, within our experimental uncertainties, the observed lifetime is the same both for spinor and $m_F = 0$ condensates. Researchers have observed relaxation dynamics of multiple-spin components, which usually evolve during time towards equilibrium of the spin-projection populations [28]. In the experiments carried out with $m_F = 0$ condensates, no relaxation dynamics has been observed. We believe that these spin-changing collisions are energetically suppressed due to the second order Zeeman effect. Indeed, Ho showed that for a $F = 1$ spinor condensate, the interaction energy between two atoms in a Bose-Einstein condensate, with spins $\mathbf{F}_1$ and $\mathbf{F}_2$, is given by the following expression

$$V(\mathbf{r}_1 - \mathbf{r}_2) = \delta(\mathbf{r}_1 - \mathbf{r}_2)(c_0 - c_2 \mathbf{F}_1 \cdot \mathbf{F}_2), \tag{4.12}$$

where $c_0 = \frac{4\pi\hbar^2}{m}(a_0 + 2a_2)/3$ and $c_2 = \frac{4\pi\hbar^2}{m}(a_2 - a_0)/3$. Let us note that a_0 and a_2 are the s-wave scattering length in the total spin F channel [27]. Depending on the value of the singlet and triplet scattering length, a ferromagnetic or an antiferromagnetic behavior of the spinor condensate is observed. Klausen *et al*. predicted a ferromagnetic behavior for F=1 ^{87}Rb condensates [101]. In general, for the $F = 1$ manifold, the collisions among bosons which preserve the angular momentum are the following:

$$2|m_F = 0\rangle \rightleftharpoons |m_F = 1\rangle + |m_F = -1\rangle. \tag{4.13}$$

The effect of the ferromagnetism is to raise the energy of the $m_F = 0$ component with respect to the average of the $m_F = \pm 1$ components. The system spontaneously tends to the right of the above process, since this has then the lowest energy. This analysis is valid in case of zero external magnetic field.

In our experiments, because of an external bias field on the order of ~ 1 G, it is anticipated that the state of both atoms being in the $m_F = 0$ state, as shown on the left hand side of (4.13), has the lowest energy. The interplay between the two regimes is ruled by the ferromagnetic energy $|c_2|n/2$ and the difference in Zeeman energies, which reads $(E_{+1} + E_{-1} - 2E_0)/2$ [27, 95].

In this last formula, $E_{\pm 1,0}$ are the Zeeman energies of the three spin-projections $m_F = \pm 1, 0$. In our experiments, the ferromagnetic energy is 38 Hz. On the other hand, for a magnetic bias field of 1 G, the Zeeman energy is -135 Hz, which is caused by the quadratic Zeeman effect. The $m_F = 0$ state has a lower energy, and then it is stable against spin changing collisions. Very recently, the dynamics of $F = 1$ and $F = 2$ spinor condensates of ^{87}Rb have been investigated in [97] and [98], respectively. In particular, Chang *et al*. showed

the ferromagnetic nature of the $F = 1$ spinor condensate when the external magnetic field was opportunely reduced below a certain value. In this experiment, the variation of the lifetime of the $m_F = 0$ condensate was studied as function of magnetic bias field.

Chapter 5

All-optical Formation of an Atom Laser Beam

In this chapter, a novel type of atom laser is described. The device is based on the output coupling of the generated magnetic-field-insensitive Bose-Einstein condensate, and produces a well-collimated, monoenergetic atomic beam. Unlike previous devices, the operation of this atom laser does not require any magnetic shielding of the experimental apparatus or radiofrequency fields for the output coupler in order to generate a quasi-continuous coherent atomic beam [37].

In the first part of the chapter, the state of the art in this new research field is resumed. At the core of this quantum device two concepts reside: coherence and bosonic stimulation. This two concepts are also fundamental for a common photon laser. A critical issue is the output coupling scheme, which should preserve the coherence properties of the trapped Bose-Einstein condensate, from which the atom laser is generated. In virtue of these properties, a brief analogy with a common photon laser is presented.

A simple theoretical model of the output coupling mechanism is developed here. This model is based on Newton's equation for a $m_F = 0$ Bose-Einstein condensate initially confined in a time-dependent external potential. When the optical potential is smoothly ramped down, gravity extracts Bose condensed atoms, and a well collimated atomic beam can be observed.

In the final part of this chapter, the experimental realization of the all-optical atom laser is presented. Coherent atomic beams of up 1 mm length have been observed. Measurements of the brightness and the transverse mode profile are presented.

5.1 A brief History of Atom Lasers

An atom laser beam is generated when Bose condensed atoms are extracted from a trap. The first demonstration of such a device was given in 1997 by Ketterle at MIT [33]. In that experiment, a sodium condensate was confined in a magnetic trap and exposed to a series of radiofrequency pulses which drove spin-flip transitions from trapped to untrapped states. Under the effect of the gravity, untrapped sodium atoms propagated in free space, originating a pulsed coherent atomic beam. In 1998, Kasevich showed a pulsed coherent atomic beam based on the interference of matter waves released from an optical lattice by tunneling effect [34]. The first demonstration of a quasi-continuous atom laser was given by Phillips and collaborators in 1999 at NIST laboratories. The outcoupling mechanism consisted of stimulated Raman transitions between different magnetic sublevels [35]. Also in 1999, the group of Hänsch in München demonstrated a quasi-continuous output coupler for magnetically trapped Bose condensed atoms. The extraction technique was similar to that employed by Ketterle. However, a stabilization of the residual magnetic field fluctuations below 100 µG allowed the application of continuous weak radiofrequency output coupling [36].

In all those experiments, coherent atomic beams were extracted from Bose-Einstein condensates based on atoms in magnetic-field sensitive states, for which any stray magnetic field causes fluctuations of the chemical potential. It is experimentally challenging to suppress the fluctuations of the chemical potential of a Bose-Einstein condensate in a magnetic field-sensitive spin-projection.

Although successfully generating a quasi-continuous beam, when applying a magnetic shielding, the experiments cannot be easily scaled. Reductions of fluctuations of the chemical potential on the order of fK seem unattainable with the present technology employed in magnetically trapped spin-polarized Bose-Einstein condensates.

The scenario changes completely, if one consider the possibility to create Bose condensates with atoms in magnetic field-insensitive states ($m_F = 0$ states), as demonstrated in this work. Indeed, in this case, the residual fluctuations of the chemical potential are only $\sim 10\,\mathrm{fK}/(\mathrm{mG})^2$, and at a rather low value even without a magnetic shield of the experimental apparatus. It is clear that atom lasers based on such $m_F = 0$ states would display an exceptional robustness to stray magnetic fields.

In this work, I demonstrated for the first time an atom laser whose realization is based on all-optical methods only. A $m_F = 0$ Bose-Einstein condensate is confined in a single CO_2-laser dipole trap, and constitutes the "source" of "coherent matter". In this work, the output coupling mechanism is realized by smoothly lowering the potential depth over time. Quasi-continuous, well collimated atomic beams are generated by gravity. The output coupler does not require any magnetic shielding of the experimental apparatus or radiofrequency fields. The stability of the chemical potential is improved by orders of magnitude over conventional atom lasers based on Bose condensates in magnetic field-sensitive states.

5.2 Analogy between a "photon" laser and an "atom" laser

The definition of an "atom laser" is not trivial [102, 103, 104, 105]; nevertheless, the accepted one is the following: *atom laser is a device which produces a bright coherent beam of atoms through a stimulated process* [106].

Two concepts stand behind this definition: coherence and bosonic stimulation. Coherence means that two atom laser beams, if overlapped in space, can produce a macroscopic interference pattern. This behavior derives from the long range coherence embedded in a Bose-Einstein condensate, as recently observed in two impressive experiments [29, 30].

Similarly to laser light, an atom laser is created by stimulated amplification of bosons. In a photon laser the amplification is created by stimulated emission of photons by the atoms or molecules constituting the active medium. On the other hand, the analogy between optical lasers and current atom lasers is not perfect, since the latter ones rely on equilibrium, while the former ones are far from that. In an atom laser the bosons are represented by massive atoms, which exhibit a strong interaction.

A photon laser requires a cavity, an active medium and an output coupler. The quantum-mechanical description of an oscillating laser mode is given through a coherent state. Usually, above the laser threshold photons mostly occupy one laser cavity mode.

For atom lasers, the "cavity" is represented either by a magnetic trap or by an optical dipole trap. The macroscopic population of the ground state of the bosonic system is achieved when a Bose-Einstein condensate is formed. The population of bosons builds up in the ground state of the external trap through elastic collisions, which bring the system into thermal equilibrium. Atoms are taken out from a thermal reservoir and transformed into coherent matter. At room temperatures, atoms scatter among a myriad of possible quantum states. Below a critical temperature however, atoms scatter predominately into the lowest energy state of the system. This makes the formation of a Bose condensate a stimulated process, as in the case of laser light sources. A scheme of the bosonic stimulation process is depicted in Fig. 5.1. The probability that an atom from the thermal gas reservoir scatters into the "condensate cloud" is enhanced by a factor $N_C + 1$, where N_C is the number of the atoms already in the condensate state [31]. Thermal equilibrium is reached when the number of collisions into and out of the condensate are equal. However, evaporative cooling creates an extremely cold thermal cloud not in thermal equilibrium. After relaxation, the condensate fraction grows.

Similarly to photon lasers, the high population per mode results in an exceptional high brightness of the atomic beam. Thermal atomic beams have a population per mode of typically only 10^{-12} atoms, whereas that of an atom laser beam is $\gg 1$.

The output coupling of Bose condensed atoms can be accomplished in several ways. In any case, the adopted technique must preserve the long range coherence of the trapped Bose condensate. In this work, the extraction method is straightforwardly implemented by reducing the depth of the confining optical potential with time. Gravity extracts Bose condensed atoms to form well collimated monoenergetic atomic beams.

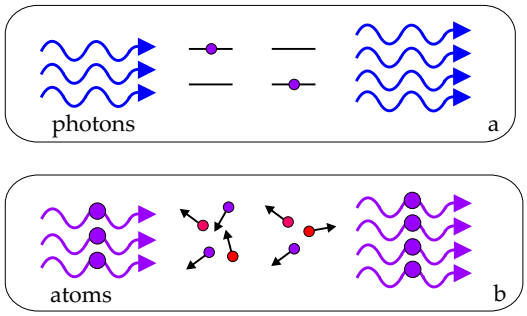

Figure 5.1: Bosonic stimulation: (a) For laser light, atoms of the active medium are stimulated to emit photons with a probability proportional to the number of photons in the laser mode. (b) For matter wave amplification process, the presence of a Bose-Einstein condensate enhances the probability that an atom from the thermal cloud scatters into the condensed cloud itself, with a probability proportional to the number of condensed atoms.

5.3 Outcoupling of the field-insensitive Bose-Einstein condensate

The starting point for the experiments on the realization of the all-optical atom laser is the production of a magnetic field-insensitive Bose-Einstein condensate in a single running wave CO_2-laser dipole trap. After the forced evaporation phase, which lasts 7 s, an almost pure $m_F = 0$ Bose-Einstein condensate is formed when the final CO_2-laser power is chosen to be 200 mW. After this cooling stage, the magnetic field gradient is switched off, and the Bose condensed atoms are confined in the optical dipole trap. At this stage, no output coupling of condensed atoms is observed, as the value of the chemical potential is much smaller than the height of the optical potential barrier.

To allow for an output coupling of the Bose condensed atoms, the optical trapping potential is further reduced with time. The used output coupling ramp is 100 ms long and it is chosen to be relatively smooth to minimize condensate excitations. The CO_2-laser power is reduced from an initial value of 200 mW (the value at which a $m_F = 0$ Bose-Einstein condensate is formed) down to a value of 35 mW. Outcoupling of atoms is experimentally observed when the optical trapping power is near 40 mW, for which the confining optical force cannot anymore support the Bose condensed cloud against gravity.

In Fig. 5.2 it is shown the atom laser formation. In particular, in Fig. 5.2a an incoherent atomic beam is shown. For this measurement, the evaporation ramp is stopped before the onset of Bose-Einstein condensation so that the atomic cloud ensemble is still thermal. Outcoupling is accomplished by lowering in 100 ms the trapping optical potential. Let us note that this output coupling ramp is too short for a forced evaporation of the trapped sample. The produced atomic beam is clearly not well collimated, since the "source" of atoms is thermal (the atoms populate a myriad of quantum states). However, when a Bose condensate is formed, the outcoupling process results in a well collimated monoenergetic

atomic beam, as clearly shown in Fig. 5.2b. The velocity spread of the atomic beam is assumed to be limited by the uncertainty principle. From the length of the atomic beam displayed in Fig. 5.2b, it is possible to estimate an output coupling time of 9 ms. This length is 400 µm.

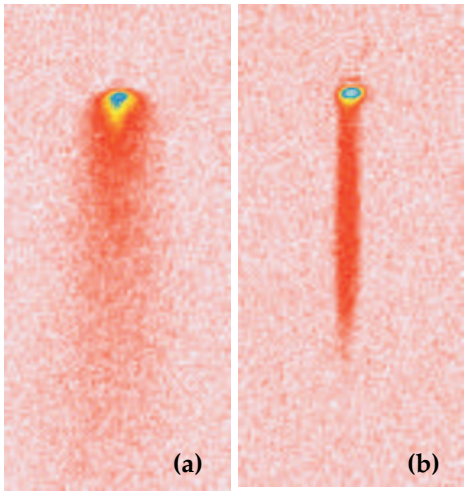

incoherent atomic beam | atom laser

Figure 5.2: Atom laser formation: absorption images of the released atomic beam. (a) Output coupling of thermal atoms. (b) For an almost pure Bose condensate, a well collimated beam is observed. In both images the field of view is 300 µm × 625 µm.

In other measurements, with longer and slower ramps, also spatially "fragmentated" beams were observed, whose origin still remains to be exploited.

5.4 All-optical atom laser: a toy model

In this section a simple model is developed for describing the output coupling rate.

The external potential, in which the $m_F = 0$ Bose condensate is trapped, is the sum of the optical dipole potential and the gravitational potential:

$$V_{ext}(\mathbf{r}) = -\frac{1}{2}\alpha_S |\vec{E}(\mathbf{r})|^2 - mgx \tag{5.1}$$

where we assume that gravity is directed along the x axis, and m is the mass of the single atoms. For our experimental parameters, the gravity force can be neglected for high values of the laser intensity. However, when the optical trapping power is reduced down to values of ~ 100 mW, gravity plays an important role. Generally, the gravity force reduces the

confining potential depth and deforms the trap geometry, as shown in Figs. 5.3. In particular, Fig. 5.3a shows the external potential without gravity correction, whereas in Fig. 5.3b the external potential also include the gravity term. For typical experimental parameters, at the end of the evaporation ramp, the optical confining potential has a depth of 8 μK, whereas the value of the chemical, for a number of 7×10^3 condensed atoms, is near 65 nK.

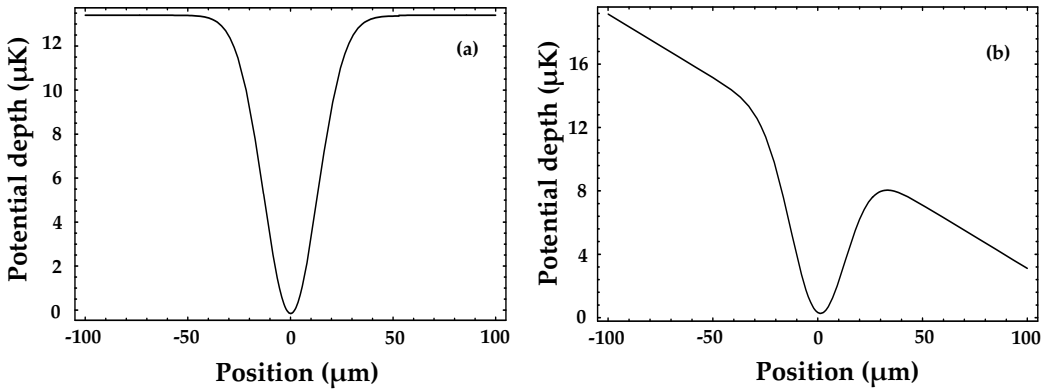

Figure 5.3: External trapping potential at the end of the evaporation ramp. (a) Trapping potential without gravity correction. (b) Trapping potential when the gravitational potential is included. In both plots, the CO_2-laser power is 200 mW, and the beam waist is 27 μm.

At this stage of the experimental sequence, no output coupling of the Bose condensed atoms is observed. However, output coupling of atoms is induced by reducing in a controlled way the optical confining potential over time. Figs. 5.4 show the variation of the potential depth and the chemical potential versus the power of the confining CO_2-laser single dipole trap. These two plots refer to the used experimental ramp for the atom laser generation, as described in the previous section. It is interesting to note that both the potential depth and the chemical potential decrease when the CO_2-laser power is reduced with time. Nevertheless, the variation of the chemical potential is slower than that of the potential depth.

Fig. 5.5a shows the used trapping laser power versus time for the last 50 ms of the ramp. When the confining laser power is near 40 mW, the chemical potential equals the height of the potential barrier, and for lower laser powers the condensate gradually starts to spill over the potential barrier. This allows to extract Bose condensed atoms into a coherent atom laser beam. Fig. 5.5b shows both the trapping potential and the chemical potential as a function of CO_2-laser power in this range.

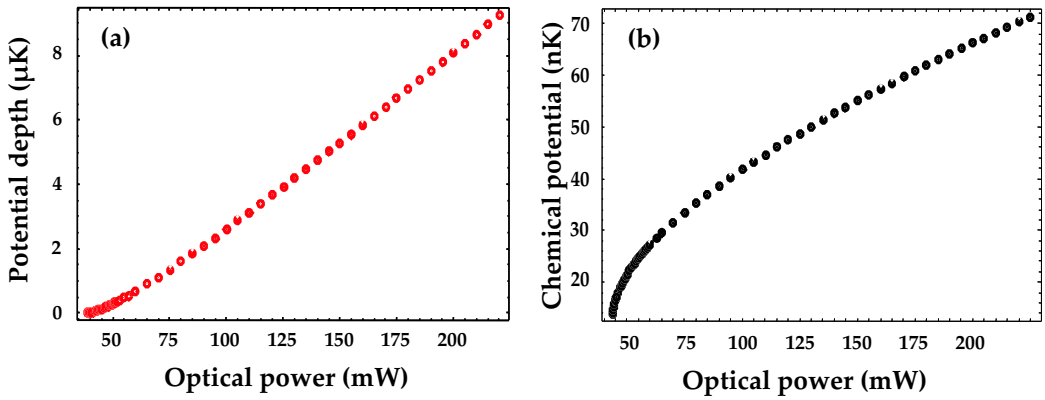

Figure 5.4: (a) Potential depth versus the CO_2-laser power. (b) Chemical potential versus CO_2-laser power. Both graphs include gravity correction.

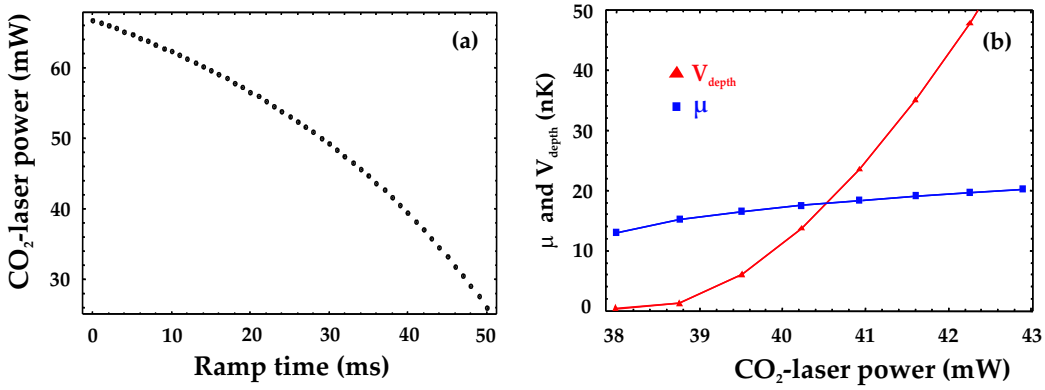

Figure 5.5: (a) CO_2-laser power versus time. (b) Chemical potential and potential depth versus CO_2-laser power.

To describe the output coupler mechanism of the atom laser, we develop a simplified classical model for the behavior of the trapped atoms.

1. When $\mu < V_{depth}$, the atoms do not posses enough energy to overcome the potential barrier. The chemical potential is given by

$$\mu = \frac{\hbar\omega_{ho}}{2}\left(\frac{15Na}{a_{ho}}\right)^{2/5}. \tag{5.2}$$

   In this regime, the number of condensed atoms is supposed constant and no output coupling is observable.

2. As soon as $V_{depth} = \mu$, output coupling of atoms takes place. Initially, we shall assume that all unconfined atoms are instantly removed from the trapping region by gravity, *i.e.* we shall neglect the inertia of the atoms. The chemical potential during this outcoupling stage is not given through the formula (5.2) but rather follows the variation of V_{depth} over time. During the output coupling, the chemical potential is, in this model, locked to the height of the potential barrier:

$$\mu(t) = V_{depth}(t). \tag{5.3}$$

The number of the still trapped atoms can be estimated inverting the relation (5.2), and using the potential depth V_{depth} instead of μ:

$$N(t) = \frac{a_{ho}(t)}{15a}\left(\frac{2V_{depth}(t)}{\hbar\omega_{ho}(t)}\right)^{5/2}. \tag{5.4}$$

From this equation the number of atoms that are output coupled is estimated from the decrease of the number of the still trapped atoms. Fig. 5.6 shows the number of the residing atoms in the CO_2-laser dipole trap during the final stage of the smooth output coupling ramp.

From this model, the flux of the atom laser is approximately constant in the first 4 ms of the extraction process, and it is estimated to be about 1.3×10^6 atoms/s. This value is a factor ~ 1.5 bigger than the experimental one of 8.4×10^5 atoms/s, as presented in the next section. The reason of this overestimation will be clarified soon. Moreover, a closer look at Fig. 5.6 reveals that the number of the trapped atoms is almost zero already after 5 ms the beginning of the extraction process (at a ramp time of 45 ms in the plot). In contrast, the observed value of the temporal length of the atom laser beam for the used ramp is such that the Bose condensed cloud is still populated after 9 ms, as discussed in the previous section.

It is believed that the reason of this difference is the lack of the inclusion of the atomic inertia: it implicitly assumes that the atoms near the height of the potential depth immediately spill out of the trap. In reality, this is true only for those residing on the trap edge, whereas for the ones residing inside the Bose condensed cloud, a finite time is required for

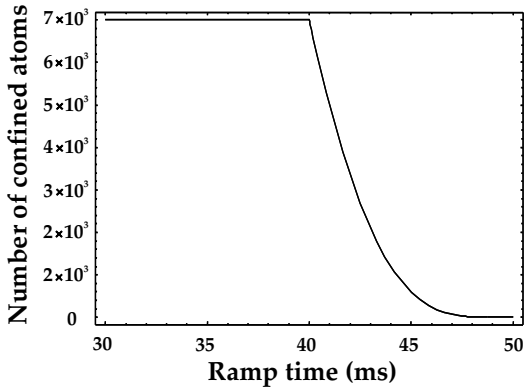

Figure 5.6: Number of atoms still confined by the trapping potential during the final stage of the output coupling ramp (the last 20 ms).

the output coupling. This time can be comparatively long since the atoms inside the Bose condensed cloud still experience the optical dipole force. To introduce a simple dynamics of the process, which also qualitatively takes into account the contribution of the mean-field energy, we assume that Bose condensed atoms in the trap have to roll down a linear potential, as schematically represented in Fig. 5.7.

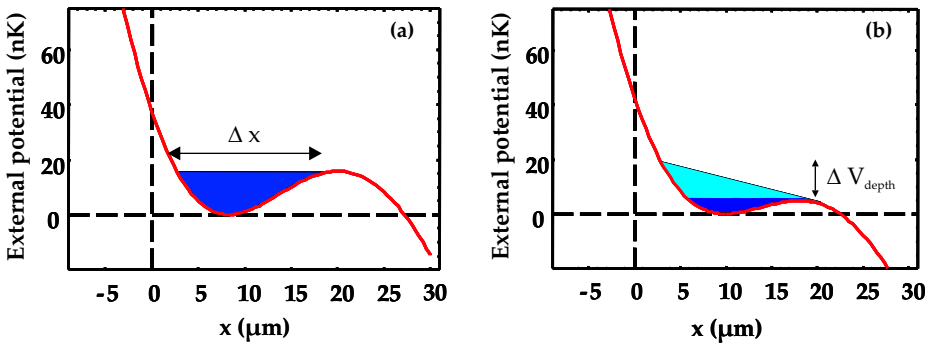

Figure 5.7: Simple output coupling model including the atomic inertia. (a) The Bose condensed cloud has a chemical potential $\mu \sim V_{depth}$. The extraction starts. (b) After a time Δt, the Bose condensed atom which have an energy higher than ΔV_{depth} roll down the potential.

The Bose condensed atoms that have an energy higher than the potential depth V_{depth} see a linear potential whose slope is determined by the variation of the chemical potential over time. The acceleration possessed by these atoms can be estimated as follows. Let us

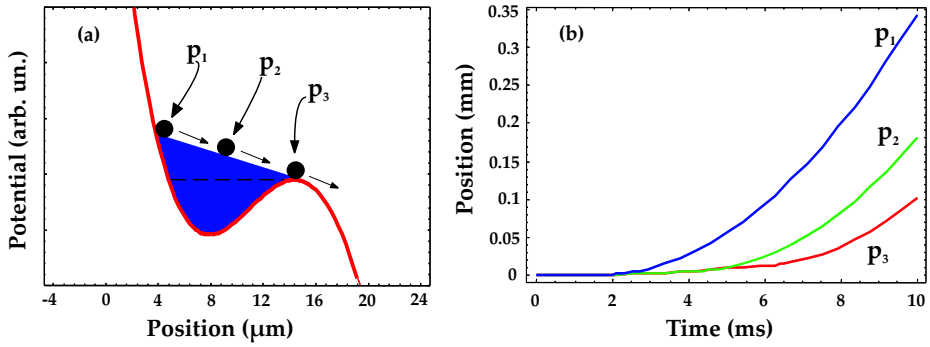

Figure 5.8: Simplified dynamic model of the output coupling time. (a) Atoms at three different initial positions in the trap (p_i). (b) Trajectories of atoms for different initial positions in the trap. Atoms at different positions leave the trapping region at different times.

suppose that at time $t = 0$ the relation $\mu(0) = V_{depth}(0)$ holds, and therefore the extraction starts. After a time t, the height of the trap is $V_{depth}(t)$, and the reduction of the potential depth is therefore $\Delta V_{depth}(t) = V_{depth}(t) - V_{depth}(0)$, as schematically shown in Fig. 5.7. The acceleration possessed by the trapped atoms (whose energy is greater than $V_{depth}(0)$) is then

$$a(t) = \frac{1}{m}\frac{\Delta V_{depth}(t)}{\Delta x}. \tag{5.5}$$

This acceleration is a time dependent function and changes during the extraction process. However, in order to estimate the output coupling time of the atom laser beam, we can introduce an average acceleration defined as $a_{av} = \Delta V_{depth}(\Delta t)/m\Delta x$, where Δt is taken as the time in which the number of atoms confined by the trapping potential decreases to $1/e$ of the initial atom number. In other words, we can determine Δt from the value of the plot of Fig. 5.6, from which we arrive at $\Delta t \approx 2.8$ ms.

With this assumption, the average acceleration of the atoms inside the optical trap is found to be $\simeq 0.075g$, where g is the earth's gravity acceleration. From the knowledge of a_{mean}, one can derive the dynamics of the outcoupling for classical atoms in different regions of the trap. Fig. 5.8 presents a scheme of the outcoupling for atoms initially located in three different positions. Each atom has its own trajectory and thus its own outcoupling time. The temporal spread of the trajectories far from the trap is estimated ≈ 4 ms. If we take into account an additional delay of this order due to the atomic inertia, the experimentally observed value of time 9 ms seems to be much better understood.

It is clear that atoms in a Bose-Einstein condensate are indistinguishable, *i.e.* before the position measurement each atom actually is in a coherent superposition of all possible spatial positions.

In chapter 1, we have derived the hydrodynamic equations for a trapped Bose-condensate in a time-dependent potential, see equations (1.29) and (1.30). The full dynamics of the ex-

traction process, as well as the profile of the monoenergetic atomic beam is embedded in a non-linear time dependent Schrödinger equation. The solution of this problems is difficult to obtain because of the presence of a inharmonic external potential which varies in time. To the best of our knowledge, this problem has not yet been faced. At the present stage, we are collaborating with Dr. Kramer in München to obtain a more realistic model of the output coupling process [107].

5.5 Transverse mode and Brightness of the atom laser beam

Recently, experiments characterizing the physical properties of an atom laser, such as its temporal coherence or the angular divergence have been performed [38, 39].

In this section, we present measurements on the transverse mode and estimations of the brightness of the all-optical atom laser [37]. Fig. 5.9 shows the transverse distribution of the averaged optical column density. Particularly interesting is the transverse mode of our atom laser. The experimental data are fitted quite well with an inverted parabola. This trial function is obtained when assuming that the transverse mode of the atomic beam maps the typical Bose condensate density profile, which in the Thomas-Fermi limit is an inverted parabola. Note that in atom lasers based on radiofrequency output coupling, the

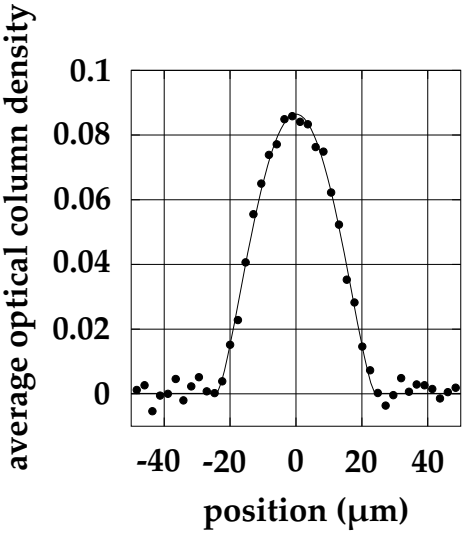

Figure 5.9: Transverse mode of the output coupled atomic beam.

transverse mode often exhibits fringes [40]. These fringes are caused by a lensing effect due to interactions among the atoms in the laser beam and the remaining atoms inside the Bose condensate. Indeed, in order to reach the high flux regime, in atom lasers based on magnetic traps the output coupling happens in the interior of the Bose condensate [36]. The

output coupled atomic beam is formed by atoms which do experience interactions with the residing, magnetically trapped atoms in the interior of the condensate. On the contrary, in the present scheme, the untrapped atoms are those residing not in the internal part of the Bose condensed cloud but rather on the downward directed side of the condensate. Mean field effects from the internal residing atoms are, in this manner, minimized.

Another physical quantity of relevance is the "brightness". This quantity is defined as the flux of atoms over the velocity uncertainty:

$$\frac{\Phi}{\Delta v_x \Delta v_y \Delta v_z} \tag{5.6}$$

where Φ is the flux of atoms and Δv_i is the velocity uncertainty in the corresponding direction x_i [108]. From a fit of the experimental data, the atomic flux is estimated to be 8.4×10^5 atoms/s. Velocity uncertainties are estimated as follows. The uncertainty over the velocity v_z (along the z direction) is well below the experimental resolution of 0.3 mm/s. We here assume that Δv_z is limited by the uncertainty principle, as it is expected for an atom laser. The uncertainty Δz is assumed as the FWHM of the transverse mode of the laser beam, see Fig. 5.9. This transversal width has a value of 26 µm. Using the uncertainty principle, we get $\Delta v_z = \hbar/(2m\Delta z) = 0.0225$ mm/s for the velocity uncertainty along z. The velocity uncertainties along the directions y and x are similarly estimated.

If we assume the dimensions x and y of the condensate almost the same end equal the condensate radius R, then we can introduce the uncertainty ΔR of the radius of the condensate as

$$\Delta R = \frac{\omega_z}{\omega_y} \Delta z, \tag{5.7}$$

where ω_z and ω_y are the trap frequencies along z and y , respectively. The uncertainty on y and therefore on x is $\Delta R = 1.894$ µm. From this we get $\Delta v_{x,y} = \hbar/(2m\Delta R) = 0.33$ mm/s. With these values, a brightness of 7×10^{27} atoms s^2 m^{-5} is inferred. This is orders of magnitude above results achieved with thermal sources, such as atomic beam produced with a Zeeman slower [109] or atoms from a MOT [110]. On the other hand, the brightness estimated here, is about a factor six below a similarly derived value obtained in conventional atom laser based on spin flip transitions [36]. However, it is important to note that in the present experimental setup, low power diode laser sources are employed. This yields to a relatively small number of atoms in the MOT and therefore in the Bose condensate. We expect atom lasers in high flux regime, when the number of the trapped atoms in the CO_2-laser optical dipole trap is increased. This would require the use of more powerful laser sources.

5.6 Discussion

As conclusion, I would like to summarize the focal points of the all-optical laser.

The peculiarity of the all-optical atom laser consists in the use of a $m_F = 0$ Bose-Einstein condensate. This results in an unprecedented stability on the chemical potential against

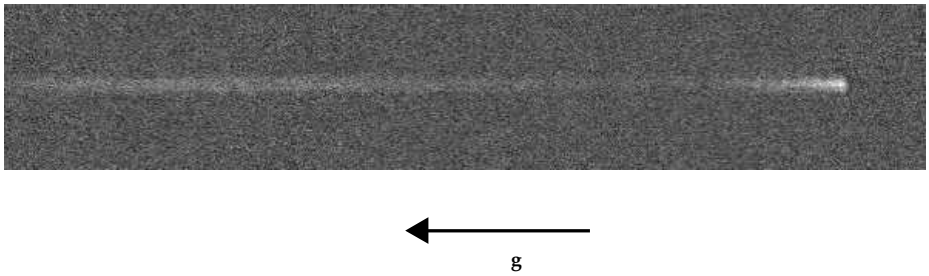

Figure 5.10: Atom laser beam for a temporally relatively slow time. The output coupling time here is 100 ms. Field of view: 1.2 mm × 220 µm

fluctuation of the magnetic field. In contrary to other coupling mechanisms, extraction by gravity does not spoil the transverse mode of the monoenergetic atomic beam. Moreover, by changing the lowering rate of the optical confining potential, both the brightness and the length of the generated beams can be varied. It is possible to observe up to 1 mm long intense, well directed beams of atoms, as Fig. 5.10 shows. Also for longer beams, the momentum spread is attributed to be limited by the uncertainty principle only.

Outlook

In this work, experiments realizing all-optical Bose-Einstein condensation of atoms in two different optical dipole trapping geometries were reported. The study successfully culminated in the demonstration of a new type of atom laser. At the hearth of this new device resides the generation of a magnetic field-insensitive Bose-Einstein condensate.

Today, Bose-Einstein condensation undoubtedly represents a starting point for a number of fascinating experiments in atom physics, ranging from strongly correlated systems in lower dimensions, to the formation of weakly bound molecules and the subsequent exploration of the crossover between BEC and BCS regimes in degenerate dilute molecular gases. Moreover, the synergy between Bose-Einstein condensates and optical lattices seems very promising for the demonstration of quantum computing with schemes based on cold coherent collision among ultracold atoms.

The ability to achieve Bose-Einstein condensation in a single optical dipole trap, as demonstrated in this work, may become a new standard procedure for the future experiments aiming to the quantum degeneracy, because of the experimental simplicity of the approach. However, CO_2-laser optical dipole traps require a suitable technology: radiation near 10.6 µm is absorbed by common quartz glass. This poses some technical constraints on the experimental setup. Further, it is technically demanding to frequency and intensity stabilize such lasers, since sensitive dc-photodiodes do not exist in the mid-infrared region.

An alternative to CO_2-lasers could be the use of tunable optical fiber lasers (OFL), which emit radiation in the spectral range $1 - 3$ µm and offer high output optical powers [111]. In this spectral range, it is possible to find atomic species whose polarizability of the first excited electronic states is positive. As described in section 4.3, it is anticipated that it is critical for the achieving of comparatively high phase space densities of the laser cooled sample that the upper electronic state of the cooling transition is bound more strongly than the ground state. This allows for a successful evaporative cooling towards BEC. Optical fiber lasers offer several advantages, e.g., they allow one to use optical elements made out of quartz or fused silica. This would cause an considerable simplification of experimental apparatus. Further, power stabilization of these lasers can be realized with well established techniques. By virtues of these considerations, optical fiber lasers traps might become a considerably simpler alternative route than magnetic traps for the achieving of quantum degeneracy.

The generation of field-insensitive Bose-Einstein condensates in optical dipole traps

might open Bose-Einstein condensates a door to the fields of precision atom interferometry and atomic clocks. For example, the application of such a magnetic-field insensitive Bose-Einstein condensate in a microgravity environment can lead to substantial improvements in high precision spectroscopy. Indeed, by adiabatically lowering the confining optical potential, Bose-Einstein condensates could then spread out by less than 1 cm/minute, which would allow for rf and microwave spectroscopy with mHz linewidths.

The improvement and the more detailed characterization of all-optical atom lasers is believed to deserve a great interest in the future. In the present experimental setup, low power diode lasers have been employed for the collection and the precooling of rubidium atoms in the MOT. Naturally, this limited the number of atoms in the $m_F = 0$ Bose-Einstein condensate. An increase in the number of Bose condensed atoms is expected when more powerful laser sources are used. This would also lead to a further increase of the flux of the atom laser. As a side effect, longer coherent atomic beams could be generated.

The achieved stability of the condensate chemical potential is in our scheme limited by intensity fluctuations of the CO_2-laser used for confining the $m_F = 0$ Bose-Einstein condensate. An active stabilization of the confining optical power may enable a series of investigations on tunneling of atoms through macroscopic barriers, which would be possible when the confining CO_2-laser power is then lowered extremely smoothly with time.

At present, the intensity noise of the used CO_2-laser is limited to 4 %, which is mainly caused by slow drift of the cavity length. This causes intensity variation, since the gain curve of the CO_2-laser is of similarly spectral width than the cavity free spectral range. However, within the atom laser outcoupling time this intensity noise is negligible.

An important issue that has to be addressed in the future is to compare the temporal coherence of all-optical atom lasers with that of atom lasers based on spin-flips output coupling. Moreover, it remains to be experimentally confirmed the angular divergence of the here demonstrated atom laser, which is expected not to be caused by interactive lensing effects.

There exist many applications in fundamental research and industry where coherent atomic beams might be used in future: atomic clocks, precision measurements of fundamental constants, tests of fundamental symmetries and atom lithography. For example, an atom laser beam could enhance interferometric capabilities, allowing for fringes to be obtained on a small scale with moderate illumination times. It is believed that all-optical atom lasers in future will help to push the experimental constraints of atom optics along these technically and fundamental fascinating physics goals.

Appendix A

Rubidium data

In the following table, important data on ^{87}Rb are resumed. In the formula of the scattering length, a_0 is the Bohr's radius: a_0=0.529 $\times 10^{-10}$ m. The transition $5S \rightarrow 5P_{1/2}$ is denoted as D1-line, whereas the transition $5S \rightarrow 5P_{3/2}$ is denoted as D2-line.

^{87}Rb Physical Properties

Atomic Number Z	37
Relative Abundance	27.83%
Nuclear Spin I	3/2
Mass	$1.44316060 \times 10^{-25}$ Kg [112]
D1-line transition energy	1.559 590 99 (6) eV [113]
D2-line transition energy	1.589 049 439(58) eV
D1-line wavelength in vacuum	794.978 850 9(8) nm [113]
D2-line wavelength in vacuum	780.241 209 686(13) nm [113]
$5P_{1/2}$ state lifetime	26.24(4) ns [113]
$5P_{3/2}$ state lifetime	27.70(4) ns [113]
D1-line natural linewidth	$2\pi \cdot 5.746$ MHz [113]
D2-line natural linewidth	$2\pi \cdot 6.066$ MHz [113]
D1-line recoil velocity	5.7754 mm/s
D2-line recoil velocity	5.8845 mm/s
D1-line recoil energy	$2\pi \cdot 3.6325$ kHz
D2-line recoil energy	$2\pi \cdot 3.7710$ kHz
D1-line saturation intensity(π light)	4.484(5) mW/cm^2
D2-line saturation intensity (π light)	2.503(3) mw/cm^2
D2-line saturation intensity ($\sigma^{\pm}$ light)	1.669(2) mW/cm^2
Triplet scattering length a_T	106 ± 4 a_0 [101]
Singlet Scattering length a_S	90 ± 1 a_0 [101]
Three body recombination rate	$4.3(1.8) \times 10^{-29}$ cm^6/s [100]

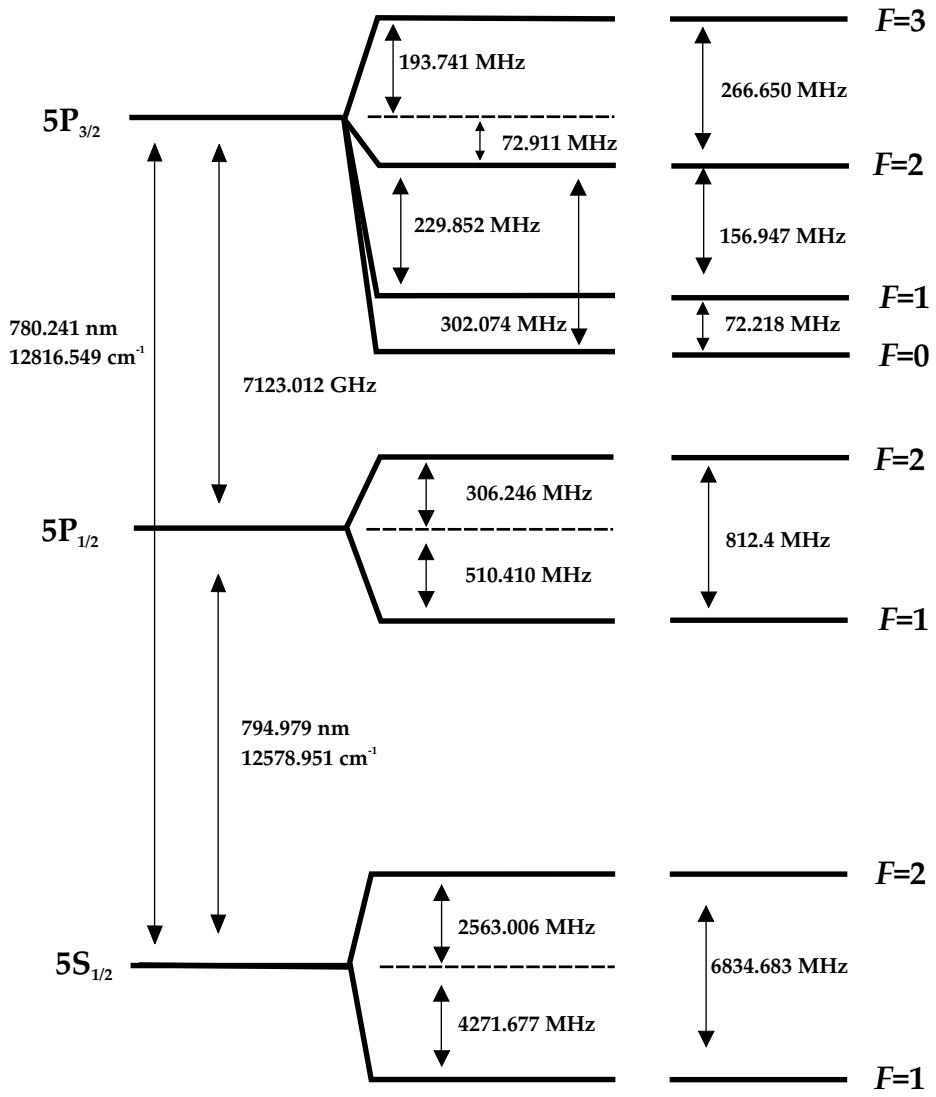

Figure A.1: ^{87}Rb level scheme (D1 and D2 lines).

Appendix B

Experimental sequence

In this section we resume the experimental sequence that leads to a $m_F = 0$ Bose-Einstein condensate. Let us remember, that for the generation of the atom laser Bose-Einstein condensation is achieved in a single running wave optical dipole trap. Once a $m_F = 0$ Bose condensate is formed, the CO_2-laser power is smoothly ramped down in few hundreds of milliseconds (50-100 ms) from an initial value of 150 mW to a final one of 30-40 mW.

Stage	**Description**	**Duration**
MOT loading phase	6×10^7 rubidium atoms are collected in the MOT. The laser cooling detuning is 18 MHz, with a power of 45 mW. The repumping laser power is 10 mW. The applied magnetic MOT field is 10 G/cm. The CO_2-laser radiation is kept on at full power 28 W. The laser beam waist is 27 µm.	30 s
dark-MOT phase	The cooling laser frequency is further "red" detuned by 160 MHz. The repumping laser power is decreased by a factor 100. More than 4×10^6 ^{87}Rb atoms are confined in the single beam CO_2-laser dipole trap. MOT field is kept on.	60 ms
Delay time	The optical potential is kept at full power: 28 W. Plain evaporation is observed, with initial atomic phase-space density 1×10^{-4}. In the first 30 ms of delay phase, the number of atoms in the single dipole trap is reduced by a factor 3, and the atomic temperature decreases from 140 µK to 90 µK. The inferred phase space density after this fast decrease is about 0.016	100 ms
Evaporative cooling	The CO_2-laser dipole trapping potential is adiabatically lowered to near 150 mW, in order to generate an almost pure Bose-Einstein condensate. MOT field is kept on.	7 s
Detection	Stern-Gerlach experiment: $m_F = 0$ Bose condensate with 7000 atoms is detected. The intensity of the probe beam is about 100 mW/cm^2	$80 - 100$ µs

Appendix C

Analysis of Ultracold Atoms

The knowledge of physical properties of the atomic ensemble realized in the experiments, is derived from the analysis of time of flight of ultracold ensemble, as already mentioned in the third chapter. Thermal clouds and Bose condensates are imaged in free expansions after release from the CO_2-laser dipole trap.

Thermal clouds

When the CO_2-laser trapping radiation is switched off, the trapped atoms fly ballistically from their position in the trap with a certain velocity. If an atom starting from point $\mathbf{r}_0$ arrives at a point $\mathbf{r}$ after a time t of free expansion, then its momentum is $\mathbf{p} = m(\mathbf{r} - \mathbf{r}_0)/t$. Integrating over all positions $\mathbf{r}_0$ it is possible to determine the density distribution as a function of the expansion time t:

$$\begin{aligned} n_{tof} &= \frac{1}{h^3}\int d\mathbf{r}_0^3 d\mathbf{p}^3 \frac{1}{e^{H(\mathbf{r}_0,\mathbf{p})/k_BT-\mu}-1}\delta^3(\mathbf{r}-\mathbf{r}_0-\mathbf{p}t/m) \\ &= \frac{1}{\lambda_{dB}^3}\prod_{i=1}^{3}\left(\frac{1}{1+\omega_i^2t^2}\right) g_{3/2}\left(exp\left[\left\{\frac{\mu}{k_BT}-\frac{m}{2k_BT}\sum_{i=1}^{3}x_i^2\left(\frac{\omega_i^2}{1+\omega_i^2t^2}\right)\right\}\right]\right). \end{aligned} \tag{C.1}$$

At larger expansion times ($t \gg 1/\omega_i$), by neglecting the collisions during the expansion, the density profile becomes isotrope, and can be well described by the equation

$$n_{tof} = \frac{1}{\lambda_{dB}^3} g_{3/2}\left(e^{(\mu-\frac{mr^2}{2t^2})/k_BT}\right), \tag{C.2}$$

where $\lambda_{dB} = (2\pi\hbar^2/mk_BT)^{1/2}$, $z(\mathbf{r}) = exp((\mu - V(\mathbf{r}))/k_BT)$, with μ the chemical potential and T the atomic temperature. The Bose function is given by $g_j = \sum_i z^i/i^j$. For high temperatures and longer expansion times, the function $g_{3/2}(z)$ is linear $z + O(z^2)$, and is approximated by a gaussian density distribution:

$$n_{tof} = \frac{n_0}{\lambda_{dB}^3} e^{-\frac{mr^2}{2t^2}/k_BT} \tag{C.3}$$

with $n_0 = e^{\mu/k_B T}$. Information about the number of atoms and atomic temperature is extracted by absorption images, as follows. The absorption function is mapped into the optical density distribution $D(x,z)$ by recurring to equation (3.3). The number of atoms is obtained by integrating the optical density in the $x-z$ plane

$$N = \frac{\Delta_x \Delta_z}{\sigma_\pi} \sum_i \sum_j D(x_i, z_j), \tag{C.4}$$

where $\Delta_x = \Delta_z = 2.36\,\mu\text{m}$ is the size of the region in the object plane which is imaged onto a single pixel of the used CCD camera. In order to extract the temperature of the atomic cloud, first the measured optical density is fitted by the theoretical optical density integrated along the y direction giving the following function

$$D_{th}(x,z,t) = \sigma_\pi \eta_{th}(x,z,t) = \sigma_\pi n_{TOF}(0,0) \frac{2k_B T}{m} \frac{(1+\omega_y^2 t^2)}{\omega_y^2} \times \\ exp\left\{ -\frac{m}{2k_B T} \left(\frac{\omega_x^2 x^2}{1+\omega_x^2 t^2} + \frac{\omega_z^2 z^2}{1+\omega_z^2 t^2} \right) \right\} \tag{C.5}$$

The temperature is deduced from the measured σ_x or σ_z width, according the following formula [11]

$$T = \frac{m}{2k_B} \left(\frac{\omega_x^2}{1+\omega_x^2 t^2} \right) \sigma_x^2. \tag{C.6}$$

Pure Bose-Einstein condensate

For pure Bose condensates, the atomic density is given by the Thomas-Fermi equation:

$$\begin{aligned} n_c(x,y,z) &= \frac{1}{g}(\mu - V_{ho}(\mathbf{r})) \\ &= \frac{15}{8\pi} \frac{N_c}{\prod_i R_i} \left(1 - \sum_i \frac{x_i^2}{R_i^2} \right), \end{aligned} \tag{C.7}$$

where R_i is the half-lengths of the condensate, determined by the chemical potential and the trap vibrational frequencies as $R_i = \sqrt{2\mu/m\omega_i^2}$. It is shown that when such a condensate is released from the trap, it evolves simply as a rescaling of its parabolic shape [114, 115]. This means that the density remains a parabola in the free expansion. For release from a cigar shaped optical dipole trap with radial frequency ω_ρ and aspect ratio $\omega_\rho/\omega_z = \epsilon^{-1}$, the half-lengths of the condensate evolve according to the following equations

$$\begin{aligned} R_\rho(t) &= R_\rho(0) \sqrt{1+\omega_\rho^2 \tau^2} \\ R_z(t) &= R_z(0) \left(1 + \epsilon^2 \left[\tau \arctan \tau - \ln \sqrt{1+\tau^2} \right] \right), \end{aligned} \tag{C.8}$$

with $\tau = \omega_\rho t$ and $\rho = x^2 + y^2$. The expansion of the condensed cloud can be divided in three stages.

1. Soon after the release from the trap interaction energy is converted into kinetic energy (for times $t < \omega_\rho^{-1}$), and the radial direction expands a little.

2. For times $\omega_\rho < t < \epsilon^{-2}\omega_\rho^{-1}$, a radial expansion and a little axial expansion beyond the original axial size are observed.

3. For expansion times $t > \epsilon^{-2}\omega_\rho^{-1}$, the radial and the axial expansions reach an asymptotic aspect ratio: $R_z(t)/R_x(t) = \pi\epsilon^2/2$.

After integration of the parabolic profile of the expanded cloud, the optical density of the condensate images is

$$D_c = \sigma_\pi \eta_c(x,z,t) = \sigma_\pi \frac{2\pi}{5} \frac{N_c}{R_x(0)R_z(0)} \left(1 - \frac{x^2}{R_x^2} - \frac{z^2}{R_z^2}\right)^{3/2} \tag{C.9}$$

The experimental data are fitted according this last function, in order to extract the value of the chemical potential as:

$$\mu = \frac{m}{2}\left(\frac{\omega_\rho^2}{1+\omega_\rho^2}\right) R_x^2(t) \tag{C.10}$$

From the knowledge of μ, the total number of the atoms is extracted:

$$N_c = \frac{a_{ho}}{15a}\left(\frac{2\mu}{\hbar\omega_{ho}}\right)^{5/2}. \tag{C.11}$$

Bimodal distribution

In the process of BEC formation, (when the atomic temperature is in the range between T_c and $T = 0$), a bimodal distribution is observed. As the temperature lowers, more and more atoms scatter into the lowest energy state of the optical dipole trap. Experimentally, it is observable a parabola distribution (which describe the Bose-Einstein condensate density in the TF-regime) sets on a isotropic gaussian, which represents the thermal distribution of the not yet condensed atoms. In this regime, the optical density can be described by the sum of two independent density distributions [11]:

$$D(x,z) = \sigma_\pi \frac{n_{th}(0)}{g_2(1)} g_2\left(e^{1-x^2/\sigma_{x,th}^2 - z^2/\sigma z,th}\right) + n_c(0)\left(1 - \frac{x^2}{R_x^2} - \frac{z^2}{R2_z}\right)^{3/2}. \tag{C.12}$$

Bibliography

[1] A. Einstein, *Zur Quantentheorie des idealen Gases*, Sitzungber. Preuss. Akad. Wiss. Phys. Math. Kl. Bericht **3**, 18 (1925).

[2] M. H. Anderson, J. R. Ensher, M. R. Matthews, C. E. Wieman and E. A. Cornell, *Observation of Bose-Einstein condensation in a dilute atomic vapor.*, Science **269**, 198 (1995).

[3] K. B. Davis, M.-O. Mewes, M. R. Andrews, N. J. van Druten, D. S. Durfee, D. M. Kurn and W. Ketterle, *Bose-Einstein condensation in a gas of sodium atoms*, Phys. Rev. Lett. **75**, 3969 (1995).

[4] C. C. Bradley, C. A. Sackett and R. G. Hulet, *Bose-Einstein Condensation in Atomic Gas with Attractive Interactions*, Phys. Rev. Lett. **75**, 1687 (1995).

[5] D. G. Fried, T. C. Killian, L. Williams, D. Landhuis, S. C. Moss, D. Kleppner and T. J. Greytak, *Bose-Einstein Condensation of Atomic Hydrogen*, Phys. Rev. Lett. **81**, 3811 (1998).

[6] S. Chu, *Nobel Lecture: The manipulation of neutral particles*, Rev. Mod. Phys. **70**, 685 (1998).

[7] W. D. Phillips, *Laser cooling and trapping of neutral atoms*, Review of Modern Physics **70**, 721 (1998).

[8] C. N. Cohen-Tannoudji, *Nobel Lecture: Manipulating atoms with photons*, Rev. Mod. Phys. **70**, 707 (1998).

[9] E. A. Cornell and C. E. Wieman, *Nobel Lecture: Bose-Einstein Condensation in a Dilute Gas, the First 70 Years and Some Recent Experiments*, Rev. Mod. Phys. **74**, 875 (2002).

[10] W. Ketterle, *Nobel Lecture: When atoms behave as waves: Bose-Einstein condensation and the atom laser*, Rev. Mod. Phys. **74**, 1132 (2002).

[11] W. Ketterle, D. S. Durfee and D. M. S. Kurn, Making probing and understanding Bose-Einstein condensates, in *Bose-Einstein Condensation in Atomic Gases*, edited by M. Inguscio, S. Stringari and C. E. Wieman, Proceedings of the International School of Physics "Enrico Fermi", Course CXL, IOS Press, 1999.

[12] A. L. Midgal, J. V. Prodan, W. D. Phillips, T. H. Bergeman and H. J. Metcalf, *First Observation of Magnetically Trapped Neutral Atoms*, Phys. Rev. Lett. **54**, 2596 (1985).

[13] E. Hott, J. Fortágh, G. Schlotterbeck, A. Grossmann and C. Zimmermann, *Bose-Einstein condensation in a surface microtrap*, Phys. Rev. Lett. **87**, 230401 (2001).

[14] W. Hänsel, P. Hommelhof, T. W. Hänsch and J. Reichel, *Bose-Einstein condensation on a microelectronic chip*, Nature **413**, 498 (2001).

[15] AA.VV., in *Proceeding of the Fifth Sysmposium on Frequency Standards and Metrology*, edited by J. C. Bergquist, World Scientific, Singapore, 1996.

[16] T. Takekoshi, B. M. Patterson and R. J. Knize, *Observation of Optically Trapped Cold Cesium Molecules*, Phys. Rev. Lett. **81**, 5105 (1998).

[17] R. Grimm, M. Weidemüller and Y. B. Ovchinnikov, *Optical dipole traps for neutral atoms*, Adv. At. Mol. Opt. Phys. **42**, 95 (2000).

[18] A. Görlitz, J. M. Vogel, A. E. Leanhardt, C. Raman, T. L. Gustavson, J. R. Abo-Shaeer, A. P. Chikkatur, S. Gupta, S. Inouye and W. Ketterle, *Realization of Bose-Einstein Ceondensates in Lower Dimensions*, Phys. Rev. Lett. **87**, 130402 (2001).

[19] M. Greiner, O. Mandel, T. Esslinger, T. W. Hänsch and I. Bloch, *Quantum phase transition from a superfluid to a Mott insulator in an ultracold gas of atoms*, Nature **415**, 39 (2002).

[20] M. D. Barret, J. A. Sauer and M. S. Chapman, *All-Optical Formation of an Atomic Bose-Einstein Condensate*, Phys. Rev. Lett. **87**, 010404 (2001).

[21] T. Weber, J. Herbig, M. Mark, H.-C. Nägerl and R. Grimm, *Bose-Einstein Condensation of Cesium*, Science **299**, 232 (2002).

[22] S. R. Granade, M. E. Gehm, K. M. O'Hara and J. E. Thomas, *All-Optical Production of a Degenerate Fermi Gas*, Phys. Rev. Lett. **88**, 120405 (2002).

[23] G. Cennini, G. Ritt, C. Geckeler and M. Weitz, *Bose-Einstein condensation in a CO_2-laser optical dipole trap*, Appl. Phys. B **77**, 773 (2003).

[24] Y. Takasu, K. Maki, K. Komori, T. Takano, K. Honda, M. Kumakura, T. Yabuzaki and Y. Takahashi, *Spin-Single Bose-Einstein Condensation of Two-Electron Atoms*, Phys. Rev. Lett. **91**, 040404 (2003).

[25] S. Friebel, R. Scheunemann, T. W. Hänsch and M. Weitz, *Laser cooling in a CO_2-laser optical lattice*, Appl. Pys. B **67**, 699 (1998).

[26] C. S. Adams, H. J. Lee, N. Davidson, M. Kasevic and S. Chu, *Evaporative Cooling in a Crossed Dipole Trap*, Phys. Rev. Lett. **74**, 3577 (1995).

[27] T.-L. Ho, *Spinor Bose condensates in optical traps*, Phys.Rev. Lett. **81**, 742 (1998).

[28] D. M. Stamper-Kurn, M. R. Andrews, A. P. Chikkatur, S. Inouye, H.-J. Miesner, J. Stenger and W. Ketterle, *Optical Confinement of a Bose-Einstein Condensate*, Phys. Rev. Lett. **88**, 2027 (1998).

[29] M. R. Andrews, G. G. Townsend, H.-J. Miessner, D. S. Durfee, D. M. Kurn and W. Ketterle, *Observation of Interference between two Bose condensates*, Science **275**, 637 (1998).

[30] I. Bloch, T. W. Hänsch and T. Esslinger, *Meaurements of the phase coherence of a Bose gas at the phase transition*, Nature **403**, 4213 (2000).

[31] H.-J. Miessner, D. M. Stamper-Kurn, M. R. Andrews, D. S. Durfee, S. Inouye and W. Ketterle, *Bosonic Stimulation in the Formation of a Bose-Einstein Condensate*, Science **279**, 1005 (1998).

[32] M. Köhl, M. J. Davis, C. W. G. nad T. W. Hänsch and T. Esslingen, *Growth of Bose-Einstein Condensates from Thermal Vapor*, Phys. Rev. Lett. **88**, 080402 (2002).

[33] M.-O. Mewes, M. R. Andrews, D. M. Kurn, D. S. Durfee, C. G. Townsed and W. Ketterle, *Output Coupler for Bose-Einstein Condensed Atoms*, Phys. Rev. Lett. **78**, 582 (1997).

[34] B. P. Anderson and M. A. Kasevic, *Macroscopic Quantum Interference from Atomic Tunnel Arrays*, Science **282**, 1686 (1998).

[35] E. W. Hagley, L. Deng, M. Kozuma, J. Wen, K. Helmerson, S. L. Rolston and W. D. Phillips, *A Well-Collimated Quasi-Continuous Atom Laser*, Phys. Lett. A **283**, 1706 (1999).

[36] I. Bloch, T. W. Hänsch and T. Esslinger, *Atom Laser with a cw Output Coupler*, Phys. Rev Lett. **82**, 3008 (1999).

[37] G. Cennini, G. Ritt, C. Geckeler and M. Weitz, *All-Optical Realization of an Atom Laser*, Phys. Rev. Lett. **91**, 240408 (2003).

[38] M. Köhl, T. W. Hänsch and T. Esslingen, *Measuring the Temporal Coherence of an Atom Laser Beam*, Phys. Rev. Lett. **87**, 160404 (2001).

[39] Y. L. Coq, J. H. Thywissen, S. A. Rangwala, F. Gerbier, S. Richard, G. Delannoy, P. Bouyer and A. Aspect, *Defining the Laser Divergence*, Phys. Rev. Lett. **87**, 170403 (2001).

[40] T. Busch, M. Köhl, T. Esslinger and K. Mølmer, *Transverse mode of an atom laser*, Phys. Rev. A **65**, 043615 (2002).

[41] S. N. Bose, *Plancks Gesetz und Lichtquantenhypothese*, Z. Phys. **26**, 178 (1924).

[42] F. Dalfovo, S. Giorgini, L. P. Pitaevskii and S. Stringari, *Theory of Bose-Einstein condensation in trapped gases*, Rev. Mod. Phys. **71**, 463 (1999).

[43] A. J. Leggett, *Bose-Einstein condensation in alkali gases: Some fundamental concepts*, Rev. of Mod. Phys. **73**, 307 (2001).

[44] K. Huang, *Statistical Mechanics*, John Wiley & Sons, Inc., 1963.

[45] R. P. Feynman, *Statistical Mechanics: A Set of Lectures*, Addison-Wesley, 1972.

[46] V. Bagnato, D. E. Pritchard and D. Kleppner, *Bose-Einstein condensation in an external potential*, Phys. Rev. A **35**, 4354 (1987).

[47] R. P. Feynman, *The Feynman Lectures on Physics, Vol III: Quantum Mechanics*, Addison-Wesley, 1965.

[48] J. Dalibard, Collisional dynamics of ultra-cold atomic gases, in *Bose-Einstein Condensation in Atomic Gases*, edited by M. Inguscio, S. Stringari and C. E. Wieman, Proceedings of the International School of Physics "Enrico Fermi", Course CXL, IOS Press, 1999.

[49] N. N. Bogoliubov, *On the theory of suprefluidity*, Journal of Physics U.S.S.R. **11**, 23 (1947).

[50] O. Penrose and L. Onsager, *Bose-Einstein Condensation and Liquid Helium*, Phys. Rev. **104**, 576 (1956).

[51] C. N. Yang, *Concept of Off-Diagonal Long-Range Order and the Quantum Phase of Liquid He and of Superconductors*, Rev. Mod. Phys. **34**, 694 (1962).

[52] A. L. Fetter, heory of a dilute low-temperaturetrapped Bose condensate, in *Bose-Einstein Condensation in Atomic Gases*, edited by M. Inguscio, S. Stringari and C. E. Wieman, Proceedings of the International School of Physics "Enrico Fermi", Course CXL, IOS Press, 1999.

[53] F. Dalfovo, L-Pitaevskii and S. Stringari, *Order parameter at the boundary of a trapped Bose gas*, Phys. Rev. A **54**, 4213 (1996).

[54] Y. Castin, *Bose-Einstein condensation in atomic gases: simple theoretical resuts*, (2001).

[55] G. A. Askar'yan, *Effects of the gradient of a strong electromagnetic beam on electrons and atoms*, Sov. Phys. JEPT **15**, 1088 (1969).

[56] A. Ashkin, *Trapping of atoms by resonance radiation pressure*, Phys. Rev. Lett. **40**, 729 (1978).

[57] J. P. Gordon and A. Ashkin, *Motion of atoms in a radiation field*, Phys. Rev. A **21**, 1606 (1980).

[58] S. Friebel, C. D'Andrea, J. Waltz, M. Weitz and W. Hänsch, *CO_2-laser optical lattice with cold rubidium atoms*, Phys. Rev. A **57**, 57 (1998).

[59] I. H. Deutsch and P. S. Jessen, *Quantum-state control in optical lattices*, Phys. Rev. A **57**, 1972 (1998).

[60] J. D. Jackson, *Classical electrodynamics, 3rd ed.*, John Wiley & Sons, Inc., 1998.

[61] C. Cohen-Tannoudji, J. Dupont-Roc and G. Grynberg, *Atom-Photon Interactions, Basic Processes and Applications*, John Wiley & Sons, Inc., 1992.

[62] K. L. Corwin, S. J. M. Kuppens, D. Cho and C. E. Wieman, *Spin-Polarized Atoms in a Circularly Polarized Optical Dipole Trap*, Phys. Rev. Lett. **83**, 1311 (1999).

[63] T. Takekoshi, J. R. Yeh and R. J. Knize, *Quasi-electrostatic trap for neutral atoms*, Optics Comm. **114**, 421 (1995).

[64] A. S. Davydov, *Quantum Mechanics*, Pergamon, Oxford, 1976.

[65] A. Corney, *The Theory of Atomic Spectra*, Clarendon Press, Oxford, 1977.

[66] A. Khadjavi, A. Lurio and W. Happer, *Stark effect in the Excited States of Rb, Cs, Cd, and Hg*, Phys. Rev. **167**, 128 (1968).

[67] H. Gould, E. Lipworth and M. C. Weisskopf, *Quadratic Stark Shift between Zeeman Substates in Cs^{133}, Rb^{87}, Rb^{85}, K^{39}, and Na^{23}*, Phys. Rev. **188**, 24 (1969).

[68] R. W. Schmieder, A. Lurio and W. Happer, *Quadratic Stark Effect in the $^2P_{3/2}$ States of the Alkali Atoms*, Phys. Rev. A **3**, 1209 (1971).

[69] C. C. Agosta, I. F. Silvera, H. C. T. Stoof and B. J. Verhaar, *Trapping of Neutral Atoms with Resonant Microwave Radiation*, Phys. Rev. Lett. **62**, 2361 (1989).

[70] R. Loudon, *The Quantum Theory of Light, 2nd ed.*, John Wiley & Sons, Inc., 1983.

[71] A. Yariv, *Quantum Electronics, 3rd ed.*, John Wiley & Sons, Inc., 1989.

[72] R. Scheunemann, F. S. Cataliotti, T. W. Hänsch and M. Weitz, *Resolving and addressing atoms in individual sites of a CO_2-laser optical lattice*, Phys. Rev. A **62**, 051801 (2000).

[73] E. L. Raab, M. Prentiss, A. . Cable, S. Chu and D. E. Pritchard, *Trapping of Neutral Sodium Atoms with Radiation Pressure*, Phys. Rev. Lett. **59**, 2631 (1987).

[74] L. Ricci, M. Weidemüller, T. Esslinger, A. Hemmerich, C. Zimmermann, V. Vuletic, W. König and T. W. Hänsch, *A Compact Grating-Stabilized Diode Laser System for Atomic Physics*, Opt. Comm. **117**, 541 (1995).

[75] G. Ritt, G. Cennini, C. Geckeler and M. Weitz, *Laser frequency offset locking using a side of filter technique*, Appl. Phys. B **00**, 1 (2004).

[76] C. Geckeler, *Ultrakalte Rubidiumatome in einer CO_2-Laser Dipolfalle*, Master thesis, Physikalishes Institut Eberhard-Karls-Universität Tübingen, 2002.

[77] A. Aspect, E. Arimondo, R. Keiser, N. Vansteenkiste and C. Cohen-Tannoudji, *Laser Cooling below the One-Photon Recoil Energy by Velocity-Selective Coherent Population Trapping*, Phys. Rev. Lett. **61**, 1714 (1988).

[78] C. Monroe, D. Meekhof, B. King, S. Jefferts, W. Itano, D. Wineland and P. Gould, *Resolved-sideband Raman cooling of a bound atom to the 3D zero-point energy*, Phys. Rev. Lett. **62**, 403 (1989).

[79] M. Kasevich and S. Chu, *Laser Cooling below a Photon Recoil with Three Level Atoms*, Phys. Rev. Lett. **69**, 1741 (1992).

[80] H. Perrin, A. Kuhn, I. Bouchoule and C. Salomon, *Sideband cooling of neutral atoms in a far detuned optical lattice*, Europhy. Lett **42**, 395 (1998).

[81] S. Hamann, D. Haycock, G. Klose, P. Pax, I. Deutsch and P. Jessen, *Resolved-Sideband Raman Cooling of an Optical Lattice*, Phys. Rev. Lett. **80**, 4149 (1998).

[82] A. Kerman, V. Vuletic, C. Chin and S. Chu, *3D Raman Sideband Cooling of Atomic Cesium to High Phasespace Density*, Phys. Rev. Lett. **84**, 439 (2000).

[83] D. J. Han, S. Wolf, S. Oliver, C. McCormick, M. T. DePue and D. S. Weiss, *3D Raman sideband Cooling of Cesium Atoms at High Density*, Phys. Rev. Lett. **85**, 724 (2000).

[84] C. Monroe, W. Swann, H. Robinson and C. Wieman, *Very Cold Trapped Atoms in a Vapor Cell*, Phys. Rev. Lett. **89**, 090402 (2002).

[85] C. Cohen-Tannoudji, *Atomic Motion in Laser Light*, volume Fundamental Systems in Quantum Optics, North-Holland, 1992.

[86] D. W. Sesko, T. G. Walker and C. E. Wieman, *Behavior of neutral atoms in a spontaneous force trap*, J. Opt. Soc. Am. B **8**, 946 (1990).

[87] A. M. Steane, M. Chowdhury and C. J. Foot, *Radiation force in the magneto-optical trap*, J. Opt. Soc. Am. B **9**, 2142 (1992).

[88] C. G. Townsed, N. H. Edwards, C. J. Cooper, K. P. Zetie, C. J. Foot, A. M. Steane, P. Szriftgiser, H. Perrin and J. Dalibard, *Phase-space density in the magneto-optical trap*, Phys. Rev. A **52**, 1423 (1995).

[89] W. Ketterle, K. B. Davis, M. A. Joffe, A. Martin and D. E. Pritchard, *High Densities of Cold Atoms in a Dark Spontaneous-Force Optical Trap*, Phys. Rev. Lett. **70**.

[90] H. F. Hess, *Evaporative cooling of magnetically trapped and compressed spin-polarized hydrogen*, Phys. Rev. B **34**, 3476 (1986).

[91] W. Ketterle and N. J. van Druten, *Evaporative Cooling of Trapped Atoms*, Adv. At. Mol. Opt. Phys. **37**, 181 (1996).

[92] K. B. Davis, M.-O. Mewes and W. Ketterle, *An analytical model for evaporative cooling of atoms*, Appl. Phys. B **60**, 155 (1995).

[93] K. M. O'Hara, M. E. Gehm, S. R. Granade and J. E. Thomas, *Scaling laws for evaporative cooling in time-dependent optical traps*, Phys. Rev. A **64**, 051403 (2001).

[94] S. J. M. Kuppens, K. L. Corwin, W. W. Miller, T. E. Chupp and C. E. Wieman, *Loading an optical dipole trap*, Phys. Rev. A **62**, 013406 (2000).

[95] J. Stenger, S. Inouye, D. M. Stamper-Kurn, H.-J. Miesner, A. P. Chikkatur and W. Ketterle, *Spin domains in ground-state Bose-Einstein condensates*, Phys.Rev. Lett. **396**, 345 (1998).

[96] H.-J. Miesner, D. M. Stamper-Kurn, J. Stenger, S. Inouye, A. P. Chikkatur and W. Ketterle, *Spin domains in ground-state Bose-Einstein condensates*, Phys.Rev. Lett. **396**, 345 (1998).

[97] M.-S. Chang, C. D. Hamley, M. D. Barrett, J. A. Sauer, K. M. Fortier, W. Zhang, L. You and M. S. Chapman, *Observation of Spin Dynamics in Optically Trapped ^{87}Rb Bose-Einstein Condensates*, Phys. Rev. Lett. **92**, 140403 (2004).

[98] H. Schmaljohann, M. Erherd, J. Kronjäger, M. Kottke, S. van Staa, L. Cacciapuoti, J. J. Arlt, K. Bongs and K. Sengstock, *Dynamics of F=2 Spinor Bose-Einstein Condensates*, Phys.Rev. Lett. **92**, 040402 (2004).

[99] G. Breit and I. Rabi, *Measurement of Nuclear Spin*, Phys. Rev. **38**, 2082 (1931).

[100] E. A. Burt, R. W. Ghirst, C. J. Myatt, M. J. Holland, E. A. Cornell and C. E. Wieman, *Coherence, correlations and collisions: What One Learns about Bose-Einstein Condensates from Their Decay*, Phys. Rev. Lett. **79**, 337 (1997).

[101] N. N. Klausen, J. L. Bohn and C. H. Greene, *Nature of spinor Bose-Einstein condensates in rubidium*, Phys. Rev. A **64**, 053602 (2001).

[102] M. Holland, K. Burnett, C. Gardiner, J. I. Cirac and P. Zoller, *Theory of an Atom Laser*, Phys. Rev. A **54**, 1757 (1996).

[103] G. M. Moy, J. J. Hope and C. M. Savage, *Atom laser based on Raman transitions*, Phys. Rev. A **55**, 3631 (1997).

[104] H. M. Wisemann, *Defining the (atom) laser*, Phys. Rev. A **56**, 2068 (1997).

[105] D. Kleppner, *Experimental Studies of Bose-Einstein Condensation.*, Physics Today **50**, 8 (1997).

[106] W. Ketterle, *Atom Laser*, McGraw-Hill Yearbook of Science & Technology , 43 (1998).

[107] T. Kramer, private communication.

[108] E. Riis, D. S. Weiss, K. A. Moler and S. Chu, *Atom Funnel for the production of a Slow, High-Density Atomic Beam*, Phys. Rev. Lett. **64**, 1658 (1990).

[109] W. D. Phillips and H. Metcalf, *Laser Deceleration of an Atomic Beam*, Phys. Rev. Lett. **48**, 596 (1982).

[110] Z. T. Lu, K. L. Corwin, M. J. Renn, M. H. Anderson, E. A. Cornell and C. E. Wieman, *Low-Velocity Intense Source of Atoms from a Magneto-optical Trap*, Phys. Rev. Lett. **77**, 3331 (1996).

[111] T. W. Hänsch, private communication.

[112] M. P. Bradley, J. V. .Porto, S. Rainville, J. K. Thompson and D. Pritchard, *Penning Trap Measurements of the Masses of ^{133}Cs,$^{85,87}Rb$, and ^{23}Na*, Phys. Rev. Lett. **83**, 4510 (1999).

[113] A. A. Radzig and B. M. Smirnov, *Reference Data on Atoms, Molecules and Ions*, Springer-Verlag, 1985.

[114] Y. Castin and R. Dum, *Bose-Einstein condensation in time dependent traps*, Phys. Rev. Lett. **77**, 5315 (1996).

[115] Y. Kagan, E. L. Surkov and G. B. Shlypanikov, *Evolution of a Bose-Condensed gas under variations of the confining potential*, Phys. Rev. A **54**, 1753 (1996).